EVALUATION OF THE LATERAL STIFFNESS FOR THE SEISMIC ANALYSIS AND DESIGN OF SQUAT RC WALLS

by

Andres F. Ocampo-Escobar

Dissertation submitted in partial fulfillment of the requirements for the degree of

DOCTOR OF PHILOSOPHY
in
CIVIL ENGINEERING

UNIVERSITY OF PUERTO RICO
MAYAGÜEZ CAMPUS
2019

Approved by:

Aidcer L. Vidot-Vega, Ph.D. President, Graduate Committee	Date
Luis A. Montejo-Valencia, Ph.D. Member, Graduate Committee	Date
Ricardo R. López-Rodríguez, Ph.D. Member, Graduate Committee	Date
Luis E. Suárez, Ph.D. Member, Graduate Committee	Date
Barbara Calcagno, Ph.D. Representative of Graduate School	Date
Ismael Pagán-Trinidad, M.S.C.E. Chairperson of the Department	Date

ABSTRACT

Reinforced concrete (RC) squat walls provide most of the structure lateral strength and stiffness to resist earthquakes and wind loadings in nuclear power plants and other buildings. A reduction factor is usually applied to the stiffness to compensate for the effect of cracking in linear analysis. An appropriate definition of lateral stiffness is important to properly capture cracking effects and to accurately design and evaluate the behavior of RC shear walls. The basis for the effective stiffness values or expressions and their applicability to nuclear power plant elements is not clearly presented in current seismic standards. This research studies the effective stiffness of reinforced concrete (RC) squat walls under lateral loads. RC squat walls have height to length ratios less than or equal to 2. Prediction of the seismic response and proper capturing of the effective stiffness of squat walls is a challenging task since these walls exhibit a shear dominated behavior with strong coupling between shear and flexure responses. Finite element models of several RC squat walls are developed using the commercial software Abaqus and OpenSees. The main objective of these models is to predict the lateral stiffness of RC squat walls appropriately and to identify the parameters that have main influence in the lateral stiffness of these walls. The results from analytical modeling are compared with the results of experimental tests available in the literature. Available expressions and reduction factors in current seismic standards and in the literature for the calculation of effective stiffness for RC squat walls are also evaluated. Improved predictive equations for lateral stiffness are developed by calibration against the available data. Multiple-linear regression analysis is used to develop the predictive equations. Key parameters influencing the effective stiffness are identified during the nonlinear analyses and from existing experimental data.

RESUMEN

Los muros de concreto reforzado (CR) de baja altura proporcionan la mayor parte de la resistencia y rigidez en las estructuras para resistir las cargas sísmicas y de viento en plantas nucleares y otros edificios. Usualmente se usan factores de reducción para reducir la rigidez en los muros y compensar el efecto del agrietamiento en el análisis lineal. Una adecuada definición de rigidez lateral es importante para capturar apropiadamente los efectos de agrietamiento y para diseñar y evaluar con precisión el comportamiento de los muros de corte (CR). La base para los factores de reducción o expresiones para el cálculo de la rigidez efectiva y su aplicabilidad en muros de plantas nucleares no se presenta claramente en las normas sísmicas actuales. Esta investigación estudia la rigidez efectiva de los muros de corte de baja altura (CR) bajo cargas laterales, estos muros tienen una relación de altura a longitud menor o igual a 2. La predicción de la respuesta sísmica y la captura adecuada de la rigidez efectiva de estos muros es una tarea difícil, ya que tienen un comportamiento dominado por el cortante pero también con un fuerte acoplamiento entre las respuestas a cortante y flexión. Se desarrollaron varios modelos de muros de corte en elementos finitos utilizando el software comercial Abaqus y el software Opensees. El objetivo principal de estos modelos es el de predecir la rigidez lateral de muros de corte bajos (CR) de forma apropiada e identificar los parámetros que tienen mayor influencia en la rigidez lateral de estos muros. Los resultados de rigidez lateral de los modelos analíticos fueron comparados con resultados de pruebas experimentales disponibles en la literatura. También se evaluaron las expresiones disponibles y los factores de reducción de los estándares sísmicos actuales y en la literatura para el cálculo de la rigidez efectiva de estos muros. Se desarrollaron ecuaciones para predecir la rigidez lateral con base en datos experimentales disponibles de muros bajos (CR) y mediante el análisis de regresión lineal múltiple. Se identificaron los parámetros más importantes en la rigidez efectiva con los análisis no lineales y datos experimentales.

I dedicate this thesis to my parents who taught me the value of education, they will always be in my mind.

ACKNOWLEDGEMENTS

I would like to thank professors Dr. Luis Montejo and Dra. Aidcer Vidot for trusting in me and giving me the opportunity to pursue my doctorate degree.

Special thanks to my advisor professor Dra. Aicer Vidot for her constant guidance, patience, dedication and her support to carry out this research.

I would also like to thank my friend Carlos Andres Gaviria for recommending me to professors Dr. Luis Montejo and Dra. Aidcer Vidot.

I also want to thank professors Dr. Luis Suarez and Dr.Ricardo Lopez for being part of my graduate committee and for the teachings taught in their courses and especially as human beings.

Thanks to my family for their support in my academic career.

Thanks to my friends and my girlfriend for being part of this process.

This work was performed under award NRC-HQ-84-14-G-0057 from the US Nuclear Regulatory Commission. The statements, findings, conclusions, and recommendations are those of the authors and do not necessarily reflect the view of the US Nuclear Regulatory Commission.

TABLE OF CONTENTS

LIST OF FIGURES

LIST OF TABLES

CHAPTER I. BACKGROUND

1.1 Introduction

Reinforced concrete (RC) shear walls with height to length ratios less than or equal to two are commonly used in nuclear power plants buildings as part of the lateral-load-resisting system of the structure, those walls are known as squat or short walls. Three types of failure can be found in squat RC walls: diagonal tension, diagonal compression and sliding shear (Paulay and Priestley, 1992). The type or combination of failure will depend on the design parameters such as horizontal and vertical web reinforcement ratio, wall geometry and axial force level of each squat RC wall. Several experimental studies (Kolozvari et al. 2014, Gulec and Whittaker 2009, Tang and Su 2014) have shown that shear walls with aspect ratio higher than 3.0 will yield in flexure and not fail in shear, but shear walls with aspect ratio less than1.5 will fail in shear, meanwhile walls with aspect ratio between 1.5 and 2.5 will fail in a combination of shear and flexure.

Figure 1 shows those types of failures in shear walls and their associated characteristic cracking pattern. According to Sozen and Moehle (1993), the total displacement in a squat shear wall is comprised on three types of displacements, one related to the flexural behavior, another related to the shear deflection and the last one comes from the slippage between the foundation and the wall, as shown in the Figure 2.

a) Diagonal tension failure of wall 27 tested by Hidalgo et al. (2001)

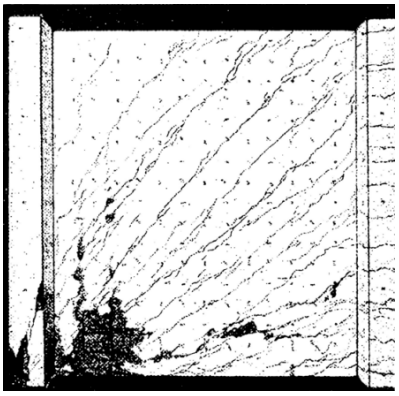

b) Diagonal compression failure of wall S1 tested by Maier and Thürlimann (1985)

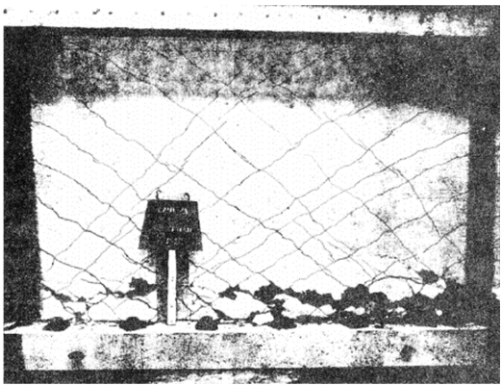

c) Sliding shear failure [Synge 1980].

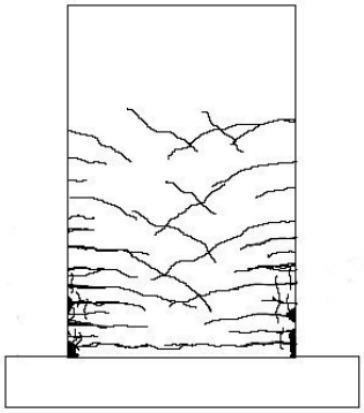

d) Representative cracking pattern for flexural failure [ATC (1998b)]

Figure 1. Types of failures in shear walls

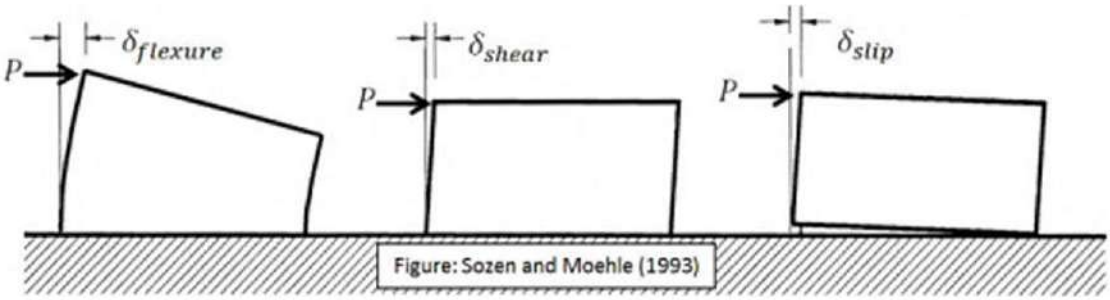

Figure 2. Types of displacements found in squat walls

In general, reinforced concrete structures subjected to earthquakes always tend to crack even if these structures are in a low to moderate seismic region. Structures with walls as the main seismic resistance structural system also tend to crack and depending of the cracking level those cracks could be devastating specially in nuclear plants where radiation is an imminent risk. The walls in those types of structures provide most of the structure lateral strength and stiffness to resist earthquakes and wind loadings. A reduction factor is usually applied to the stiffness to compensate for the effect of cracking in linear analysis. An appropriate definition of lateral stiffness is important to proper capture cracking effects and to accurately design and evaluate the behavior of RC shear walls. Estimation of the lateral stiffness of structural members especially for squat RC walls is not something straightforward. Lateral stiffness of squat RC walls depends on multiple factors besides the young modulus of the concrete and reinforcement steel. Some of these factors are: a) geometrical effect, b) the intensity of axial loads, c) the deterioration in stiffness, and d) the use of special details. Regarding the geometrical effects, walls with aspect ratios (h_w/l_w) less than 1.5 have a stiffness controlled by shear, meanwhile walls with aspect ratios higher than 3.0 are controlled by flexural behavior that will impact the cracking pattern and estimation of their stiffness. Furthermore, a higher axial load can reduce the crack formed by tensile stress in concrete increasing the stiffness in the walls. The degradation of the flexural stiffness and shear stiffness are different and could be affected by the bond-slip deformation and slipping resistance between the wall and the foundation. The use of special details can modify the response of squat walls and have impact in their stiffness. For example, the use of diagonal reinforcement details can increase the ductility and the effective stiffness of the wall due to a reduction of cracks.

An accurate model for the prediction of the response of squat walls that capture initial stiffness and its degradation as multiple cycles of deformations beyond yielding occurs is necessary. Several approaches have been proposed to predict the cyclic behavior of squat walls based on experimental data and/or analytical modeling theories such as fracture mechanics (Thomson and Florez-López 2004, Massone et al. 2006, Fischinger et al. 2012, Kolozvari 2013, Epackachi et al. 2015, and others). Some of these models are already implemented in finite element analysis programs, such as OpenSees and the commercial software Perform-3D which is a program from CSI for implementing displacement-based design. Other models have been implemented as subroutines in commercial programs like ABAQUS and LS-DYNA, however not all subroutines are available to

the public. In general different modeling approaches and computer programs have its inherent advantages and disadvantages to properly model the behavior of squat RC walls and to capture stiffness changes that will be discussed later.

1.2 Research significance and motivation

In the seismic analysis and design of RC structures, the stiffness properties of the elements must account for the effects of concrete cracking, member strength and axial load. A reduction factor is usually incorporated in the lateral stiffness to compensate for the effect of cracking in linear analysis. Design codes and seismic standards (e.g FEMA, ASCE, ACI) provide factors to reduce stiffness to account for the effects of cracking in the analyses and design. However, the basis for these stiffness reduction factors or stiffness expressions is not clearly presented in these standards and their applicability to nuclear plant elements could not be assessed (NUREG/CR 6926). The ASCE Standard 4-98 indicates that care should be exercised in modeling the stiffness of reinforced concrete elements depending on the level of stress and critical seismic load combinations in safety-related nuclear structures. Assumptions in stiffness can have a profound effect in the frequency of the system, could affect greatly the design seismic loads, and has an impact in the evaluation of RC elements or walls in NPPs for different performance objectives. The Nuclear Energy Agency (NEA) Committee on the Safety of Nuclear Installations (CSNI) has pointed out (NEA-CSNI 2003) that for the evaluation of NPPs at different performance limit states, a better understanding and prediction of the actual structural response is needed. In this regard, it is important to have a robust modeling scheme capable to capture initial stiffness and its changes as cracking occurs in the element in special for squat RC walls. Prediction of the seismic response and proper capturing of the effective stiffness for squat walls is a challenging task since these walls exhibits a shear dominated behavior with strong coupling between shear and flexure responses. In addition, this type of walls can present significant shear sliding as cycles of inelastic excursions occur. While significant research has been performed during the past years to address this situation, more research is still necessary to improve current modeling approaches for the seismic analysis of squat RC walls and to produce better equations to obtain the effective stiffness that can be used in the design office environment.

The research to be performed around this topic will be focused on the evaluation of the available expressions for the calculation of effective stiffness and reduction factors for RC squat walls since these are one of the most important structural elements encountered in nuclear facilities. In addition, several modeling schemes will be evaluated in order to find a robust and capable model to predict the lateral response of these systems that could be used for preliminary assessment and design.

1.3 Research objectives and scope

The research objectives of this thesis are twofold: (1) to provide better tools for lateral stiffness calculation to be used in the design of squat RC walls and (2) to provide a modeling approach capable of capturing accurately the lateral response of these structural systems to be used for the seismic assessment and more detailed analyses.

The main research objectives of this study can be summarized as follows:

- Evaluation of the available expressions for the calculation of effective stiffness and secant stiffness at peak strength for RC squat walls.
- Evaluation of the most relevant existing nonlinear modeling methodologies for squat RC walls.
- Development of improved equations for the calculation of effective stiffness and secant stiffness at peak strength for RC squat walls based on the results obtained from the analytical studies and multi-variable linear regressions.
- Provide recommendations about appropriate modeling conditions and parameters for lateral analysis of RC squat walls.

1.4 Literature review

1.4.1 Previous research on effective stiffness

1.4.1.1 Fenwick and Bull (2000)

These authors derived an equation for the calculation of the effective stiffness of slender walls (walls with aspect ratio higher than 3.0), whose behavior is dominated by flexure and standard flexural theory could be applied. In this research the deformation associated with shear and diagonal cracking were not considered. The reinforcement varied from 0.0025 to 0.0125 and axial loads varied from 0 to $0.2A_g f'c$, in all cases longitudinal reinforcement was placed uniformly along the walls. The authors analyzed 68 rectangular reinforced concrete walls assessing the influence of concrete strength, reinforcement grade and axial loading stiffness. The following expression (Eq. 1) was found for this type of walls:

$$I_e = 0.267\left(1 + 4.4\frac{P_u}{f_c' A_g}\right)\left(0.62 + \frac{190}{f_y}\right)(0.76 + 0.005 f_c')I_g \qquad (1)$$

where I_e is the effective moment of inertia (mm^4), f'_c is the concrete compressive strength (MPa), P_u is the factored axial force (N), I_g is the gross moment of inertia of the concrete section about centroidal axis (mm^4), A_g is the gross area of the concrete section (mm^2) and f_y yield strength of longitudinal reinforcement. According to the authors, this expression is valid for concrete with moderate creep and low shrinkage characteristics and could not be used for walls dominated by shear behavior.

1.4.1.2 Paulay and Priestley (1992)

Paulay and Priestley (1992) proposed an equation (Eq. 2) for the calculation of the equivalent moment of inertia of the wall taking into account the first yield in the extreme fiber in the wall. Equation (2) depends on the moment of inertia of the uncracked gross concrete section (I_g), the yield strength of longitudinal reinforcement (f_y) and the axial load ratio ($Pu/f'cA_g$). This equation could be used to calculate the effective stiffness for flexural walls.

$$I_e = \left(\frac{100}{f_y} + \frac{P_u}{f_c' A_g}\right) I_g \tag{2}$$

Paulay and Priestley (1992) presented two more equations (3 and 4) to consider flexure and shear deformation contribution to the stiffness for cantilever walls with aspect ratio less than 4.0.

$$I_w = \frac{I_e}{1.2 + F} \tag{3}$$

$$F = \frac{30 I_e}{{}_w^2 b_w I_w} \tag{4}$$

where h_w is the wall height, b_w is the wall thickness and l_w is the wall length. This equation does not have a lower bound of aspect ratio to determine when the wall fails by shear and not by flexure contribution.

1.4.1.3 Li and Xiang (2011)

These authors proposed an analytical approach for the calculation of the effective stiffness of RC squat walls considering the deformation by flexural and shear actions and derived the Equation (5). The test results of 29 experimental squat wall specimens were compared with the analytical proposed stiffness equation (Eq. 5) showing good agreement with the experimental results. All specimens had common characteristics: aspect ratio less than 2.0, isolated walls and symmetrical wall cross section.

$$\frac{I_e}{I_g} = 0.19\left(\frac{100}{f_y} + \frac{N}{f_c' A_g}\right)\left(0.53 + 0.37\frac{{}_w}{L_w} + 0.31\frac{{}_w^2}{L_w^2}\right) \tag{5}$$

The authors investigated the effect of varying different parameters performing a total of 180 combinations. In these equations, f_y is the yield strength of longitudinal reinforcement in wall boundaries (MPa), f'_c is the concrete compressive strength (MPa), A_g is the gross area of the concrete section (mm^2), ρ_b is the reinforcement ratio in the wall boundaries, $N/f'cA_g$ is the axial

load ratio and the aspect ratio h_w/l_w (h_w is the height of the wall and l_w is the length). According to this research, the increase of aspect ratio, axial load and the longitudinal reinforcement content in wall boundaries with the same reinforcement detailing also increases the stiffness ratio (I_e/I_g) for squat walls. The stiffness ratio of the walls decreases if the yield strength of the outermost longitudinal bars increases depending on the axial load level and wall aspect ratio. The equation proposed by the authors, gives an approach to calculate the effective stiffness of RC squat walls which shows a good agreement compared with the experimental results.

1.4.1.4 Codes ACI 318-14, ASCE 43-05, ASCE 41-13 and FEMA 356.

The American Concrete Institute (ACI 318, 2014), recommends the use of factors to reduce the gross moment of inertia for cracked and uncracked walls. For the calculation of the effective stiffness of the wall, ACI 318-14 considers a gross section of 1.0 Ag and factors 0.7 Ig and 0.35 Ig for uncracked and cracked walls, respectively.

As an alternative and for refined values, ACI 318-14 recommends the use of Equation (6) to calculate the effective moment of inertia for walls. This equation depends on the axial load (P_u) and moment (M_u) that shall be calculated from the load combination under consideration. The code also recommends the minimum and maximum moment of inertia as $0.35I_g$ and $0.875\ I_g$, respectively. The problem with this equation is that the code does not specifies the wall type that covers the equation (flexural or shear controlled).

$$I_e = \left(0.8 + 25\frac{A_{st}}{A_g}\right)\left(1 \quad \frac{M_u}{P_u} \quad 0.5\frac{P_u}{P_o}\right) I_g \tag{6}$$

In this equation A_{st}, is the total area of longitudinal reinforcement (in^2), A_g is the gross area of the concrete section (in^2), I_g is the gross moment of inertia of the concrete section about centroidal axis, neglecting reinforcement (in^4), M_u is the factored moment at section (in.-lb), P_o is the nominal axial strength at zero eccentricity (lb), P_u is the factored axial force to be taken as positive for compression and negative for tension (lb) and h is the overall thickness, height, or depth of member (in).

ASCE 43-05 and ASCE 41-13 standards also recommend factors for the reduction of the flexural and shear rigidities for cracked and uncracked walls to estimate the effective stiffness. For cracked walls, ASCE 43-05 recommends a reduction of 50% in the flexural and shear rigidities and no reduction in the flexural and shear rigidities for uncracked walls. ASCE 41-13 has no recommendation about uncracked walls and for cracked walls recommends a reduction in 50% in the flexural rigidity and no reduction in the shear rigidity.

FEMA 356 recommends 80% in reduction for flexural rigidities for uncracked walls, 50% in flexural rigidities for cracked walls and no reduction for shear rigidities for uncracked and cracked walls.

1.4.1.5 Adebar et al. (2007)

In this research, the authors tested a large-scale model of a slender (height to length ratio of 7.2) reinforced concrete shear wall from the core of a high rise building and developed simple expressions to estimate the upper and lower bound effective flexural moment of inertia of RC walls based on the level of axial load compression. The test results were used to calibrate a simple nonlinear flexural model for high rise concrete walls resulting in the following expression for effective moment of inertia (Equation 7):

$$I_e = I_{cr} + \left[3\left(\frac{M_l}{M_n}\right)^{a} \quad 2\left(\frac{M_l}{M_n}\right)^{1.6a}\right]\left(I_g \quad I_{cr}\right) \leq I_g \tag{7}$$

where $a = 1.1\left(\frac{I_{cr}}{I_g}\right) \quad 0.4$, M_l is the intersection bending moment of first and second linear segments in a trilinear moment curvature diagram. M_n is the flexural capacity of section.

These authors examined different walls and observed that the most important parameter was the axial compression applied at the wall base, resulting in the following simplified expressions that give reasonable estimates of upper and lower bound effective moment of inertia of RC walls:

$$I_e = \left(0.6 + \frac{P}{f_c' A_g}\right) I_g \leq I_g \tag{8}$$

$$I_e = \left(0.2 + 2.5\frac{P}{f_c' A_g}\right) I_g \leq 0.7 I_g \tag{9}$$

According to this research the authors found the following: a) despite the combination of significant axial compression and low percentage of vertical reinforcement, when lateral force is removed the horizontal cracks get closed and residual lateral displacements are small, b) the stiffness of the wall was not affected after the wall has being reloaded and severely cracked and observed that the initial stiffness was similar to uncracked stiffness of the wall, c) the failure mode for this wall was buckling due to an unsupported vertical reinforcing bar, d) the authors calibrate a nonlinear flexural model for high rise concrete shear wall whose prediction compares well for upper and lower bound effective stiffness.

1.4.1.6 Tran (2012)

The author derived an equation for the calculation of the flexural stiffness based on test results for a cantilever wall for moderate aspect ratio walls:

$$F = k_f \quad {}_f \tag{10}$$

$$k_f = \frac{3E_c I_{eff}}{{}^3_w} \tag{11}$$

Therefore, the secant flexural stiffness normalized by the concrete gross section flexural stiffness is determined as (Equation 12):

$$\frac{I_{eff}}{I_g} = \frac{E_c I_{eff}}{E_c I_g} = \frac{k_f \quad {}^3_w}{3E_c I_g} = \frac{{}^3_w}{3E_c I_g}\left(\frac{F}{{}_f}\right) \tag{12}$$

where F is the lateral load, Δ_f is the flexural displacement at the top of the wall, E_c is the Young's modulus and h_w is the height of the wall.

This author found that flexural stiffness values when anchorage slip and extension deformation are included for uncracked and cracked walls are approximately $0.65E_cI_g$ and $0.30E_cI_g$, respectively. However, when slip and extension deformation are included the flexural stiffness values are 0.85 E_cI_g and $0.40E_cI_g$, respectively. These values according to the author are modestly lower than the values recommended by ASCE 41-06 (2007) and FEMA 356 (2000) standards.

This author also derived the secant shear stiffness of walls normalized by E_cA_w from the test results using the Equation (13).

$$\frac{GA_{eff}}{E_cA_w} = \frac{F/\gamma_s}{E_cA_w} = \frac{w}{E_cA_w}\left(\frac{F}{s}\right) \tag{13}$$

According to the Equation (13), Tran (2012) found that the secant shear stiffness for uncracked walls is approximately $0.2E_cA_w$ which is half of the value recommended by ASCE 41 and FEMA 356. For cracked walls the shear stiffness is about $0.1E_cA_w$ which is much lower of the values by ASCE 41 and FEMA 356.

1.4.1.7 Luna (2015)

This author recommends new reduction factors for E_cI_g and G_cA_g to calculate the initial stiffness according to the results of 12 RC walls tests. This stiffness was calculated from the first cycle of the first load step, which involved a force less than 15% of peak strength and a drift less than 0.025%.

E_cI_g is the flexural stiffness and G_cA_g is the shear stiffness. In this research, it was determined that the effective flexural stiffness of $0.5E_cI_g$ proposed by ASCE 43-05 and ASCE 41-13 can be used for the calculation of initial stiffness of cracked walls. However, ASCE 43-05 and ASCE 41-13 overestimate the shear stiffness of cracked RC walls. According to the author, the effective flexural and shear stiffness can be calculated as 0.5 EcI_g and $0.35G_cA_g$., respectively. These values are reasonable for forces up to 40% of the peak strength and drifts of up to 0.1%.

In summary, most of the equations for the calculation of the effective stiffness or reduction factors proposed in the literature has been calibrated or tested for RC walls with flexural dominated behavior. Li and Xiang (2011) and Luna (2015) are the authors that directly had proposed expressions or factors for the effective stiffness calculation of RC squat walls (aspect ratios less than 2.0).

1.4.2 Finite Element Simulations and Models for RC shear walls

1.4.2.1 Model proposed by Kolozvari et al (2014)

The authors of this research proposed an analytical model that couples the wall flexural and shear responses under cyclic loadings. (Figure. 3) In this study, the Multiple-vertical-line-element-model (MVLEM) implemented by Orakcal et al. (2004) was chosen as baseline in the implementation of the new cyclic Shear-flexure interaction (SFI) model. The shear behavior was modeled using a horizontal spring placed at the height *ch*. The value of c is recommended to be 0.4 (Vulcano et al. 1988, Orakcal and Wallace 2006). In this model, each microfiber from the original formulation of MVLEM was replaced with a RC panel element subjected to membrane action. The behavior of this panel is described by the constitutive relationship based on the fixed-strut-angle-model (FSAM) developed by Ulugtekin (2010) and modified by implementing shear aggregate interlock (Orakcal et al., 2012) and dowel action of the reinforcement.

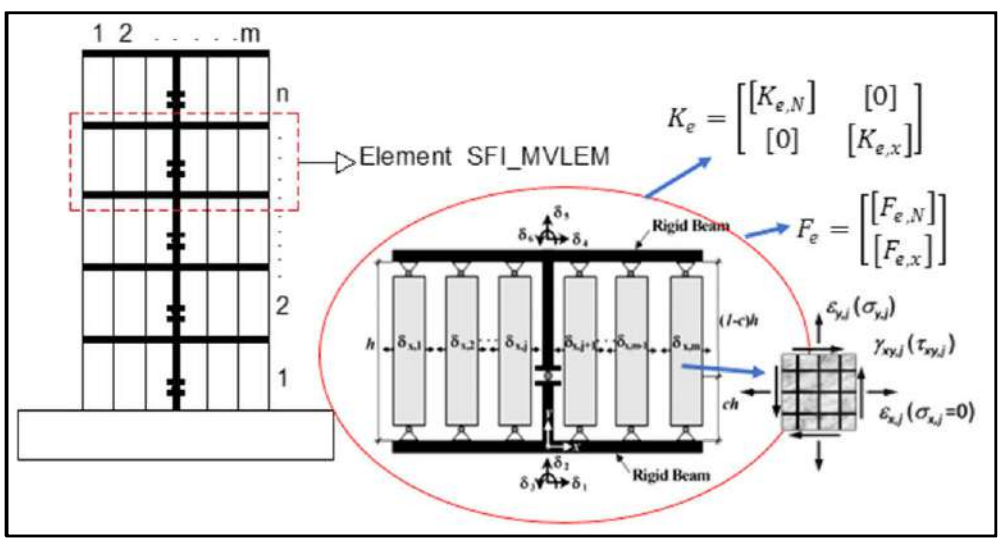

Figure 3. (a) SFI-MVLEM element (modified from Kolozvari et al. 2012)

As shown in Figure 3, the model SFI-MVLEM has six external degrees of freedom denoted as $\{\delta_N\}=\{\delta_1\ \delta_2\ \delta_3\ \delta_4\ \delta_5\ \delta_6\}$ that represent the vertical displacements, horizontal displacements and rotation at the top and bottom of each element. The deformation of each component at these degrees of freedom are used for the calculation of shear ($\gamma_{xy,j}$) and normal ($\varepsilon_{y,j}$) strains for each RC panel element based on the plane section kinematic assumption. The shear stresses are assumed to vary uniformly along the wall cross section. The normal horizontal strain ($\varepsilon_{x,j}$) component on each RC panel is defined by the use of additional (internal) deformation degrees of freedom defined in the horizontal direction $\{\delta_x\}=\{\delta_{x,1}\ \delta_{x,2}\ \delta_{x,3}\ \ldots..\ \delta_{x,m}\}$ that depend on the number of panel macrofibers (m) for each element as shown in Figure. 3. These internal deformation degrees of freedom are assumed kinematically independent from the external degrees of freedom (δ_N). Therefore, according to Kolozvari et al. (2014) the total number degrees of freedom necessary for one SFI-MVLEM element is the sum of external and internal degrees of freedom $\{\delta\}=\{\delta_N\ \ \delta_x\}^T$.

A model of a structural wall consists of n, 2D, SFI-MVLEM with "m" macrofibers connected at the top and bottom with two rigid beams (Figure.3). The rigid beam represents a body constrain between top and bottom wall nodes. A stiffness matrix is assembled for each element from element stiffness sub-matrices $[K_e]_N$ and $[K_e]_x$, since the deformations at six external degrees of freedom and deformations at internal degrees of freedom are kinematically independent.

Strains and stress in the RC panel are calculated following several cracking stages. The formulation of the RC panel SFI-MVLEM has three characteristics under cyclic loading depending on the rotating angle: 1-uncracked concrete, 2- behavior after the first crack, and 3- behavior after the formation of the second crack. The first crack is formed when the value of the principal tensile strain in concrete exceeds a specified cracking strain value. The second crack is formed when the strain along the first crack strut direction exceeds the cracking strain, the second crack will develop perpendicular to the direction of the first crack as shown in Figure. 4.

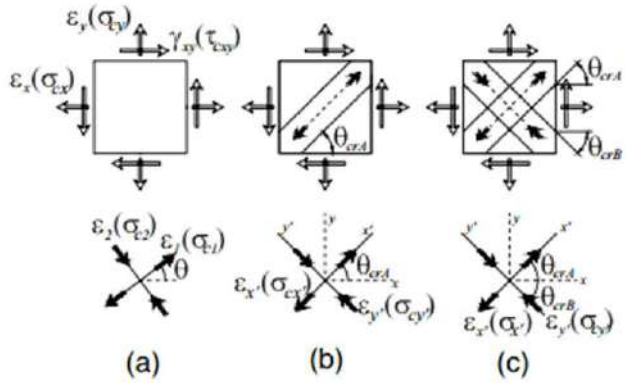

Figure 4. Concrete biaxial behavior in the FSAM: (a) uncracked behavior, (b) behavior after formation of first crack, (c) behavior after formation of second crack. (from Kolozvari et al. 2012)

The constitutive model stress-strain relationship for the reinforcing steel used in this model is the one proposed by Menegoto and Pinto (1973), and later modified by Filippou et al. (1983) to include isotropic strain hardening effects. The constitutive material model used to simulate the uniaxial hysteretic concrete behavior along the fixed struts was the proposed by Chang and Mander (1994) modified to represent the effects of biaxial loading in the concrete behavior. Additional details can be found in Kolozvari et al. (2014).

1.4.2.2 Model proposed by Thomson and Flores-López (2004)

The authors of this research proposed a simplified model for the simulation of damage in RC squat walls under monotonic and cyclic lateral loads. The model was first developed for monotonic loading. Later a yield function was proposed in conjunction with a crack resistance function which is based on the use of the Griffith criterion of fracture mechanics for cyclic loading. The model allows the representation of the following effects:

- Stiffness and strength degradation mainly due to diagonal cracking of concrete.
- Plastic deformations due to yield of the horizontal reinforcement.
- Sliding shear across diagonal cracks (pinching effect).
- Unilateral behavior.

The general matrix that describe the behavior of a frame in terms of stresses and deformations are related by:

$$\{\Phi\} = [F_O]\{M\} \tag{14}$$

where [Fo] is the flexibility matrix represented as the sum of the matrices due to axial forces [F^ao], flexure [F^fo] and shear effects [F^so]. {M} and { Φ} correspond to stresses and deformations respectively.

$$[F_O] = [F_O^a] + \left[F_O^f\right] + [F_O^s] \tag{15}$$

The model includes damage mechanics and plastic deformations but only into the shear flexibility matrix. There is no permanent elongation related to axial and flexural deformation, according to this assumption there is no yielding of the longitudinal reinforcement. However, deformations due to yielding of transverse reinforcement are taken into consideration. The shear damage variable (d_s) was included in the flexibility matrix. A value of d_s =0 indicates that there is no concrete cracking, and a value of d_s=1 indicates that the wall cracked and has no shear stiffness.

For a wall whose failure is dominated by shear, the authors determined an equation for computing the damage using the following equation (Eq. 16), in which G is the shear modulus, Av is the effective shear area, I is the moment of inertia, L is the length of the member, E is the elastic modulus, H is the height of the element, L is the length of the element and Z represents the slope of the elastic unloading.

$$d_s = 1 \quad \frac{1}{GA_vL}\left(\frac{1}{\frac{1}{Z} \quad \frac{H}{3EI}}\right) \tag{16}$$

For this model, Thomson and Flores-López (2004) defined the state law for hysteresis action as (Eq 17):

$$\{\Phi \quad \Phi^P\} = [F(d_s^+)]\{\ M\ _+\} + [F(d_s^-)\{\ M\ \}] \tag{17}$$

In a hysteretic model, the damage is defined according to the direction of the load. Figure 5 shows the definition of positive and negative loading directions in the model.

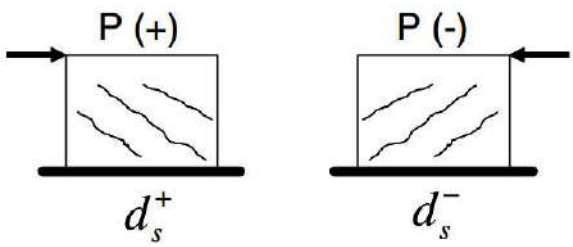

Figure 5. Representation of positive and negative damage.(from (Thomson and Flórez-lópez 2004))

In this model, the pinching effect is considered consequence of the sliding in the interface between two different elements (Figure. 6). if it is subjected to a normal stress and a shear stress characterized by the Coulomb friction criterion in which the relative horizontal displacement obeys the law described by Equations (18).

$$\begin{cases} > 0 \; if \; |\tau| & \tau_s(\sigma) = 0 \\ = 0 \; if \; |\tau| & \tau_s(\sigma) < 0 \end{cases} \tag{18}$$

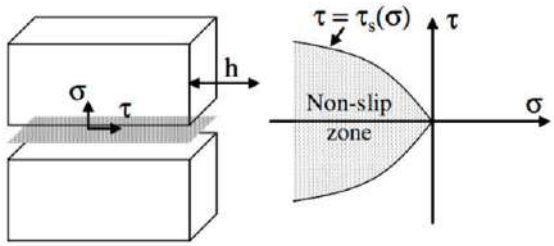

Figure 6. a) Interface between two media b) Non-slip domain.
(from Thomson and Flórez-López 2004)

To consider the process of slip across a shear crack a generalization of the concept of Coulomb friction plasticity was used introducing the Equation (19) to describe the behavior of an inelastic shear wall with slip:

$$f_s = |V| \quad k_s \tag{19}$$

In this equation, the value k_s corresponds to a hardening function proposed as:

$$k_s = V_{0.} e^{sign(V).\gamma.\phi_s^p} \tag{20}$$

The term V_o is the shear force that produces sliding when no plastic rotation has occurred yet.

The term γ for positive action (ds^+) is defined as:

$$\gamma = \frac{(1 \quad d_s^+)}{2} \frac{\ln(\frac{2GA_v R(R_s^+)}{LV_0^2}}{\sqrt{\frac{2GA_v(1 \quad d_s^+)^2 R(d_s^+)}{L}} \quad (1 \quad d_s^+)V_y \quad (1 \quad \alpha)(1 \quad d_s^+)c_s p_s} \tag{21}$$

The expression for negative action is obtained substituting ds^- for d_s^+.

1.4.2.3 Simulation model by Epackachil et al. (2015)

These authors developed a finite element model using the commercial program LS-DYNA to simulate the nonlinear cyclic response (Epackachi et al. 2015) of RC shear walls. The models were validated using experimental data from seven shear walls with low aspect ratio ranging from 0.33 to 0.94, the vertical web reinforcement ratios varied from 0.15% to 0.33%, the concrete compressive strength (f′c) ranging from 2.9 ksi to 6.5 ksi, and the length and thickness of the experimental walls were 10 feet and 8 inches, respectively. These walls were tested in the SEESL laboratory at the University of Buffalo as part of an experimental study to investigate their cyclic response.

The RC wall was modeled in LS-DYNA using a smeared crack Winfrith model (MAT085) and a plastic model Mat-Plastic-Kinematic (MAT003) for concrete and the reinforcement, respectively. The wall was modelled using solid elements for the concrete and beam type elements to represent the horizontal and vertical reinforcement.

The effect of shrinkage on the initial stiffness of RC walls was investigated using shrinkage strain. This restrained shrinkage at the base of the wall was considered applying a thermal load over a height (H_t) of the wall above the foundation, and the increment of temperature was calculated as:

$$\Delta T = \frac{\varepsilon_{sh}}{\alpha_c} \tag{22}$$

where α_c is a thermal expansion coefficient for the concrete and ε_{sh} is the ultimate drying shrinkage strain. The impact of shrinkage on the initial stiffness was investigated with different levels of restrained shrinkage. The authors found that the shrinkage strain has a considerable effect on the initial stiffness of RC walls. The larger the shrinkage strain, the smaller the initial stiffness and the restrained shrinkage has no effect on the peak shear strength and post-peak response. Ignoring the shrinkage effect lead to a significant overestimation of the initial stiffness of RC walls. This research concluded with the finite element model that the initial stiffness was better obtained using a shrinkage strain of 1600 macrostrain for the concrete within a height of 16in.

1.5 Research Methodology

The following tasks are proposed to perform the research objectives of this thesis:

- Evaluate the most relevant and common equations for the calculation of lateral stiffness for RC squat walls. Samples of some of these equations were presented previously.
- Compare the stiffness values obtained using the evaluated expressions with the results of experimental data of RC squat wall tests found in the literature. In addition, reduction factors recommended by the codes for the lateral stiffness to account for cracking effects will be evaluated and their applicability for shear-controlled members will be assessed.

- According to the results from the previous tasks, improved equations will be formulated for the calculation of effective and secant stiffness for squat walls. Recommendations for stiffness reduction factors will be put forward.

- Evaluate different walls using a nonlinear modeling approach incorporated into the software Abaqus V2016 to simulate the lateral response of RC squat walls. The goal is to identify the parameters that best fits the backbone curve which describes the hysteretic behavior of walls and that better match the lateral stiffness of these elements in comparison with the experimental results available in literature. RC squat walls with different parameters such as aspect ratio, steel reinforcement, different concrete strength, and axial loads will be considered.

1.6 Organization of the Thesis

This dissertation includes five chapters. Chapter 1 presents the motivation, objectives, scope and methodology of the research conducted as well as a discussion on RC squat walls behavior and available equations for the prediction of the lateral stiffness of RC walls. Chapter 2 describes the finite element model used in this research for the prediction of the lateral response of squat RC walls. This chapter also includes a description of the experimental specimens used for validation of the finite element model. Chapter 3 presents the development of empirical equations for the prediction of effective and secant lateral stiffness of RC squat walls with rectangular cross sections and investigates the performance of widely used equations available in the literature and U.S. standards. In Chapter 4, validations of the empirical equations for the prediction of effective stiffness of RC squat walls with the finite element model developed are discussed. Chapter 5 summarizes the key findings, conclusions, and recommendations for further studies.

CHAPTER II. FINITE ELEMENT MODELING OF RC SQUAT WALLS

2.1 Introduction

Finite element models of several RC squat walls were developed using the commercial software Abaqus (V 2016) and OpenSees. The main objective of the finite element models developed for this research is to appropriately predict the lateral stiffness of these RC squat walls. In addition, these finite models will serve to identify the parameters that have an important influence in the stiffness and lateral response of RC squat walls. The results from the analytical modeling are compared with those from experimental tests available in the literature. First, the specimens selected for the finite element models are described. Second, the generalities and results of the finite elements developed with Abaqus are discussed. Third, the models developed in OpenSees with the results are presented.

2.2 Wall specimens

Seven squat walls with four different aspect ratios were selected to develop the finite element models. These walls correspond to phase I specimens of twelve RC shear walls with low aspect ratio built and tested at NEES facility at University of Buffalo (Rocks 2012). The thickness and length of the test specimens were eight inches (203mm) and ten feet long (3048mm), respectively. The material properties of the walls are summarized in Table 1. The walls are identified as SW1 to SW7 according to their aspect ratio (hw/lw) and vertical/horizontal reinforcing steel quantities (ρv, ρh). The concrete compressive ($f'c$), steel yield stress (fy) and ultimate (fu) strength are shown in this table.

Table 1: Properties of the material of the walls

Wall	Web ρ h (%)	Web ρ v (%)	f 'c MPa(ksi)	fy MPa(ksi)	fu MPa(ksi)	hw/lw
SW1	0.7	0.7	24.8 (3.6)	462 (67)	703 (102)	0.94
SW2	1.0	1.0	48.3 (7.0)	434 (63)	600 (87)	0.54
SW3	0.7	0.7	53.8 (7.8)	434 (63)	600 (87)	0.54
SW4	0.3	0.3	29 (4.2)	462 (67)	703 (102)	0.54
SW5	1.0	1.0	29.6 (4.3)	462 (67)	703 (102)	0.33
SW6	0.7	0.7	26.2 (3.8)	462 (67)	703 (102)	0.33
SW7	0.3	0.3	26.2 (3.8)	462 (67)	703 (102)	0.33

2.3 Modeling in Abaqus

2.3.1 Material and plasticity criteria definition

In the last decades, many constitutive models have been developed for the prediction of the concrete behavior. There are three crack models approaches available in Abaqus to predict the behavior of the concrete: the smeared crack concrete model, concrete damage plasticity (CDP) and the brittle crack concrete model. The material model selected for the concrete in the walls was the CDP due to its higher potential of convergence compared with the smeared crack approach moreover, it has the potential to represent the complete behavior of the concrete in the inelastic range for both tension and compression including damage characteristics.

The concrete damage plasticity model requires the following parameters to define the concrete behavior: uniaxial response in compression, uniaxial response in tension, ratio of initial equibiaxial compressive yield stress to initial uniaxial compressive yield stress (σ_{b0}/σ_{c0}), ratio of the second deviatoric stress invariant on the tensile meridian to that on the compressive meridian (K_c), eccentricity and dilation parameters for the flow potential.

The uniaxial compressive response for unconfined concrete in the absence of reported data is represented by means of the numerical model of Popovics (1973) using the following equations:

$$f_c = f_c' \frac{r(\varepsilon_c/\varepsilon_{c0})}{r \quad 1 + (\varepsilon_c/\varepsilon_{c0})^r} \tag{23}$$

where:

$$r = \frac{E_c}{E_c \quad E_{sec}} \tag{24}$$

$$E_{sec} = \frac{f_c'}{\varepsilon_{c0}} \tag{25}$$

$$E_c = 5000\sqrt{f_c'} \tag{26}$$

where f'_c (MPa) is the compressive strength, ε_{c0} is the strain corresponding to f'_c the concrete compressive strength and E_c (MPa) is the modulus of elasticity of the concrete.

To define the compressive stress-strain relationship for concrete in Abaqus, it is necessary to enter the stress (σ_c), inelastic strain ($\varepsilon^{\sim in}_c$) corresponding to stress values and damage values with inelastic strain in tabular form. To introduce these values into Abaqus, it is necessary to convert the total strain into inelastic strain with the following equation:

$$\varepsilon_c^{\sim in} = \varepsilon_c \quad \varepsilon_{oc}^{el} \tag{27}$$

where, $\varepsilon_{oc}^{el} = \frac{\sigma_c}{E_c}$ is the elastic strain that corresponds to the undamaged material and ε_c is the total compressive strain. Special care must be taken with negative plastic strain compressive values $\varepsilon_c^{\sim pl}$. Decreasing plastic strain compressive values are indicative of incorrect damage curves which may lead to generate an error message before the analysis is performed. The plastic strain is defined by the following equation:

$$\varepsilon_c^{\sim pl} = \varepsilon_c^{\sim in} \quad \frac{d_c}{(1 \quad d_c)} \frac{\sigma_c}{E_c} \tag{28}$$

where d_c is the factor of damage for concrete defined as the ratio between inelastic strain ($\varepsilon_c^{\sim in}$) and ultimate strain (ε_u=0.004) for unconfined concrete. The Figure 7 shows the typical

compressive stress-strain relationship with damage properties and Figure 8 the calculated curves for the seven selected specimens.

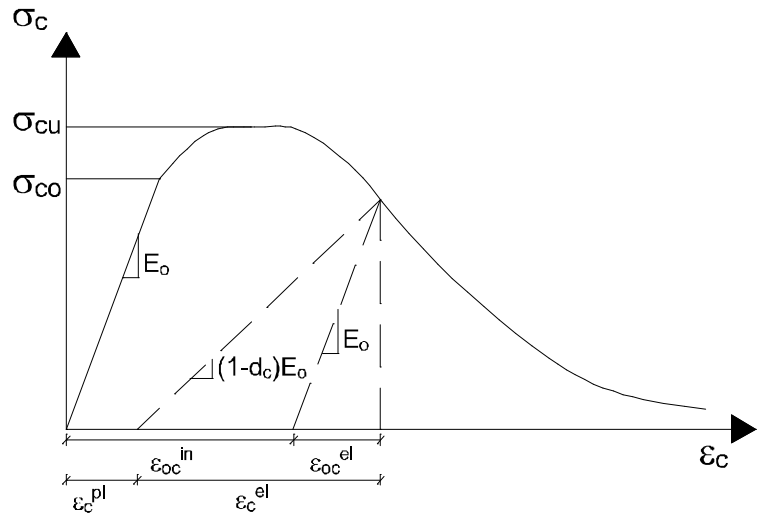

Figure 7. Compressive Stress-Strain Relationship (Abaqus manual -2016)

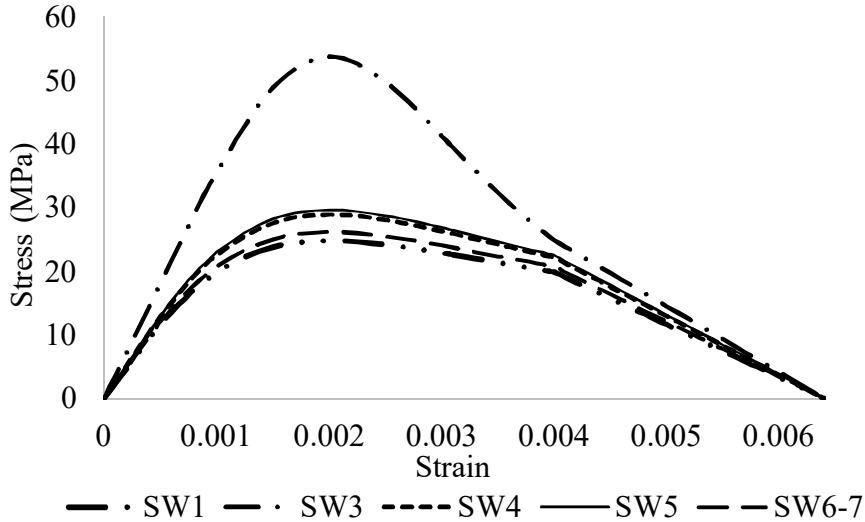

Figure 8. Compressive concrete stress-strain curves for selected specimens

To describe the stress-strain relationship for concrete in tension, the model of Belarbi and Hsu (1994) was used. The following are the equations of the constitutive model:

$$\sigma_t = E_t \varepsilon_t \quad \varepsilon_t \leq \varepsilon_{cr} \tag{29}$$

$$\sigma_t = f_t \left(\frac{\varepsilon_{cr}}{\varepsilon_t}\right)^{0.4} \varepsilon_t > \varepsilon_{cr} \tag{30}$$

where $E_t = 3900\sqrt{f_c'}(MPa)$ is the modulus of elasticity, $f_t = 0.31\sqrt{f_c'}(MPa)$ is the direct tensile strength of concrete and $\varepsilon_{cr} = 0.00008$ is the strain associate to critic tension stress. Figure 9 shows the typical tensile stress-strain relationship with damage properties. Figure 10 presents the calculated curves for the selected specimens.

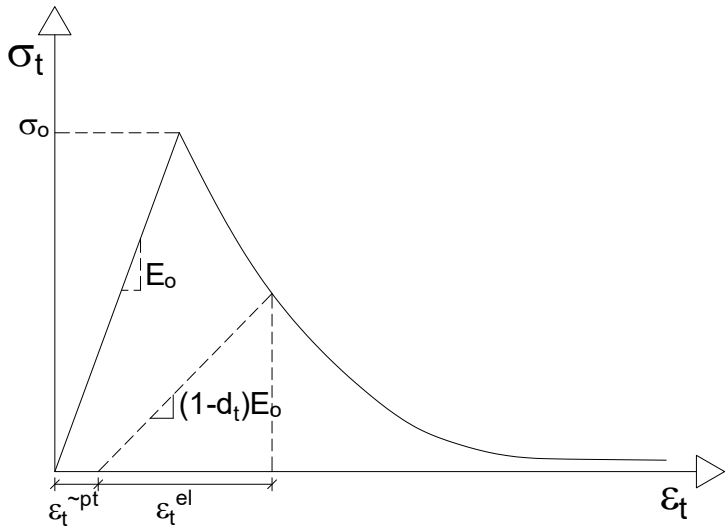

Figure 9. Parameters for Tensile Stress-Strain Relationship (Abaqus manual)

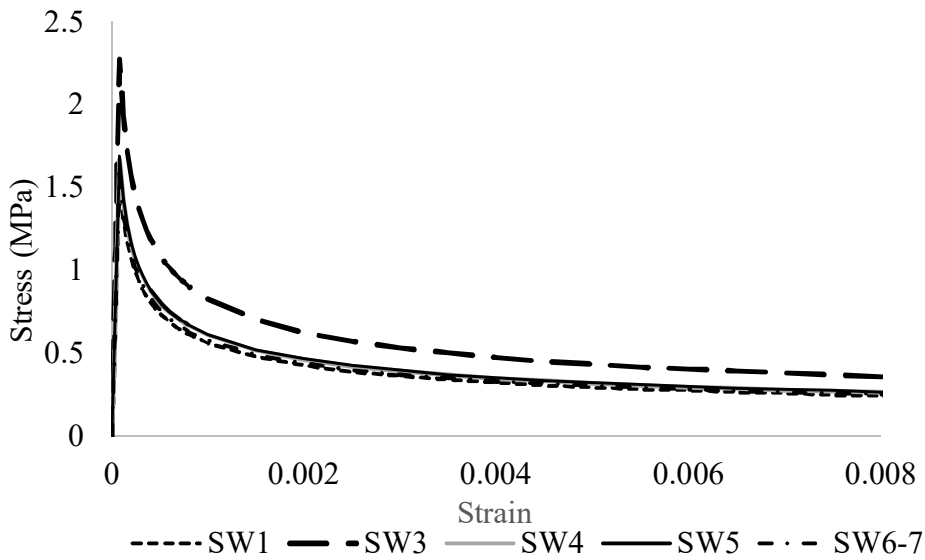

Figure 10. Calculated tensile concrete stress-strain for all specimens

To develop this model in Abaqus it is required the Young's modulus, the tension stress (σ_t), the cracking strain values ($\varepsilon_t^{\sim ck}$), and the damage parameter (d_t) defined as the ratio between . The cracking strain is calculated from the total strain according the next equation:

$$\varepsilon_t^{\sim ck} = \varepsilon_t \quad \varepsilon_{ot}^{el} \tag{31}$$

where $\varepsilon_{ot}^{el} = \frac{\sigma_t}{E_o}$ is the elastic strain corresponding to the undamaged material and ε_t is the total tensile strain. Special care must be taken with the negative plastic tensile strain values $\varepsilon_t^{\sim pl}$. Decreasing plastic tensile strain values are indicative of incorrect damage curves which may lead to generate error message before the analysis is performed. The plastic tensile strain is calculated as:

$$\varepsilon_t^{\sim pl} = \varepsilon_t^{\sim in} \quad \frac{d_t}{(1 \quad d_t)} \frac{\sigma_t}{E_o} \tag{32}$$

The parameters required to define the yield function for the CDP model already mentioned are taken as follows: the compressive yield stress ratio (σ_{b0}/ σ_{c0}) ranges between 1.10 and 1.16 (Lubliner et al., 1989), where σ_{b0} is the initial equibiaxial compressive yield stress and is obtained

from a biaxial concrete test (Figure. 11) and σ_{c0} is the uniaxial compressive yield stress (Figure. 7). The value adopted for the analysis was 1.16.

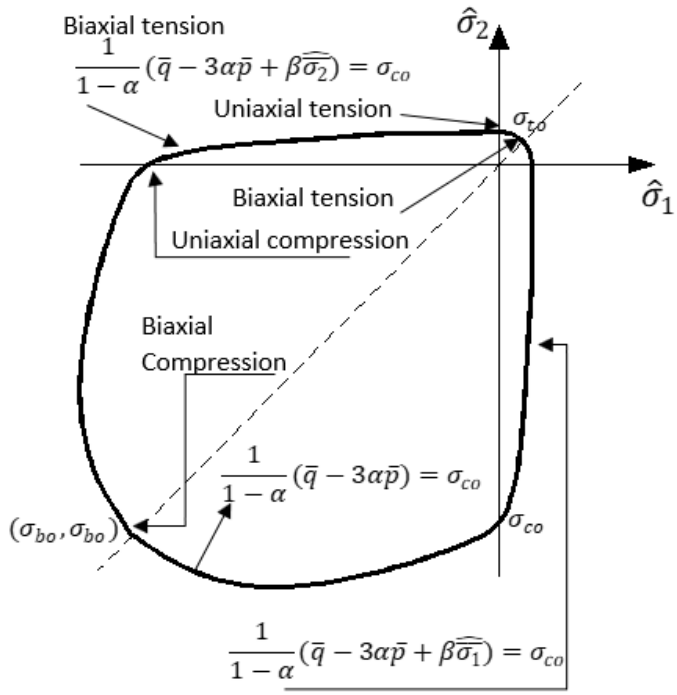

Figure 11. Yield surface in plane stress. (Abaqus, 2016)

The parameter K_c is the ratio of the second stress invariant on the tensile meridian to compressive meridian at initial yield. The values should be into the range $0.5 < K_c \leq 1.0$. Some researches recommend values that varied from 0.64 (Schickert and Winkler, 1977) and 0.66 (Richart et al., 1982) to 0.8 (Mills and Zimmerman, 1970). A typical value use for concrete is 0.67 (Figure. 12). The flow potential eccentricity parameter (ε) is a small positive number that defines the rate at which the hyperbolic flow potential approaches its asymptote. A value of $\varepsilon = 0.1$ is used for the analysis because according to Gulec and Whittaker (2009) it enables a near constant value of the dilatation angle over a wide range of confinement stress. The viscosity parameter (μ) is used for the visco-plastic regularization of the concrete constitutive equations in Abaqus/Standard analyses. This parameter is ignored in Abaqus/Explicit. The default value is 0.0 (Abaqus, 2016).

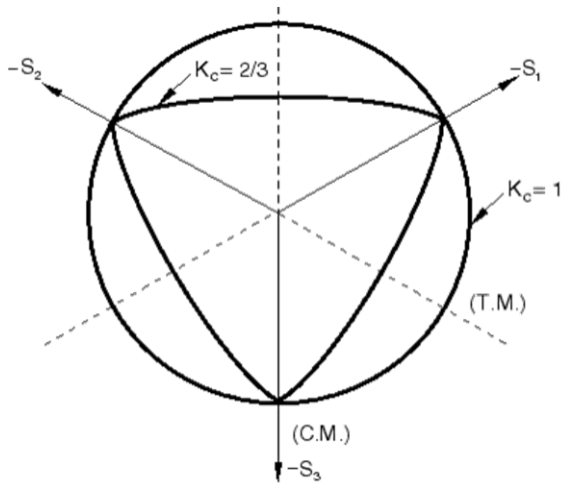

Figure 12.Yield surfaces in the deviatoric plane, corresponding to different values of Kc (Abaqus, 2016)

The last parameter for the CDP formulation is the angle of dilation which controls an amount of plastic volumetric strain developed during plastic shear and is assumed constant during plastic yielding. A value of $\psi = 0$ means that the volume preserves its deformation while in shear (Figure. 13). This parameter can be calculated from the Mohr's circle of strain or the triaxial test. Since there is not recommended value for the dilation angle and it is a critical parameter in the CDP formulation because it determines the direction of the plastic flow, this parameter will be calibrated by parametric studies of the models.

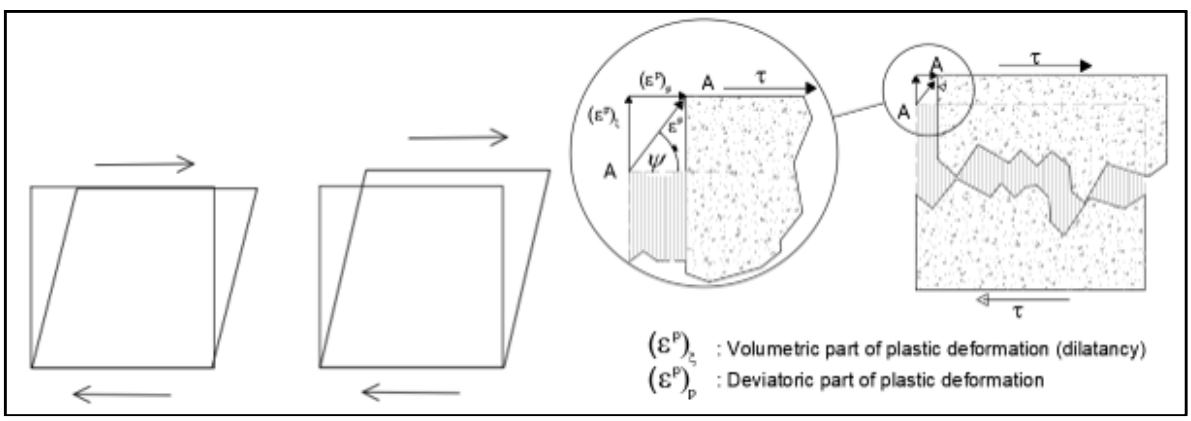

a) No dilatancy ψ=0 b) Dilatancy during shear c) Dilation angle scheme

Figure 13. Interpretation of the dilation angle

All these parameters defined before are used in the model for the definition of Plastic flow and Yield function. The flow potential G used for the CDP is the Drucker-Prager hyperbolic function given by Equation 33.

$$G = \sqrt{(\epsilon\sigma_{t0}\tan\psi)^2 + q^2} \quad p\tan\psi \tag{33}$$

In this equation, ψ is the dilation angle measured in the p-q plane at high confining pressure, σ_{t0} is the uniaxial tensile stress at failure, and ϵ is the eccentricity parameter that defines the rate at which the function approaches the asymptote (the flow potential tends to a straight line as the eccentricity goes to zero).

The CDP model uses the yield function of Lubliner et al. (1989), with the modifications proposed by Lee and Fenves (1998) to account for the different evolution of strength under tension and compression. The evolution of the yield surface is controlled by the hardening variables, ε_t^{pl} and ε_c^{pl}. In terms of effective stresses, the yield function is given by Equation 34.

$$F = \frac{1}{1 \quad \alpha}(\bar{q} \quad 3\alpha\bar{p} + \beta(\varepsilon^{pl})\ \hat{\bar{\sigma}}_{max} \quad \gamma \quad \hat{\bar{\sigma}}_{max}) \quad \bar{\sigma}_c(\varepsilon^{pl}{}_c) \tag{34}$$

Where

$$\alpha = \frac{(\sigma_{b0}/\sigma_{c0}) \quad 1}{2(\sigma_{b0}/\sigma_{c0}) \quad 1}\ ;\ 0 \le \alpha \le 0.5 \tag{35}$$

$$\beta = \frac{\bar{\sigma}_c(\varepsilon_c^{pl})}{\bar{\sigma}_t(\varepsilon_t^{pl})}(1 \quad \alpha) \quad (1+\alpha) \tag{36}$$

$$\gamma = \frac{3(1 \quad K_c)}{2K_c \quad 1} \tag{37}$$

The uniaxial tensile response of the wall reinforcement is modeled as an elasto-plastic material with isotropic hardening, based on the constitutive model proposed by Chang and Mander (1994). In this model the steel behavior is divided in three parts:

The elastic branch $0 \leq \varepsilon_s \leq \varepsilon_y$

$$f_s = E_s \varepsilon_s, \; E_t = E_s \tag{38}$$

where, $\varepsilon_y = f_y / E_s$, ε_y is the yield strain, f_y is the yield stress, E_s is the modulus of elasticity and the yield plateau is defined between $\varepsilon_y < \varepsilon_s < \varepsilon_{sh}$, $f_s = f_y$, $E_t = 0$, and ε_{sh} is the hardening strain.

The strain hardening branch is defined when $\varepsilon_s \geq \varepsilon_{sh}$.

$$f_s = f_{su} + (f_y \quad f_{su}) \left| \frac{\varepsilon_{su} \quad \varepsilon_s}{\varepsilon_{su} \quad \varepsilon_{sh}} \right|^P \tag{39}$$

$$P = E_{sh} \frac{\varepsilon_{su} \quad \varepsilon_{sh}}{f_{su} \quad f_y} \tag{40}$$

where ε_{su} is the strain at ultimate stress, and f_{su} is the ultimate (maximum) stress.

The two reinforcement parameters that should be defined in Abaqus are: true-stress $f_{tru} = f_s(1 + \varepsilon_s)$ and plastic -strain $\varepsilon_{pl} = \varepsilon_{true} \quad f_{true}/E_s$, where $\varepsilon_{true} = \ln(1 + \varepsilon_s)$ is defined as true strain of the material. Figure 13 shows the reinforcing steel curve obtained for all the studied RC wall specimens.

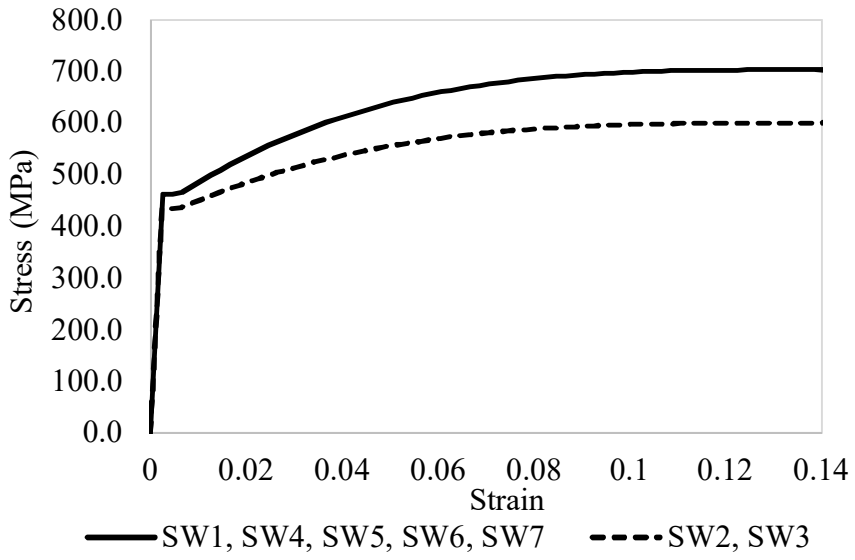

Figure 14. Stress-strain steel reinforcement curve

2.3.2 Three-dimensional model analysis

The analysis was conducted in the software Abaqus using 8-node linear brick, reduced integration with hourglass control (C3D8R) elements, to represent the concrete. This element with reduced integration takes into consideration the shear locking and increases the computational efficiency of the model compared to full integration, using a single integration point scheme instead of eight integration points in the full integration version (Figure. 14). In addition, the element with reduced integration is tolerant of shape distortions, for this reason the shear locking phenomena is not a problem as in the C3D8 element. Shear locking is an error that sometimes occurs in finite element analysis due to the linear nature of quadrilateral elements that do not accurately model the curvature that is present in materials under bending. This generates an additional shear stress that reduces the displacements and makes the element looks stiffer than in the reality.

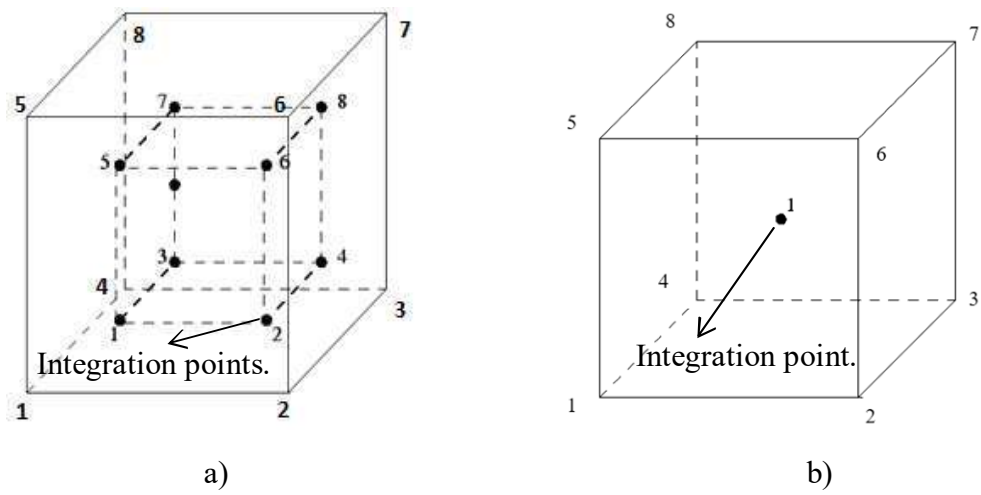

Figure 15. Brick type finite element a) 8-node linear brick C3D8, b) 8-node linear brick, reduced integration with hourglass control (C3D8R)

However, the element exhibits other shortcomings:

- The element tends to be not stiff enough in bending.
- Stresses and strains are most accurate in the integration points. The integration point of the C3D8R element is located in the middle of the element. Thus, small elements are required to capture stress concentrations at the boundary of a structure.
- There are 12 spurious zero energy modes leading to massive hourglassing: this means that the correct solution is superposed by arbitrarily large displacements corresponding to the zero energy modes. In practice, the C3D8R element is not very useful without hourglass control.

The wall reinforcement was modeled using 2-node linear truss elements (T3D2). To connect the concrete to the steel reinforcement an embedded constrain type was used. This type of constrain is used to specify an element or a group of elements that lie embedded in a group of host elements whose response will be used to constrain the translational degrees of freedom of the embedded nodes. Abaqus searches for the geometric relationships between nodes of the embedded elements and the host elements. If a node of an embedded element lies within a host element, the translational degrees of freedom at the node are eliminated and the node becomes an “embedded node.” The translational degrees of freedom of the embedded node are constrained to the interpolated values of the corresponding degrees of freedom of the host element. Embedded

elements are allowed to have rotational degrees of freedom, but these rotations are not constrained by the embedding (Abaqus 2016).

To connect the wall with the foundation a constraint type “tie” was used. This constraint connects two or more parts into the model no matters the type of meshes that are used on each part (wall or basement, Figure. 16).

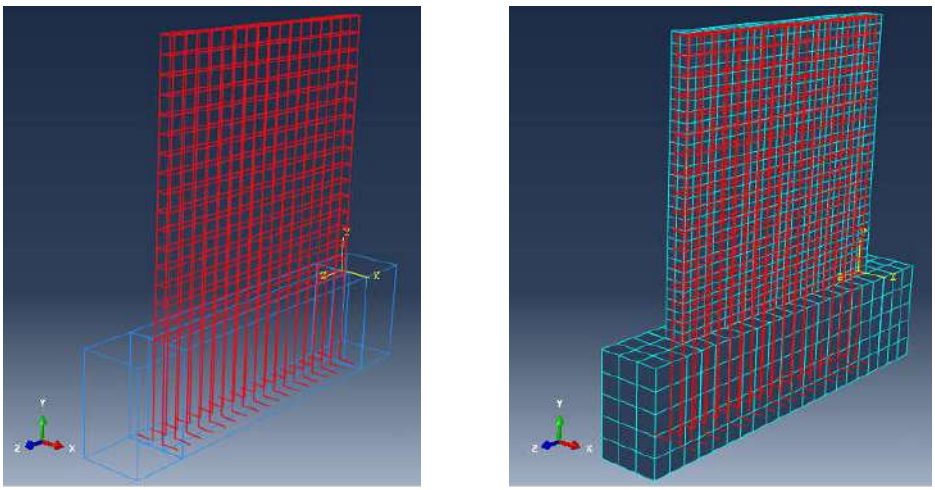

Figure 16. a) Reinforcement of the wall with Truss Elements ; b)Wall with bricks elements and steel reinforcement embedded into the wall.

2.3.2.1 Parametric study of Kc and σb_0/ σc_0

According to Richart et al. (1982) and Lubliner et al. (1989), the parameter K_c and σ_{b0}/ σ_{c0} can take values of 0.67 and 1.0, respectively. A parametric study of how these parameters affect the behavior of squat wall models in a pushover analysis was performed in Abaqus. For the K_c parameter, two extreme values of 0.5 and 1.0 were considered to analyze the wall models. The analyses were also performed varying the parameter σ_{b0}/ σ_{c0} with values 1.1 and 1.16 (Figure. 17). The models used in this analysis were the walls SW1 and SW7 with aspect ratios of 0.94 and 0.33, respectively. Minimal changes in the wall response were obtained with the variation of these parameters.

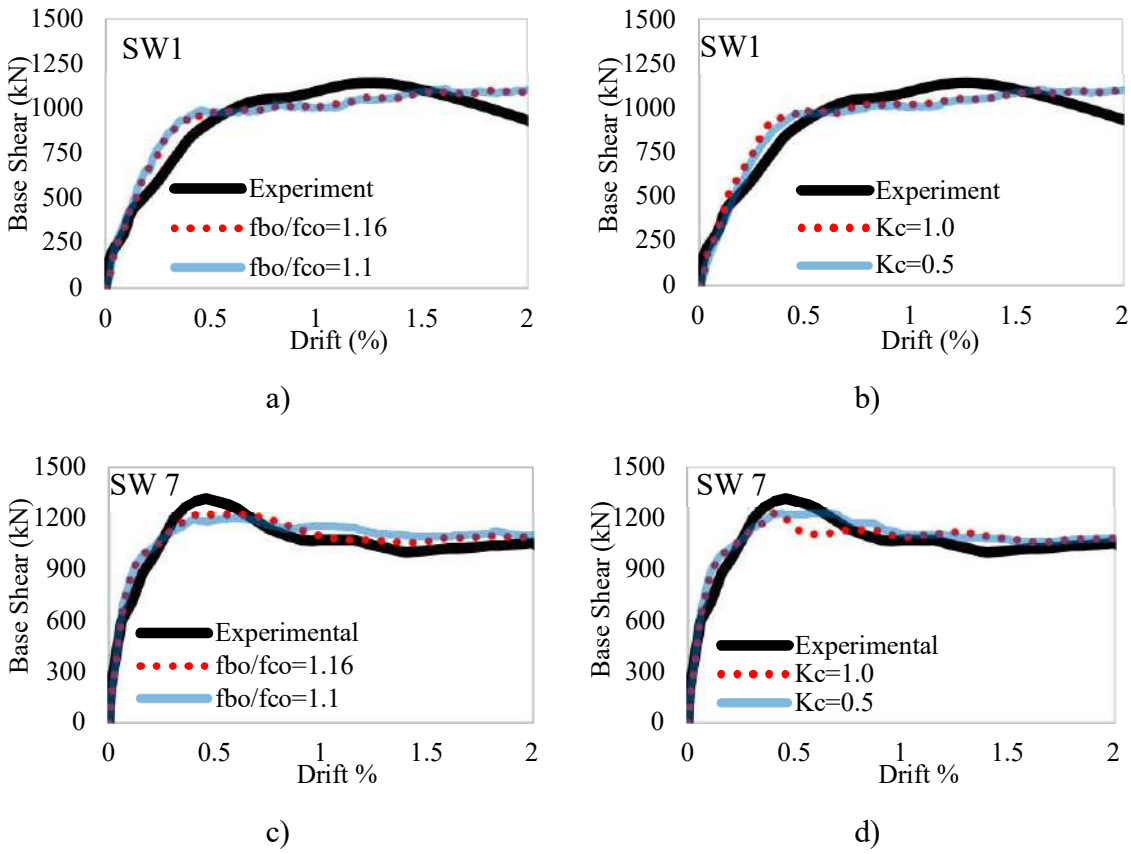

Figure 17. Variation of parameters Kc and σ_{b0}/ σ_{c0}, for walls SW1 and SW7

2.3.2.2 Parametric study of the Dilatation angle (ψ)

For all seven squat walls, it was necessary to determine an appropriate dilation angle (ψ). For this purpose a parametric analysis was conducted for all wall models varying the dilation angles from 35° to 56° (maximum dilation angle 56.31°). The models were subjected to increasing lateral loads (pushover analysis). Figure 17 shows how dilation angle affects the wall shear vs drift response for walls SW1-SW7 for three dilation angle cases (35°, 45° and 56°). As shown in this figure, as the dilation angle increases the results improve when compared with the experimental test values. From these analyses, it was determined that the dilation angle that better predicts the lateral response wall of these squat walls is 56°.

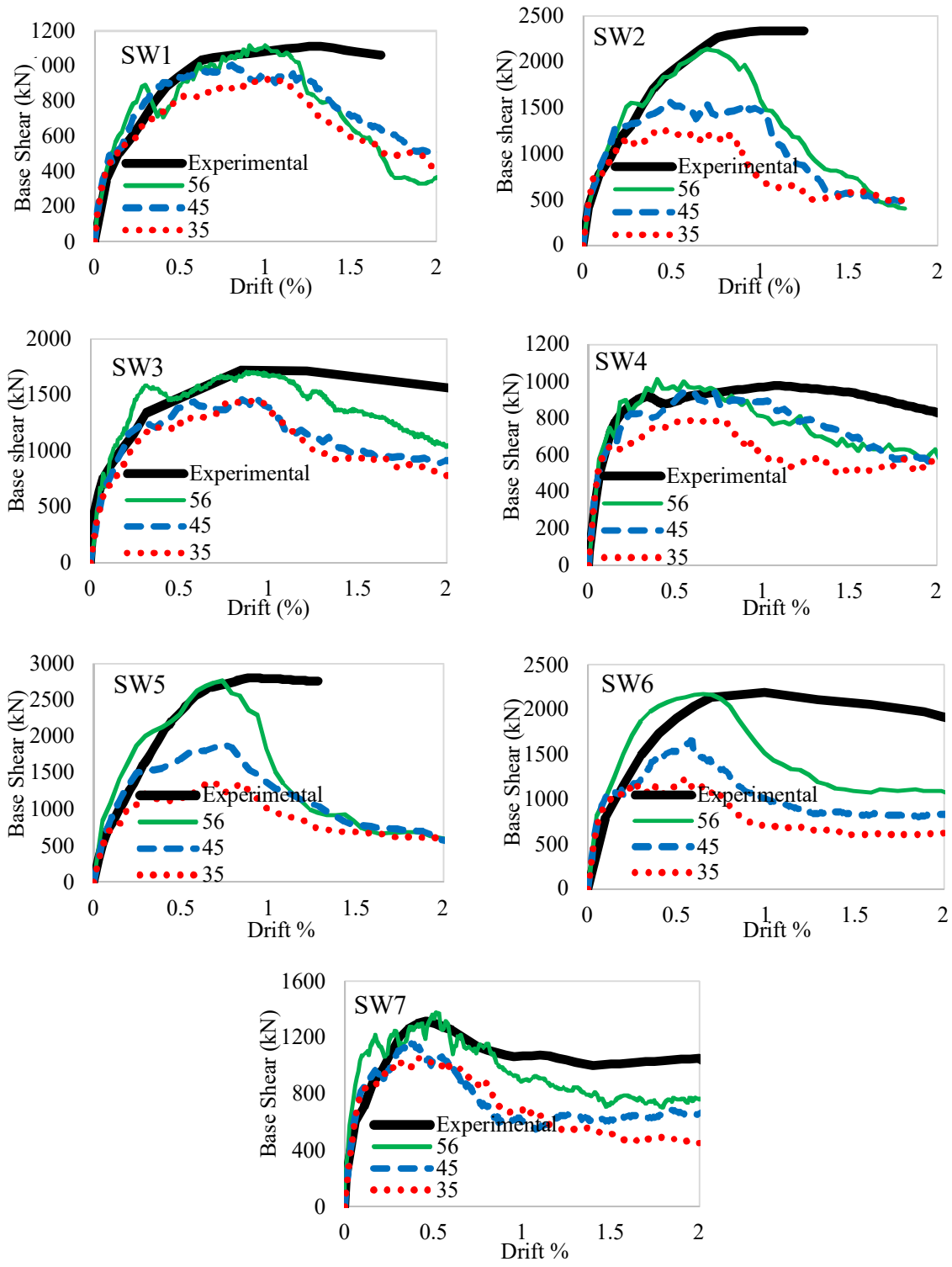

Figure 18. Pushover analysis of shear walls with different Dilation angles

2.3.2.3 Mesh sensitivity analysis for three-dimensional model

A mesh sensitivity analysis was made to the three-dimensional model in Abaqus to determine an appropriate mesh size for the models. The size of meshes used for this analysis were 25x25x25mm, 50x50x50mm, 75x75x75mm and 100x100x100mm corresponding to finite elements in hexahedral form. The mesh size of the wall base is 100x100x100mm, it is not necessary that the base has the same mesh size of the wall because of tie constrain used between the wall and the base. Figures 19 and 20 show the different mesh configurations for the two selected walls. These walls SW1 and SW7 have aspect ratios of 0.94 and 0.33, respectively.

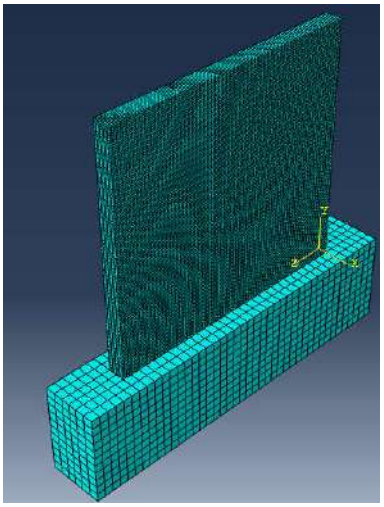

a) Mesh size 25x25x25

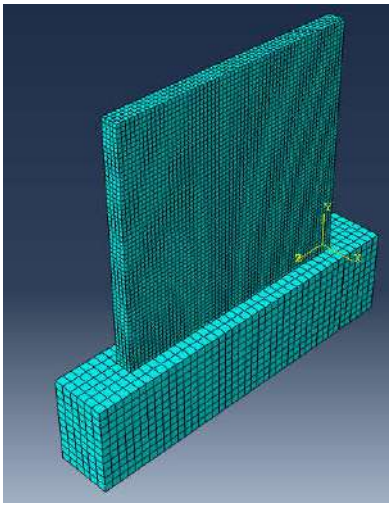

b) Mesh size 50x50x50

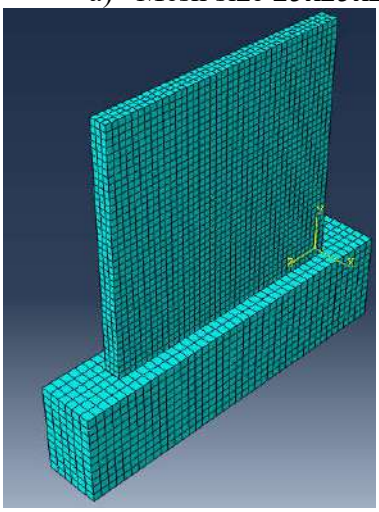

c) Mesh size 75x75x75

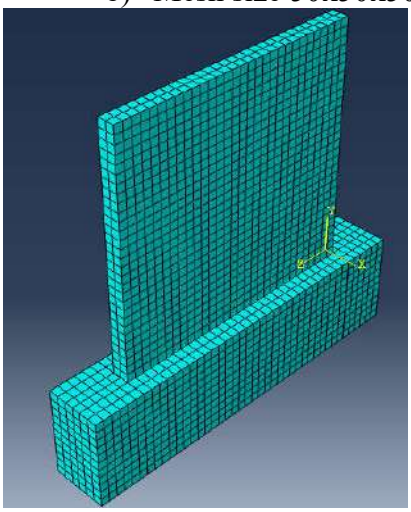

d) Mesh size 100x100x100

Figure 19. Different wall mesh sizes for mesh sensitive analysis (SW1 wall)

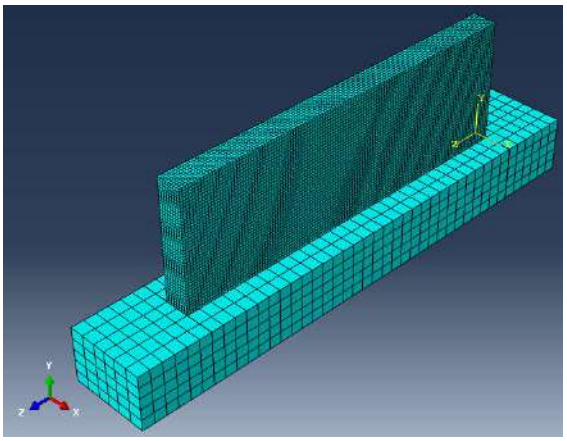

a) Mesh size 25x25x25

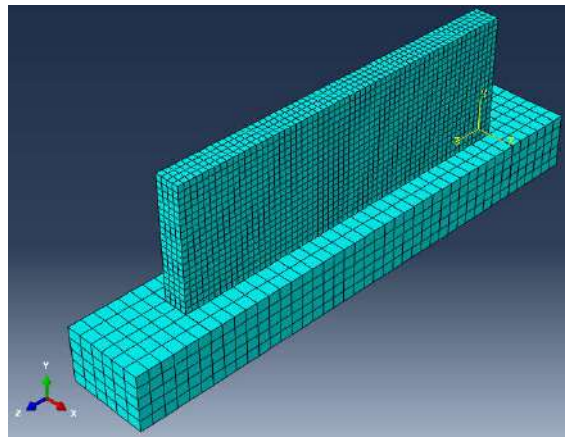

b) Mesh size 50x50x50

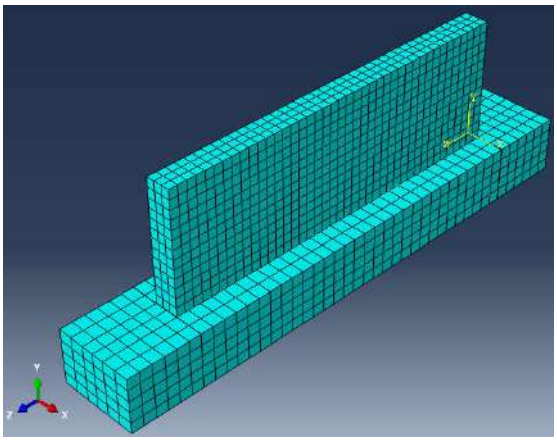

c) Mesh size 75x75x75

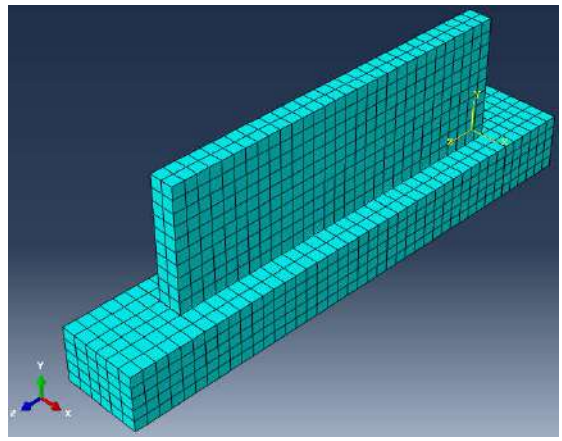

d) Mesh size 100x100x100

Figure 20. Different wall mesh sizes for mesh sensitive analysis (SW7 wall)

Each one of these walls were subjected to a pushover load and the results were compared with the experimental data of walls tested at NEES. Figures 20 and 21 show the base shear as function of drift results obtained for walls SW1 and SW7 with the different meshes. As shown in these figures, all models with different meshes have similar behavior until the plastic range starts approximately at 0.5% drift. The mesh of 100x100x100 produces the best results since it captures better the shear peak values compared with the experimental results, not only for the SW1 and SW7 walls, but for all seven wall models analyzed in Abaqus. For this reason, a mesh of 100x100x100mm was chosen for modeling the walls in Abaqus corresponding to walls tested at the NEES facility at the University of Buffalo.

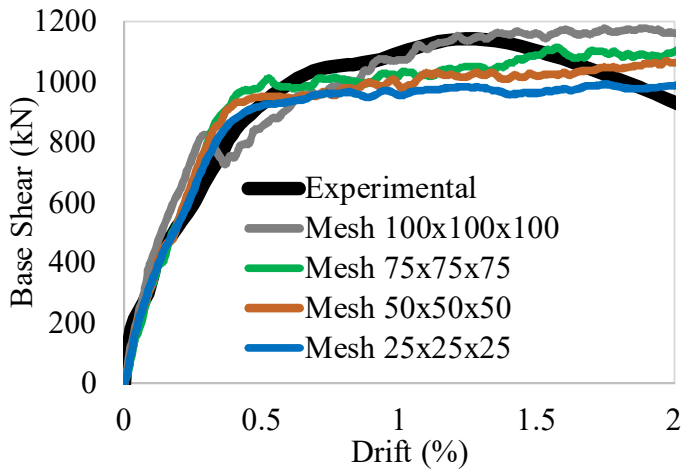

Figure 21. Mesh sensitivity analysis for wall SW1

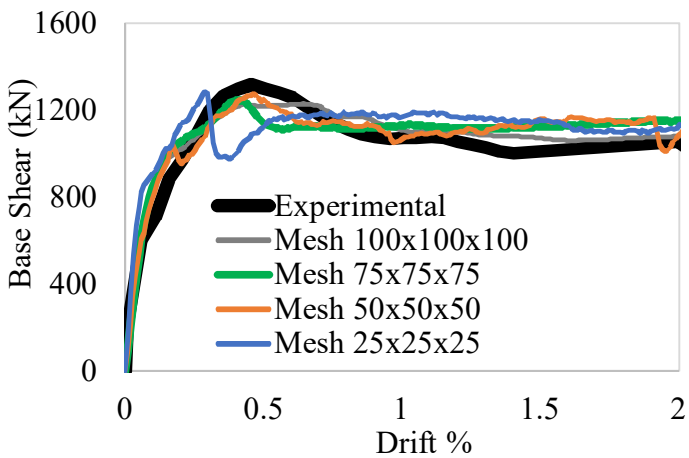

Figure 22. Mesh sensitivity analysis for wall SW7

2.3.2.4 Results for different concrete compressive curve strain limits

Once the appropriate dilation angle and mesh size for the analyses were found, additional calibrations were performed. Two tests were performed in which the concrete compressive constitutive curve was varied. The first analyses were performed with a variation of the Popovic's curve that is more typical of an unconfined concrete. In this curve, when the concrete reaches a strain of 0.004 the strength begins to drop linearly until a strain of 0.0064. The second analyses were performed with the whole compressive concrete curve obtained from the Popovic's Equation (27). These two curves are shown in Figure 23.

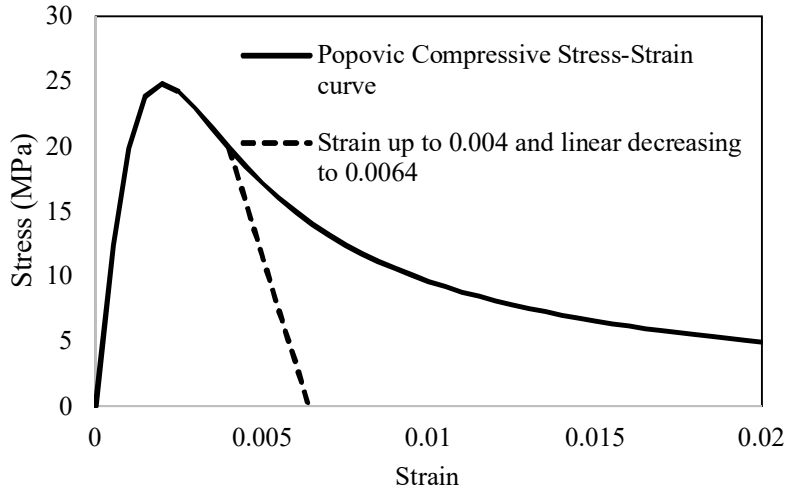

Figure 23. Compressive concrete curves used in the analyses

Figures 24 shows the results of the finite element model in Abaqus (shear vs drift) using the two different concrete curves and the average backbone curve from the experimental tests obtained from the average results of the two first and third quadrants of loading curves. As seen in these figures, the best results are obtained using the Popovic's curve until a concrete deformation of 0.02. This concrete curve allows a better estimation of the peak and post peak response of these walls. Nevertheless, using a concrete curve with a drop of strength until a strain of 0.0064 can give a good estimation of shear peak and its respectively strain, but the post peak response is not predicted well (Figure. 24)

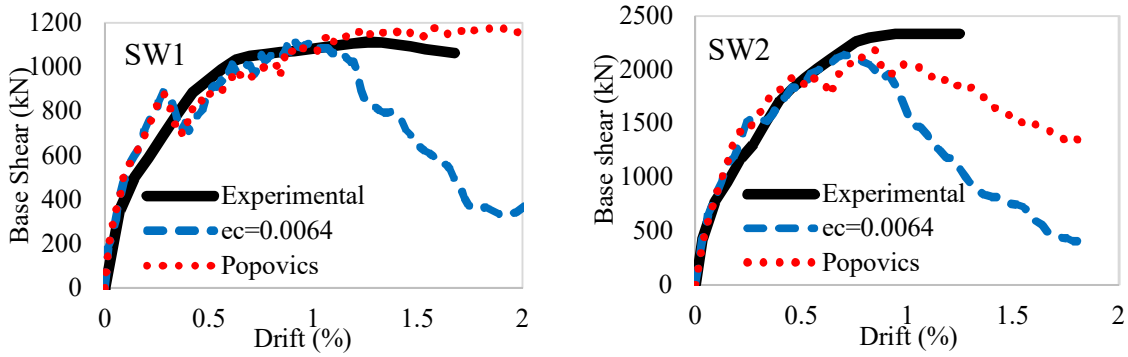

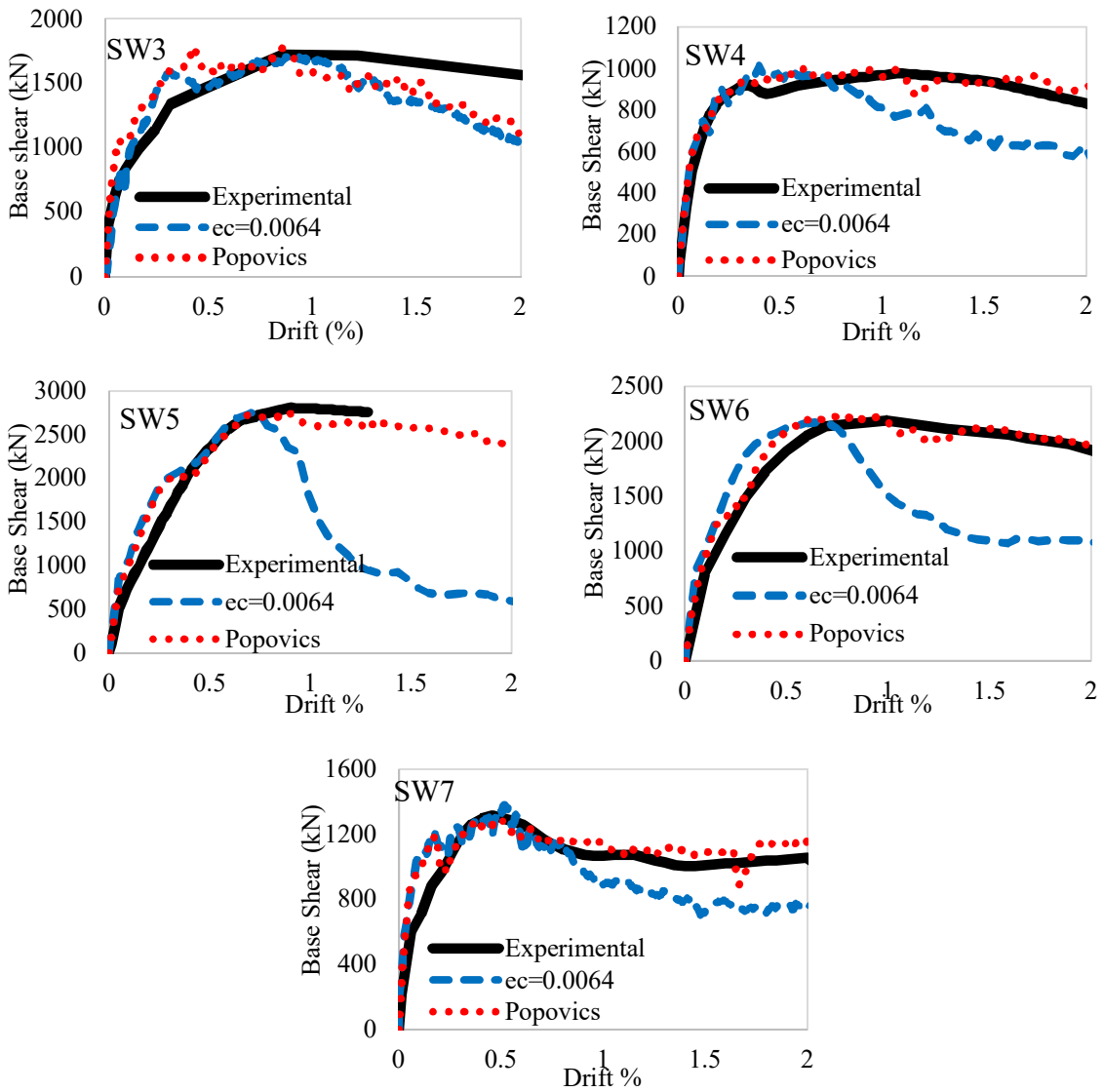

Figure 24. Base shear vs Drift for different concrete models

2.3.3 Two-dimensional model analysis in Abaqus

A two-dimensional model was also developed in Abaqus to assess its potential to model the walls in a simpler way. The 2D model was created using a quadrilateral finite membrane strain element S4R, which is a 4-node, quadrilateral, stress/displacement shell element with reduced integration and a large-strain formulation, with hourglass control (Figure. 25). This type of element was used for modeling the concrete in the wall. The material model used for concrete was the Concrete Damage Plasticity used in the three-dimensional model and explained in previous sections. Table

2 shows a summary of these parameters. The parameters for this concrete model were the same used for the 3D model with the whole compressive concrete curve obtained from the Popovics Equation (27). The reinforcement steel material was the same used for three-dimensional analysis.

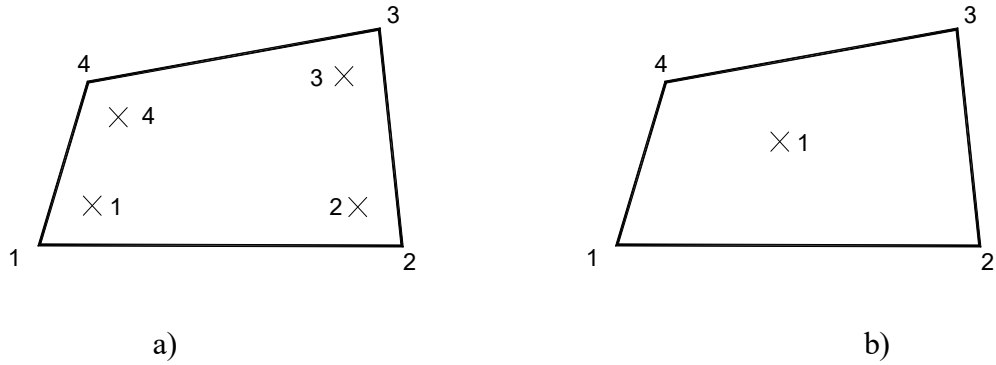

Figure 25. Finite element type shell: a) S4 4-node general-purpose shell, finite membrane strains 4 node finite element b) S4R 4-node general-purpose shell, reduced integration with hourglass control, finite membrane strains

Table 2: Concrete damage plasticity parameters

Walls	Dilation angle	Eccentricity	fb0/fc0	Kc	Viscosity Parameter
SW1-SW7	56º	0.1	1.16	0.67	0

For modeling the reinforcement steel, this type of continuum homogenous shell allows to introduce the reinforcement properties of the wall directly into this element. This is an advantage compared with the three-dimensional model because there is no need to model the steel reinforcement as a conjunction of independent truss elements. The data required for the reinforcement in the model are: layer name, rebar material previously defined, area per bar, spacing, orientation angle, and the position into the shell (this position is taken across the section of the wall).

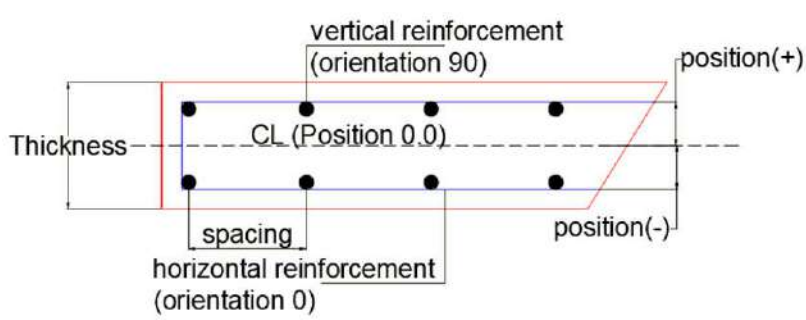

Figure 26. Reinforcement for Abaqus shell in 2D model

2.3.3.1 Mesh sensitive for two-dimensional model

Similar to the 3D model, to determine an appropriate mesh size, four types of meshes were analyzed in Abaqus and their accuracy was compared. The four-mesh size were: 25x25mm, 50x50mm, 75x75mm and 100x100mm. Figures 27 and 28 present the mesh configurations for two selected walls, SW1 and SW7.

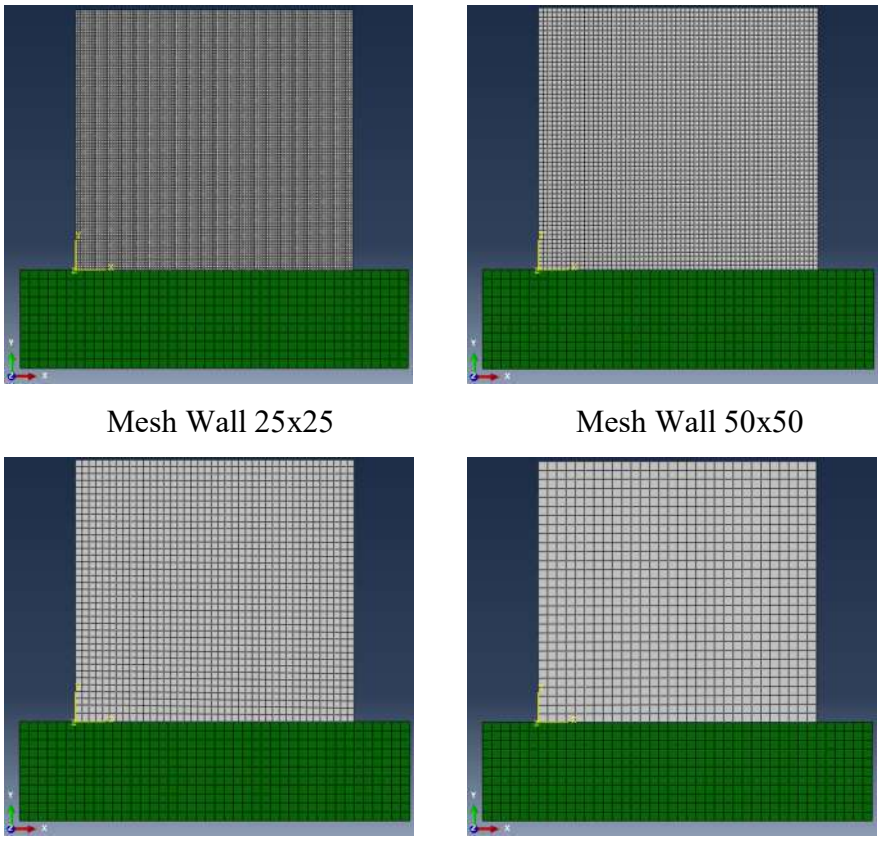

Mesh Wall 25x25 Mesh Wall 50x50

Mesh Wall 75x75 Mesh Wall 100x100

Figure 27. Several types of meshes for model wall SW1

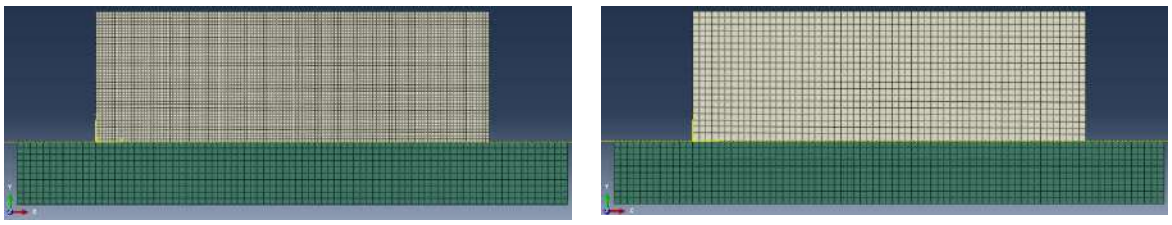

Mesh Wall 25x25 Mesh Wall 50x50

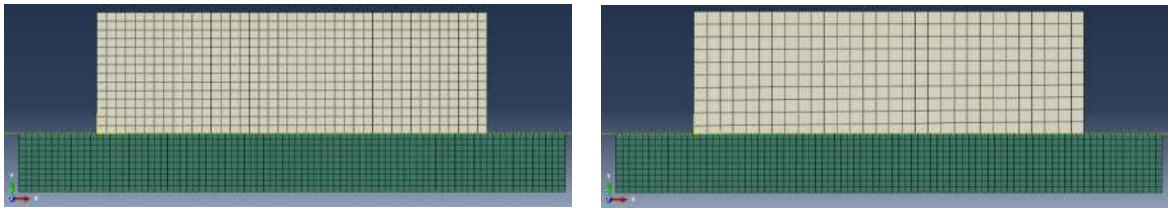

Mesh Wall 75x75 Mesh Wall 100x100

Figure 28. Several types of meshes for model wall SW7

The wall models were subjected to a lateral load of increasing magnitude (pushover). Figures 29-30 show the base shear and drift response obtained from all the mesh cases for walls SW1 and SW7, respectively. As shown in these figures, the behavior of the models with different mesh sizes is very similar up to a drift of 0.5% and 0.25% for walls SW1 and SW7, respectively. After that, the smaller mesh shows the lower capacity and worst prediction of the peak and post peak response. One possible explanation of this behavior could be that the wall with small mesh elements reaches the damage faster due to stress concentration on the element, therefore the larger element presents less stress concentration and predict the peak response much better.

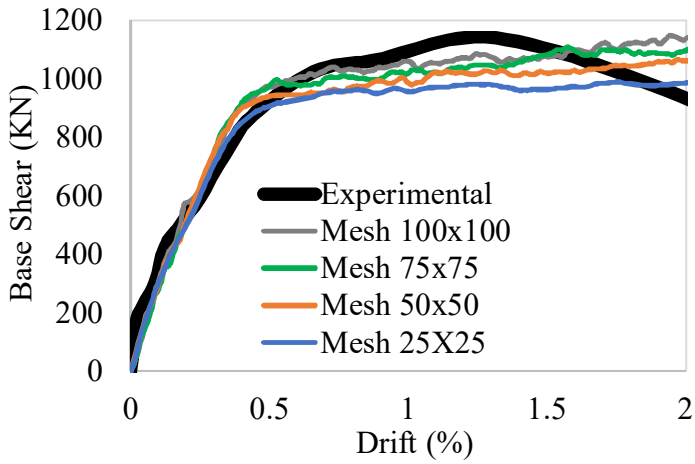

Figure 29. Mesh sensitive for 2D models of Wall SW1

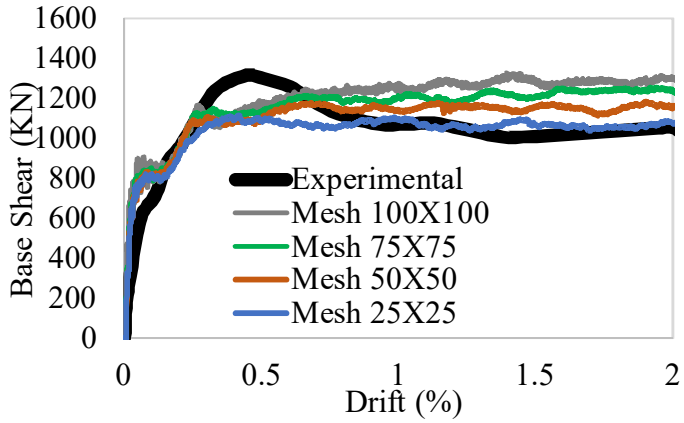

Figure 30. Mesh sensitive for 2D models of Wall SW7

2.3.3.2 Pushover results for two-dimensional analysis

Considering the results obtained from the previous parametric studies of the dilation angle in the response of the three-dimensional models of RC wall, the value of $\psi = 56°$ was used for the pushover analysis of the two-dimensional wall models. All seven wall specimens tested at the NEES facility at the University of Buffalo were also analyzed in two-dimensional fashion. Figure 30 shows the shear vs drift curves obtained from the two-dimensional models of the seven walls compared with the experimental backbones obtained from the NEES database. The analytical results are in good agreement with the experimental data. The model predicts the response up to the peak with better accuracy, any after the peak it shear shows more variability depending on the type of wall.

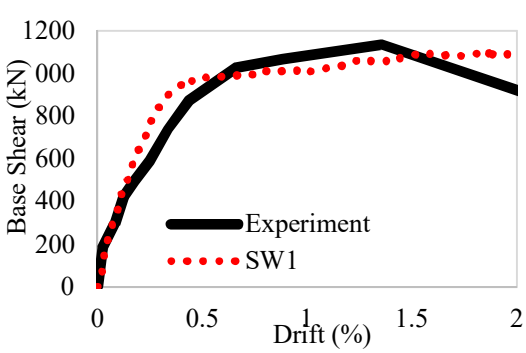

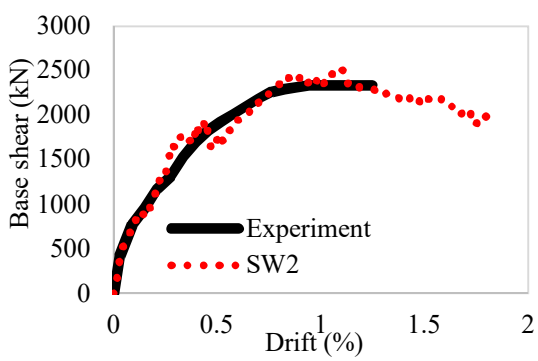

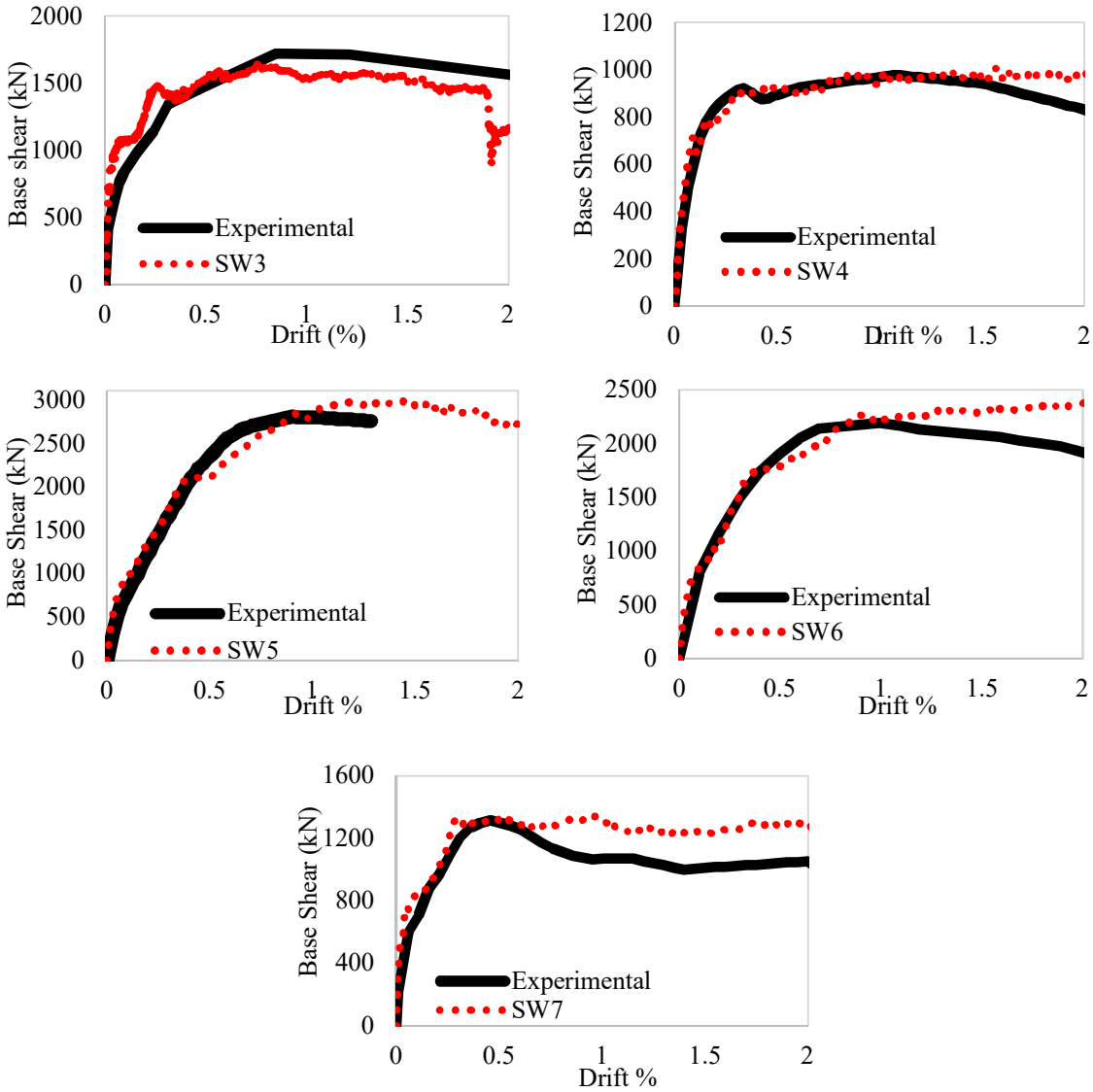

Figure 31. Pushover analyses for the two-dimensional model in Abaqus

2.4 Modeling in OpenSees

An additional analysis was conducted in the software OpenSees using an element defined as Shear-Flexure Interaction Multiple-Vertical-Line-Element Model (SFI-MVLEM, Kolozvari et al., 2015). This model was explained in Chapter I of this thesis. The objective of modeling these walls in OpenSees was to determine if this model could predict better the response of RC squat walls under lateral pushover and/or cyclic loadings than the models used in Abaqus. The wall model was developed by varying several parameters to find the combination that provides the best results. First, the number of vertical elements (n) and number of horizontal panel fibers (m) were varied.

Second, the factor height where the relative rotation between top and bottom of rigid beams (ch) is concentrated was varied. Third, the dowel action parameter was also changed. Other variables taken into consideration that impact the analysis convergence were the displacement increment step and the tolerance error (Tol).

The concrete was modelled using the constitutive relationship defined in OpenSees as uniaxialMaterial ConcreteCM (Kolozvari et al., 2015). This is a uniaxial hysteretic constitutive model for concrete developed by Chang and Mander (1994) that allows calibration of the monotonic and hysteretic material modeling parameters. This model can simulate the hysteretic behavior of confined and unconfined, ordinary and high-strength concrete, in both cyclic compression and tension (Figure. 32). The reinforcement was modelled as uniaxialMaterial SteelMPF (Kolozvari et al., 2015), which represents the well-known uniaxial constitutive nonlinear hysteretic material model for steel proposed by Menegotto and Pinto (1973) and extended by Filippou et al. (1983) to include isotropic strain hardening effects (Figure. 33).

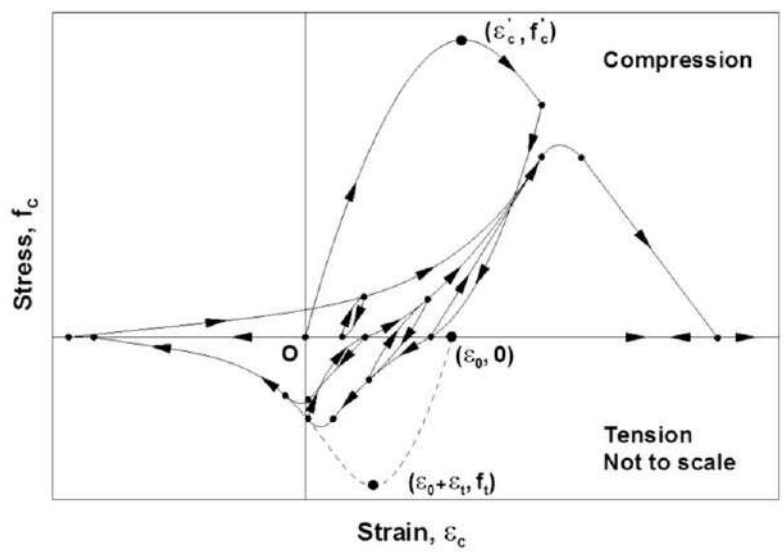

Figure 32. Uniaxial hysteretic constitutive model for concrete developed by Chang and Mander (1994)

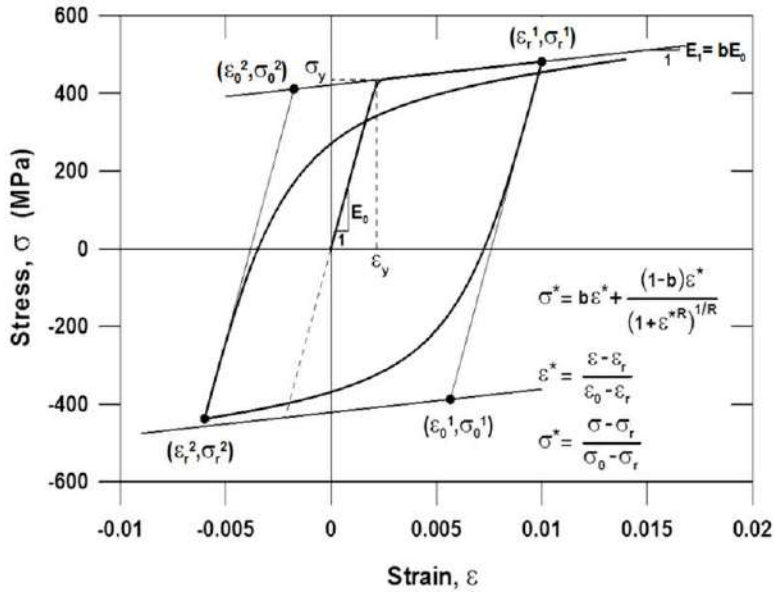

Figure 33. Constitutive Model for Steel (Menegotto and Pinto, 1973) (Figure from OpenSees)

Figure 34 shows an example of the mesh used to model wall SW1 with m = 5 and n = 16 elements, in which m is the horizontal panel fiber divisions and n is the vertical number of elements.

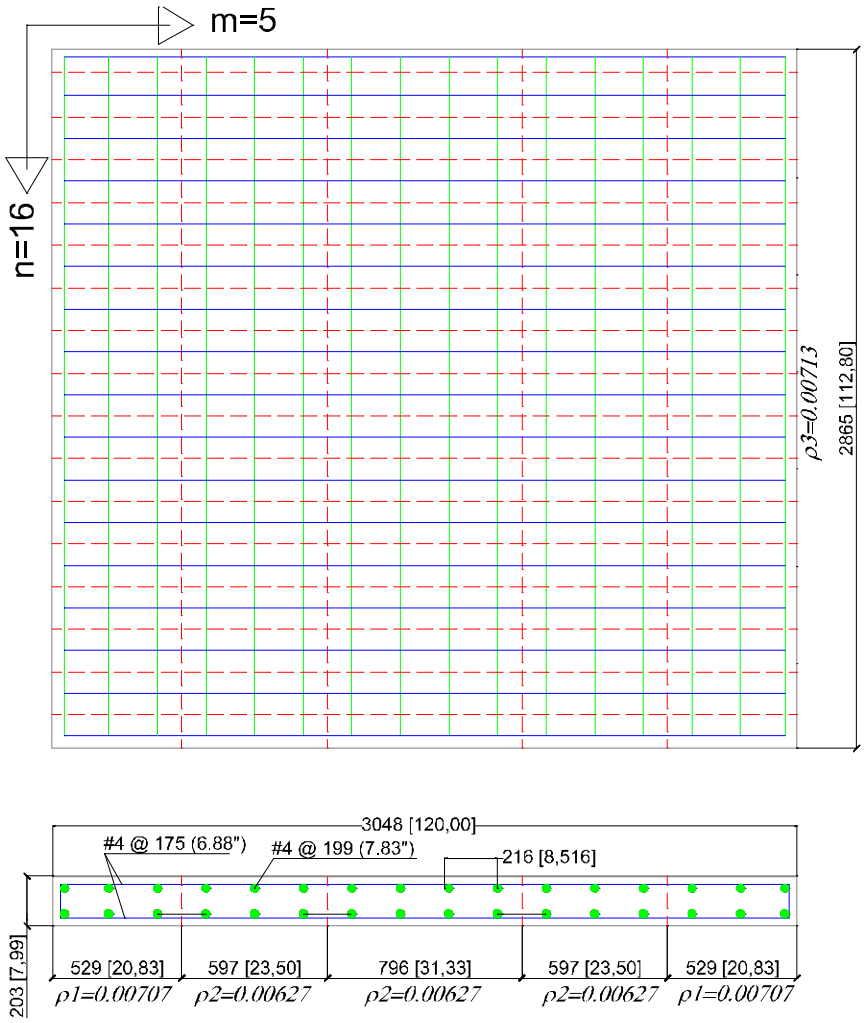

Figure 34. Mesh wall SW1 OpenSees

This type of model in Opensees is very sensitive to mesh size. Despite that the SFI-MVLEM element was created for walls with moderate aspect ratio 1.5-2.5, two walls with aspect ratio of 0.94 and 0.33 were analyzed to determine how good are the modeling capabilities of this element for walls with aspect ratio lower than 1.5.

The following Figure 35 present the results of the analysis of wall SW1 in OpenSees with a mesh size of n=16 and m=5. The variable ch, was varied using values of 0.38, 0.39, 0.46 and 0.47. The friction coefficient (η) parameter which ranges between 0 and 1.5 was not varied and was set to 1.5. The dowel action stiffness factor (α) varied from 0 to 0.05. A value of 0.0001 was used for all the analyses. These last two parameters are responsible of the shear resisting mechanism. The friction coefficient value was based on examples from Kolozvari (2014) and according to this

research, this parameter has minimum effect on the shear mechanism along a crack when compared with the dowel action parameter. There is not a method or an equation yet to estimate the dowel action parameter values. It was found that the majority of models did not converge unless this parameter was very small. Figure 35 shows the shear vs drift response of wall SW1 for different values of ch. It was only possible to get results until 0.5% drift. Other values close to 0.4 were analyzed, but unfortunately the model did not converge.

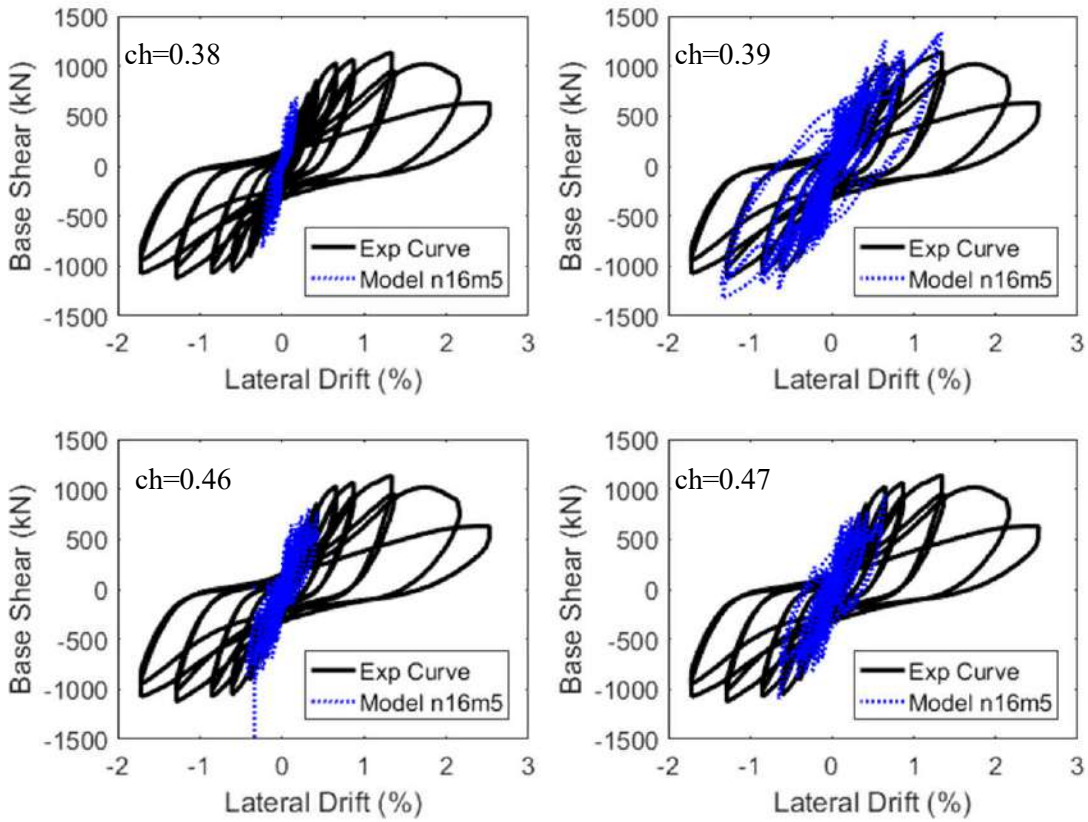

Figure 35. Results of Wall SW1 Opensees mesh with n=16 and m=5

A different mesh for the wall SW1 with n=8 and m=9 was also tried to improve results. The shape parameter (shp) or the Tsai's parameter *r* that defines the shape of the compression envelope was varied. The other parameters like the height ch=0.41, friction coefficient (η=1.5), dowel action parameter (α=0.0001) remained constant. The results (Figure 36) shows a different behavior compared with the previous mesh (n=16, m=5). For this reason and the difficulties to get convergence of the model after 0.5% drift, this analysis is not recommended for other walls with aspect ratio different from intermediate (1.5-2.5).

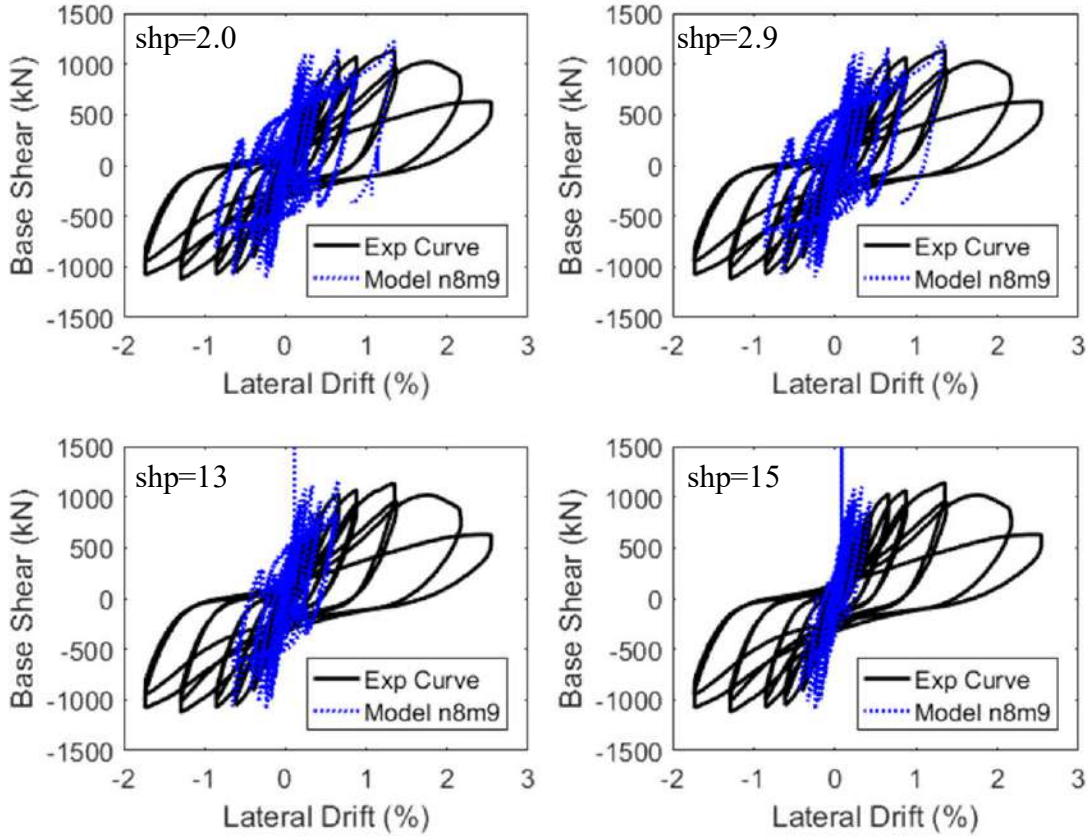

Figure 36. Results of Wall SW1 OpenSees mesh with n=8 and m=9

The wall SW3 which is a lower wall with an aspect ratio of 0.33 was also analyzed using the same model in OpenSees. Figure 37 presents the configuration of the mesh for this wall with a size of n=5 and m=8. In this analysis the variable ch was varied using values of 0.41,0.42,0.43 and 0.44. The remaining parameters; the friction coefficient (η=1.5), dowel action (α=0.0001) and shape factor (shp=8.5) were kept constant. Unfortunately, after many attempts with several values of ch close to 0.4 and even varying the rest of the parameters, the model did not converge. This corroborated one more time that this type of model does not work on walls with aspect ratios less than 1.5. It is not recommended the use of Opensees for these types of walls until further improvements are made.

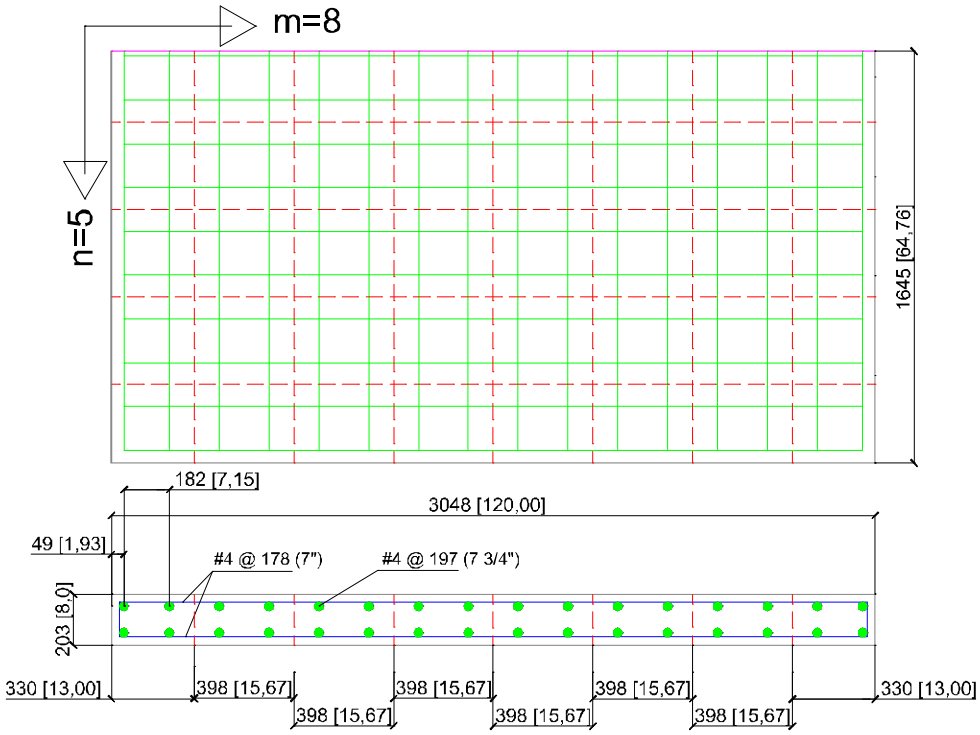

Figure 37. Mesh wall SW3 Opensees

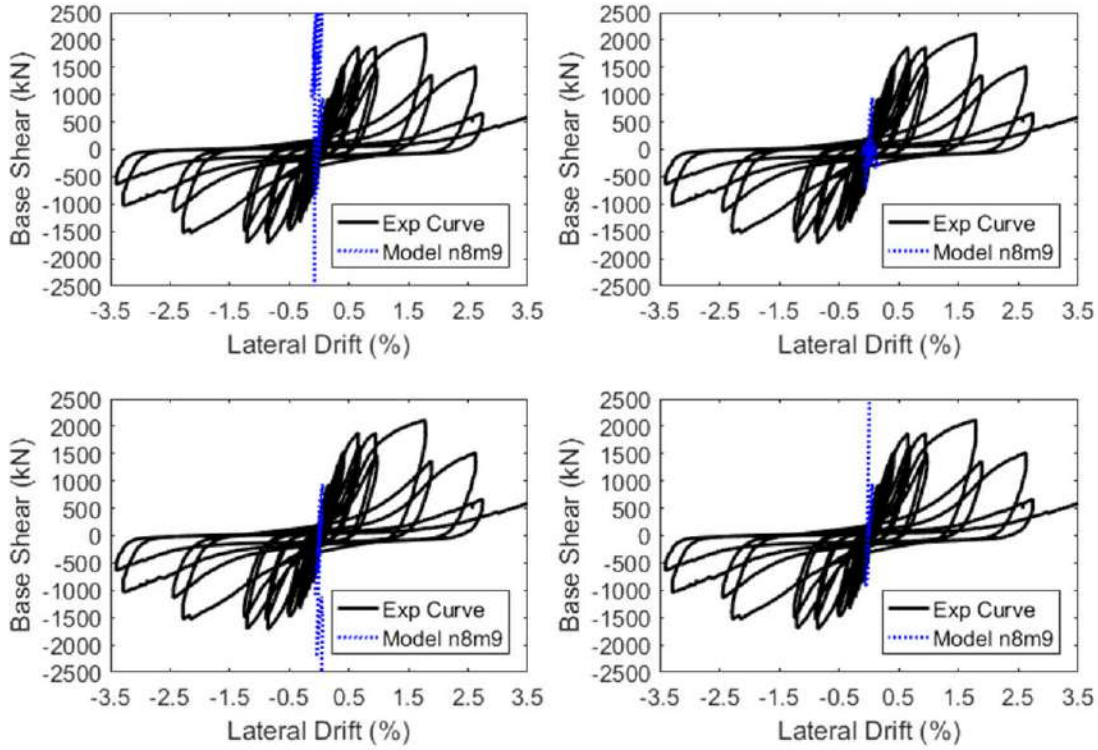

Figure 38. Results of Wall SW7 Opensees mesh n=8 m=9

2.5 Lateral stiffness calculation

The effective stiffness of experimental walls was compared with different stiffness calculated by codes using reduction flexural and shear factors (Table 3). The experimental effective stiffness data was obtained from Luna (2015). From Table 3, it can be noticed that the reduction factors that provide a better approximation of the effective stiffness are the factors proposed by Luna and ASCE 43-05 for cracked walls. The other factors provided in the ASCE 43-05 for uncracked walls, ASCE 41-13 for cracked walls, ACI 318-14 and FEMA 356 standards overestimate the results. The effective stiffness was also calculated for the calibrated 3D model using the software Abaqus 2016. It was obtained at 15% of the shear peak and its respectively displacement as recommended by Luna (2015) (Table 3). Figure 39 presents the error percentages of all the different effective stiffness calculations in relation with the experimental data. Error percentages varied from 5.7% to 22.5% for the finite element model developed in Abaqus. The analytical model predicts with good approximation the effective stiffness taking into consideration that the wall response at low levels of drifts presents more variability. Theoretical stiffness (K_t) values were calculated using the formulas derived from Mechanics of Materials (Eqs. 41-44), where E_c is the modulus of elasticity of the concrete, G_c is the shear modulus, A_g is the gross area, I_g is the gross moment of inertia, h_w is the height of the wall and υ is the Poisson's ratio. In these equations K_s and K_f are shear and flexural rigidities, respectively.

$$K_t = \frac{1}{\frac{1}{K_f} + \frac{1}{K_s}} \tag{41}$$

$$K_s = \frac{G_c A_g}{w} \tag{42}$$

$$K_f = \frac{3E_c I_g}{\overset{3}{w}} \tag{43}$$

$$G_c = \frac{E_c}{2(1+\upsilon)} \tag{44}$$

Table 3. Effective stiffness wall values

Wall Type	K_{eff} (kN/mm)					
	Data	Theoretical	Luna	ASCE 43-05	ASCE 43-05	ASCE 41-13
	K_{eff}	Stiffness (K_t)	cracked	uncracked	cracked	cracked
	Exp	No reduction	EcIg=0.5	1.00	0.50	0.50
			GcAg=0.35	1.00	0.50	1.00
SW1	322.23	845.07	354.88	845.07	422.54	543.40
SW2	735.53	3268.73	1253.68	3268.73	1634.36	2530.98
SW3	805.09	3450.46	1323.39	3450.46	1725.23	2671.70
SW4	499.11	2531.95	971.10	2531.95	1265.97	1960.49
SW5	1558.63	5130.70	1870.44	5130.70	2565.35	4527.95
SW6	1325.71	4823.19	1758.33	4823.19	2411.59	4256.57
SW7	2147.06	4823.19	1758.33	4823.19	2411.59	4256.57

Table 3 (Cont.) Effective stiffness wall values

Wall Type	K_{eff} (kN/mm)					
	ACI 318-14	ACI 318-14	FEMA 356	FEMA 356	FE Abaqus	Error
	uncracked	cracked	uncracked	cracked		Test/
	0.70	0.35	0.80	0.50		FE Abaqus
	1.00	1.00	1.00	1.00		%
SW1	682.65	416.09	742.08	543.40	369.86	14.8
SW2	2905.74	2120.72	3046.71	2530.98	853.16	16.0
SW3	3067.29	2238.63	3216.10	2671.70	905.76	12.4
SW4	2250.77	1642.70	2359.97	1960.49	579.41	16.1
SW5	4853.79	4113.72	4965.45	4527.95	1720.99	10.4
SW6	4562.88	3867.16	4667.84	4256.57	1623.97	22.5
SW7	4562.88	3867.16	4667.84	4256.57	2025.11	5.7

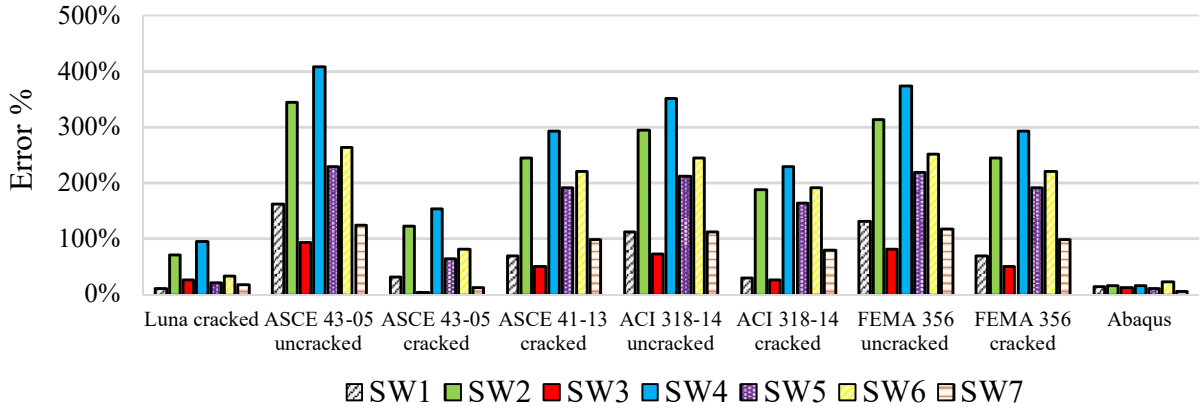

Figure 39. Error percentages of effective stiffness calculation compared with experimental data.

2.6 Summary

In this chapter were evaluated two different modeling schemes for squat reinforced concrete walls using Abaqus and OpenSees. Finite element models of seven walls were developed to determine which modeling approach provides the best agreement in lateral stiffness and peak strength. In Abaqus, the Concrete Damage Plasticity Model was evaluated by means of a parametric study focusing on important concrete parameters. From these analyses it was determined, the following:

- The parameter that has more influence in the response of the walls analyzed in this study was the dilation angle of the concrete. An angle of 56° better captures the response of these walls and provides accurate results of lateral stiffness and peak shear values.
- Different mesh sizes mostly affect the peak shear strength and post peak responses.
- The prediction of the lateral response of the walls analyzed in this research was better obtained with the constitutive relationship of the concrete based on the Popovics curve.

The Shear-Flexure Interaction Multiple-Vertical-Line-Element Model developed in OpenSees was also evaluated to determine its modeling capabilities for squat RC walls. From these analyses it was determined the following:

- The factor height (ch) where the relative rotation between top and bottom of rigid beams and shape parameter is concentrated have a great influence in the response and convergence of the analyses.
- The convergence of the results is greatly affected by the mesh size, that is, the number of horizontal and vertical fibers.
- A very small dowel action parameter is needed to run the analyses.
- The friction coefficient has less impact in the wall response.
- The convergence of this model was not possible for drifts higher than 0.5%.
- Further improvements of this model are needed to be used for squat RC walls.

From the evaluation of existing lateral stiffness factors and equations it was assessed that the reduction factors that provide a better approximation of the effective stiffness are the factors proposed by Luna, FEMA 356 and ASCE 43-05 for cracked walls. The finite element models developed in Abaqus provide results that are in good agreement with the experimental data.

CHAPTER III. EMPIRICAL EQUATIONS FOR THE PREDICTION OF EFFECTIVE LATERAL STIFFNESS OF RC SQUAT WALLS

3.1 Introduction

A proper estimation of the lateral stiffness of walls is fundamental for an accurate estimation of the fundamental period, displacements and shears in the elastic range. The magnitude of the effective stiffness depends on the reinforcement ratio, boundary elements, axial loads, concrete compressive strength and mainly on the geometric configuration of walls. Shear and flexural cracking causes reduction in the net cross-sectional area and moment of inertia, making a challenging task to predict the effective stiffness in walls and RC members in general. For that reason, in many cases it is required the use of reduction factors that affect the flexural and shear rigidities to obtain a better estimation of the wall lateral stiffness. As explained previously in Chapter 1, several researchers (Li and Xiang 2011, Tran 2012, Luna 2015) and design standards (ASCE 43-05, ASCE 41-13, ACI 318-14) have developed or established equations and reduction factors to compute the effective stiffness of RC structural members such as walls. Different equations and factors produce a great scatter in the prediction of the lateral stiffness of walls. In this chapter, the statistical analyses and procedure used to develop several equations to determine the effective stiffness of RC squat walls is described. Statistical analyses have been carried out using the assembled database developed by Adorno-Bonilla (2013). The data was divided in walls with and without axial loads to better approximate the lateral stiffness of these walls. Equations to calculate the effective stiffness and secant stiffness at peak strength of RC squat walls are developed and can be used for linear analyses, preliminary design and structural assessment. Multiple linear regression analyses were used to develop the equations.

3.2 Effective stiffness equation for squat walls without axial loads

3.2.1 Database and variables

To determine the effective stiffness equation, the walls were divided in two groups: (a) walls tested without axial loads, (b) walls tested with axial loads from the database assembled by Adorno-Bonilla (2013). A total of 33 different RC squat walls tested by different authors were used as shown in Table 4. Effective stiffness (Keff) for each of these walls were calculated at forces less than 15% of peak strength and a drift ratio less than 0.025% from the test envelope curve (Table 4) as recommended by Luna (2015). In this table, hw is the height of the wall, lw is the length of the wall, tw is the thickness, lbe is the length of the boundary zone, f'c is the compressive strength of the concrete, fy_v is the vertical steel yield strength and ρbe, ρv, ρh are the reinforcement ratios for the boundary zone, vertical and horizontal web, respectively.

To determine an appropriate equation, it is required to determine the impact of different variables in the effective stiffness such as geometric dimensions, material properties, and steel reinforcement ratios. Using the basic geometric dimensions of the walls (hw,lw,tw), other parameters were calculated such as the gross moment of inertia (Ig), the effective shear area (Aw), and variation of ratios (hw/lw, lw/tw, hw/tw) to complete the assessment of variables that affect the lateral stiffness. Geometric parameters were also combined with material parameters like the compressive strength of concrete (f'c), elasticity modulus (Ec) and shear modulus (G = 0.4Ec) to determine the combined influence in the stiffness. These analyses were performed with the software Minitab v18.1 (2017). The impact of several parameters on effective stiffness for squat walls without axial loads is presented in Figures 40 (a) to 40 (c). Every figure shows a matrix with several plots that describe how each variable placed in the diagonal is related with other variables and more important to the effective stiffness (Keff). The plots that are placed in the same line with Keff show how it is correlated with the variables in the diagonal. For example, the red dashed lines in Figures 40(a) and 40 (b) show how the effective stiffness is related to the variable 1/(Aw.fc) and to the aspect ratio hw/lw, respectively. It can be noted that the variable 1/(Aw.fc) is poorly correlated with Keff, contrary to hw/lw (Figure 40 b) that shows better correlation. From these

figures, the variables that shows better correlation with Keff correspond to those related with the geometry of the wall, and combinations of these.

Table 4. Database properties for RC squat walls tested without axial loads (assembled by Adorno-Bonilla 2013)

Researcher	ID	hw (mm)	lw (mm)	tw (mm)	hw /lw	lbe (mm)	ρ_{be} (%)	ρ_v (%)	ρ_h (%)	f'c (MPa)	fy_v (MPa)	Keff (kN/mm)
Terzioglu	SWT2S1-1	750	1500	120	0.50	130	5.16	0.67	0.67	19.3	473	588
Terzioglu	SWT1S1-2	750	1500	120	0.50	130	5.16	0.34	0.34	23.7	473	520
Terzioglu	SWT2S2-3	750	1500	120	0.50	130	5.16	0.67	0.67	25.8	473	392
Terzioglu	SWT2S3-4	750	1500	120	0.50	130	5.16	0.67	0.67	29	572	810
Terzioglu	SWT3S1-5	750	1500	120	0.50	80	1.05	0.67	0.67	32.1	572	1097
Terzioglu	SWT4S1-6	500	1500	120	0.33	130	3.95	0.67	0.67	34.8	572	1841
Terzioglu	SWT5S1-7	1500	1500	120	1.00	130	9.75	0.34	0.67	35	572	518
Terzioglu	SWT6S1-8	1500	1500	120	1.00	130	9.75	0.67	0.67	22.6	572	518
Terzioglu	SWT1S2-9	750	1500	120	0.50	130	5.16	0.34	0.34	24	572	364
Wiradinata	Wall 2	500	2000	100	0.25	320	1.25	0.71	0.21	22.0	435	2147
Wiradinata	Wall 1	1000	2000	100	0.50	320	1.25	0.71	0.21	25.0	435	1593
Pilette	Wall4	1000	2000	100	0.50	320	1.25	0.71	0.80	33	480	201
Pilette	Wall 5	1000	2000	100	0.50	250	1.60	1.15	1.15	27	480	215
Synge	Wall 1	1500	3000	100	0.50	200	2.26	0.81	1.68	27.2	300	502
NEES-UB	SW1	2865	3048	203	0.94	0	0	0.71	0.71	24.8	462	322
NEES-UB	SW2	1646	3048	203	0.54	0	0	0.96	0.96	48.3	434	736
NEES-UB	SW3	1646	3048	203	0.54	0	0	0.71	0.71	53.8	434	805
NEES-UB	SW4	1646	3048	203	0.54	0	0	0.34	0.34	29	462	499
NEES-UB	SW5	1006	3048	203	0.33	0	0	0.96	0.96	29.7	462	1559
NEES-UB	SW6	1006	3048	203	0.33	0	0	0.71	0.71	26.2	462	1326
NEES-UB	SW7	1006	3048	203	0.33	0	0	0.34	0.34	26.2	462	2147
NEES-UB	SW8	1646	3048	203	0.54	0	0	1.50	1.50	24.1	462	940
NEES-UB	SW9	1646	3048	203	0.54	0	0	1.50	0.71	29.7	462	872
NEES-UB	SW10	1646	3048	203	0.54	0	0	1.50	0.34	31.7	462	919
NEES-UB	SW11	1646	3048	203	0.54	380	1.54	0.71	0.71	34.5	462	748
NEES-UB	SW12	1646	3048	203	0.54	380	2.06	0.34	0.34	34.5	462	702
Whyte	Wall 1	1646	3048	203	0.54	0	0	0.71	0.71	35.5	464	300
Whyte	Wall 2	1646	3048	203	0.54	0	0	0.71	0.71	37.3	464	518
Doostdar	Wall 7	1500	2000	100	0.75	320	1.25	0.71	0.80	45.0	450	346
Doostdar	Wall 8	1500	1500	100	1.00	360	1.11	0.70	0.80	45.0	450	68
Salonikios	LSW1	1200	1200	100	1.00	240	1.73	0.57	0.42	22.2	610	80
Salonikios	LSW2	1200	1200	100	1.00	240	1.29	0.28	0.28	21.6	610	56
Salonikios	MSW6	1800	1200	100	1.50	240	1.73	0.57	0.42	27.5	610	57

Each figure into the matrix of figures is related with each different variable placed in the diagonal, vertical and horizontal values are the same for each variable, so it is possible to relate the horizontal value of any variable with the vertical value of Keff and viceversa (Figure 40).

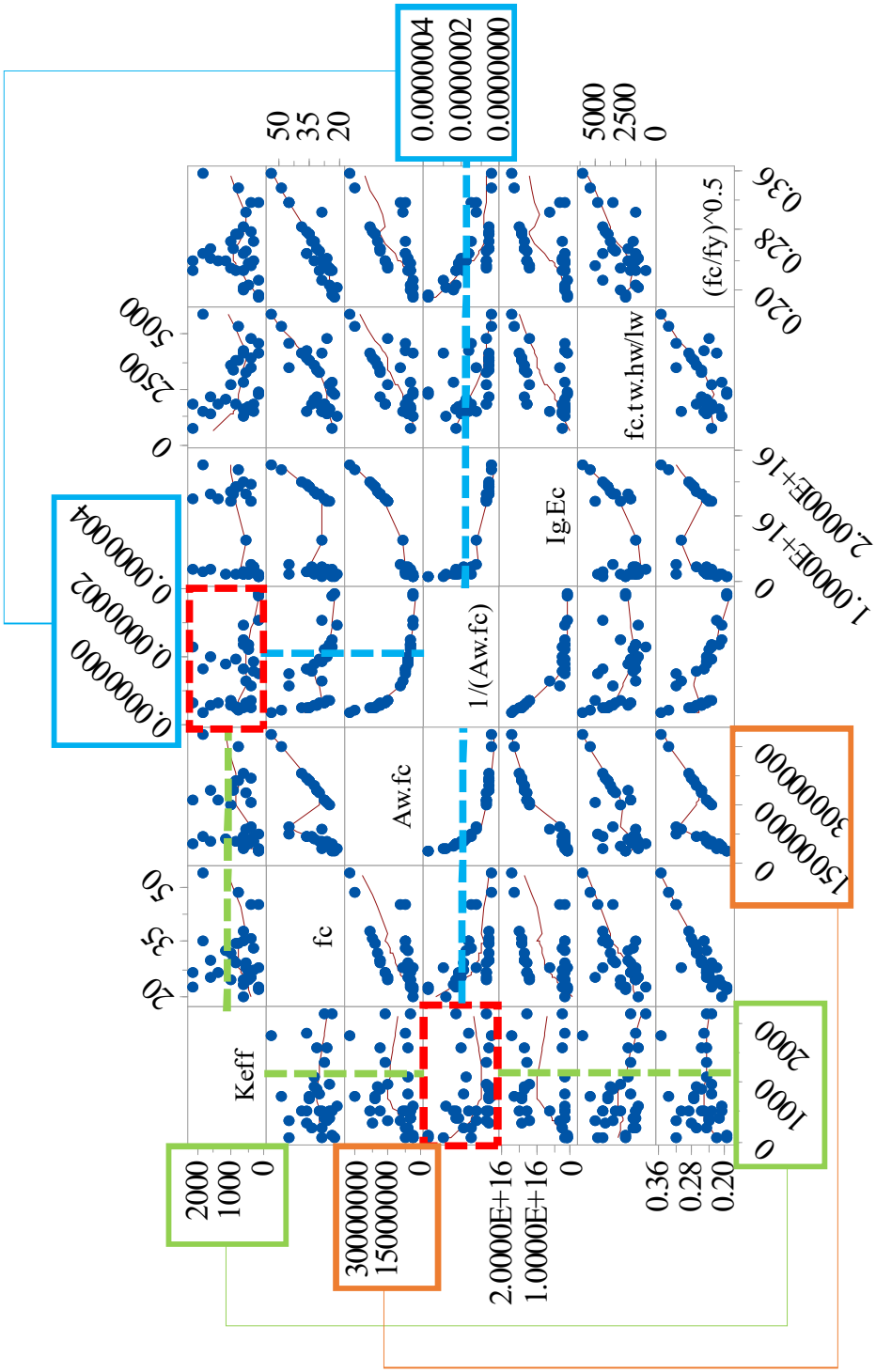

Figure 40. (a) Variables and their impact on the effective stiffness of the walls.

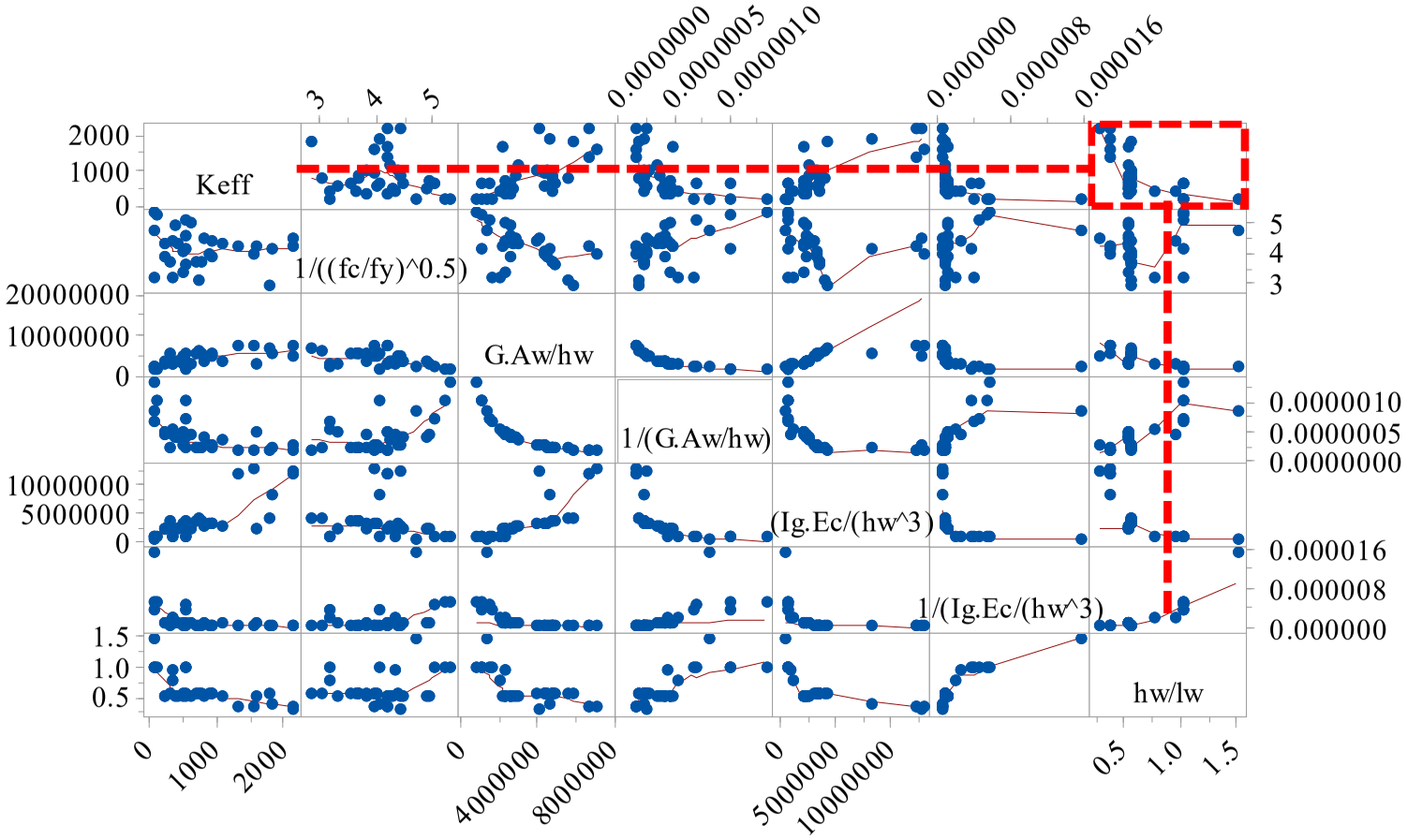

Figure 40. (b) Variables and their impact on the effective stiffness of the walls. (Cont)

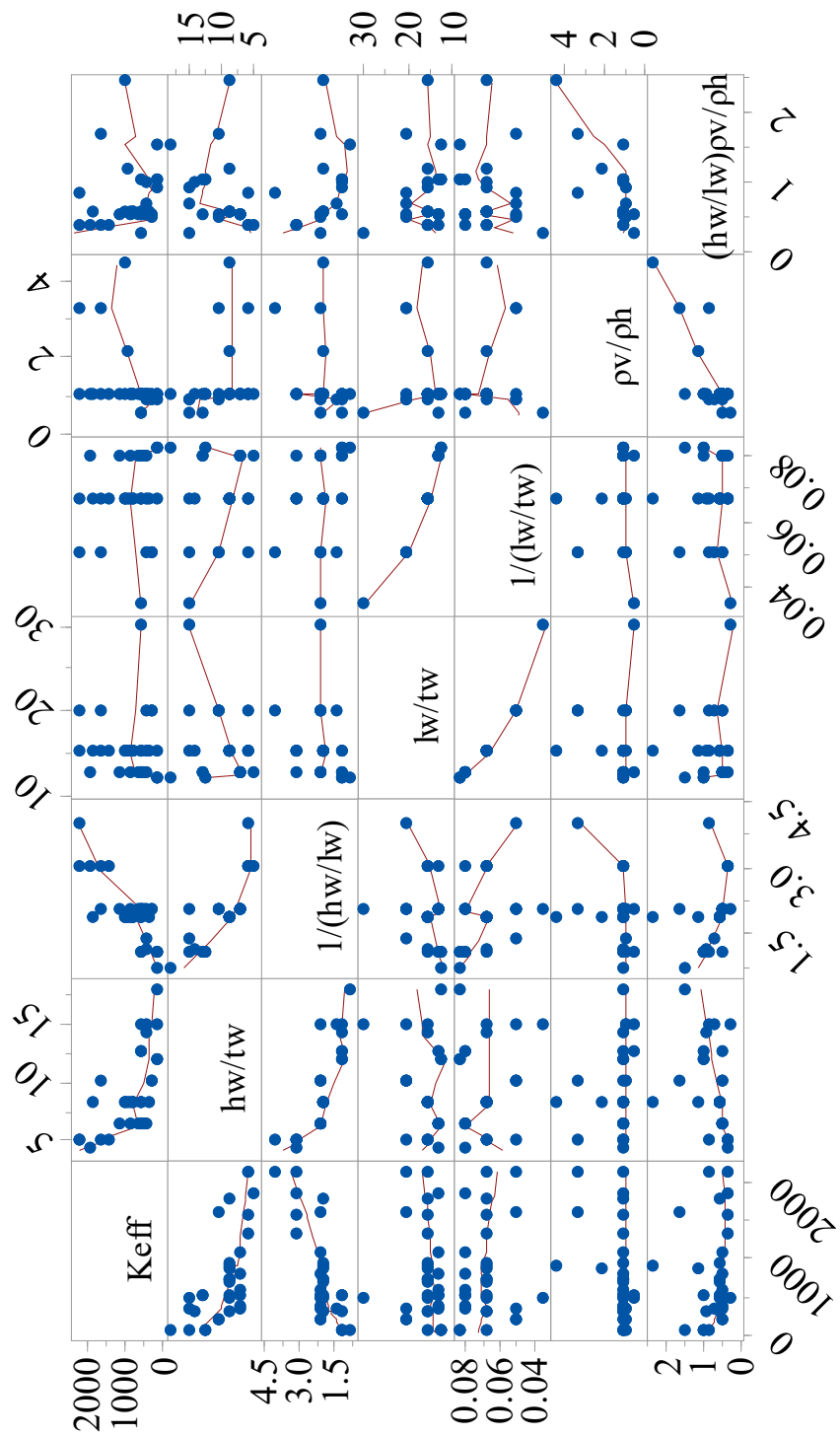

Figure 40. (c) Variables and their impact on the effective stiffness of the walls. (Cont)

Another way to determine that a variable has an impact on the effective stiffness calculation is the use of the Pearson correlation coefficient and P-value to measure how strong is a relationship

between two variables. The coefficient of correlation represented with the letter "R" has a range of -1 to +1, and values near these limits indicate a strong correlation between the independent variable and the dependent variable. A value close to cero indicates a weak correlation between the variables and if this value is cero there is no correlation. Equation 45 can be used for the calculation of the coefficient of correlation (R).

$$R = \frac{n\sum xy \quad \sum x \sum y}{\sqrt{(n\sum x^2 \quad (\sum x)^2)(n\sum y^2 \quad (\sum y)^2)}} \tag{45}$$

To determine if the correlation between variables is significant, the P-value is compared with a significance level. Typically, a significance level (α) of 0.05 is defined indicating a 5% risk of concluding that an association exists when there is no actual association. The P-value indicates if the correlation coefficient is significantly different from 0. There is no linear relationship when the coefficient is equal to 0. A P-value less than α indicates that the correlation is statistically significant. Meanwhile, a P-value higher than α indicates that the correlation is not statistically significant. Correlation coefficients (R) and P-values for all variables are shown in Table 5. According to Table 5, the parameters that were taken into consideration for the formulation of the equations to calculate the effective stiffness of walls were those with a high correlation coefficient (closer to 1.0) and with a P-value less than α=0.05. From the R and P-values it can be noticed that the strongest correlation of the stiffness is with the parameters that involve the dimensions hw, lw, gross moment of inertia and modulus of elasticity. When the compressive strength of the concrete (f'c) is incorporated with the geometric dimensions (hw,lw,tw) the correlation between the stiffness decreases as noticed before in Figures 40 (a) to 40 (c). Reinforcing steel quantities have a minimal correlation with the stiffness.

Table 5: Correlations and P-values for variables

Variable	Correlations	P-Value
fc	0.055	0.761
Aw.fc	0.273	0.124
1/(Aw.fc)	-0.329	0.061
Ig.Ec	0.278	0.117
fc.tw.hw/lw	-0.224	0.210
(fc/fy)^0.5	0.115	0.525
1/((fc/fy)^0.5)	-0.156	0.385
G.Aw/hw	0.657	0.001
1/(G.Aw/hw)	-0.556	0.001
(Ig.Ec/(hw^3)	0.797	0.001
1/(Ig.Ec/(hw^3)	-0.431	0.012
hw/lw	-0.633	0.001
hw/tw	-0.626	0.001
1/(hw/lw)	0.787	0.001
lw/tw	0.09	0.620
1/(lw/tw)	-0.172	0.339
(tw/lw)^2	-0.204	0.255
ρv/ρh	0.381	0.029
(hw/lw)ρv/ρh	-0.097	0.590
((fc/fy)^0.5)ρv/ρh	0.382	0.028
ρv (%)	0.113	0.533
ρh (%)	-0.178	0.322
ρh (%)^2	-0.119	0.509
(fc/fy)^0.5/(ρv.	0.105	0.560

3.2.2 Determination of equations for walls without axial load

Using the software Minitab V18 (2017), two effective stiffness equations were determined applying multiple regression analysis. Based on the results from the analyses described previously, the variables that have more impact in the stiffness were selected for different trial equations. Two trial equations were obtained by eliminating the variables whose P-value were higher than α with an adjusted R-squared (R^2_{adj}) higher than or equal to 85%. The R^2_{adj} is obtained with Equation 46. The $R^2_{(pred)}$ determine how well your model predicts the response for new observations.Models

that have larger predicted R2 values have better predictive ability. A predicted R^2 that is substantially less than R^2 may indicate that the model is over-fit. An over-fit model occurs when you add terms for effects that are not important in the population. In a linear regression the term R^2 shows how well terms (data points) fit a curve or line. The R^2_{adj} also indicates how well terms fit a curve or line but adjusted for the number of terms in a model. The R^2_{adj} could be negative, but it is always lower than the R-squared. Equations 47-48 show the best effective stiffness equations obtained from the database. In these equations, the variables f'c, Ec , Gc must be used in units of MPa and Ig in mm^4 . Table 6 shows the R^2, R^2_{adj}, and standard deviation (S) for the two selected trial equations. From these values it can be noticed that Equation 47 fits better the database. The units for use these equations must be the same as those in Table 4.

$$R^2_{adj} = 1 \quad \left[\frac{(1 \quad R^2)(n \quad 1)}{n \quad k \quad 1}\right] \tag{46}$$

Regression Equation A

$$Keff = \frac{0.000097\ Ec\ Ig}{w^3} + 200.3\ \frac{lw}{w} \tag{47}$$

Regression Equation B

$$Keff = \frac{0.00008\ G\ Aw}{w} + \frac{0.000114\ Ec\ Ig}{w^3} \tag{48}$$

Table 6: Summary of goodness-of-fit statistics for Keff equations of walls without axial load

No.	S	R^2	R^2 (adj)	R^2 (pred)
47	347.232	92.22%	91.69%	90.39%
48	298.07	89.84%	89.14%	86.85%

In addition to the R and standard deviation values, other calculations were performed to determine the equation that better describes the data and the one that predicts the effective stiffness with more accuracy. Figures 41-42 show the residual plots of each equation. Four plots are presented in each figure. The first one corresponds to a normal probability plot of the residuals that displays the residuals versus their expected values. When the distribution is normal this should approximately

follow a straight line. A S-curve form implies a distribution with long tails, inverted S-curve implies a distribution with short tails, downward curve implies a right-skewed distribution, upward curve implies a left-skewed distribution and a few points lying away from the line implies a distribution with outliers.

The histogram of residuals shows the distribution of the residuals for all observations. This histogram is used to determine if the data is skewed or has some outliers. A long tail in one direction means data has a skewness and a bar far away from the others means an outlier in the data. The appearance of the histogram depends on the number of intervals used in a group of data. To assess the normality of the residuals it is better to use the normal probability plot (first plot). The residual value defined as the difference between an observed value and its corresponding predicted value versus fits plot is used to verify the assumption that the residuals are randomly distributed and have constant variance (second plot on figure). The ideal distribution of points should fall randomly on both sides of 0.0, with no recognizable patterns in the points.

The residual versus order plot (four in the figure), displays the residual in the order that the data were collected and is used to verify the assumption that the residuals are independent from one another. Independent residuals show no trends or patterns when displayed in time order, a pattern in the points may indicate that residuals near each other may be correlated, and thus, not independent. Ideally, the residuals on the plot should fall randomly around the center line.

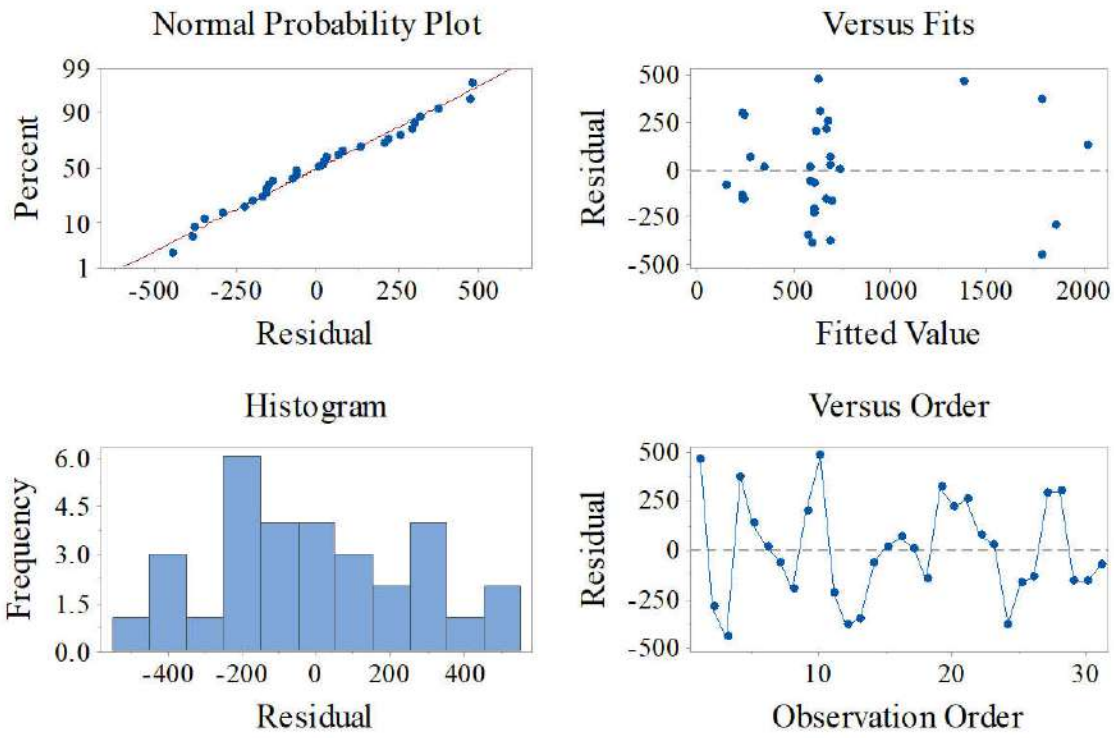

Figure 41. Residual plots for Equation 1 for walls without axial loads

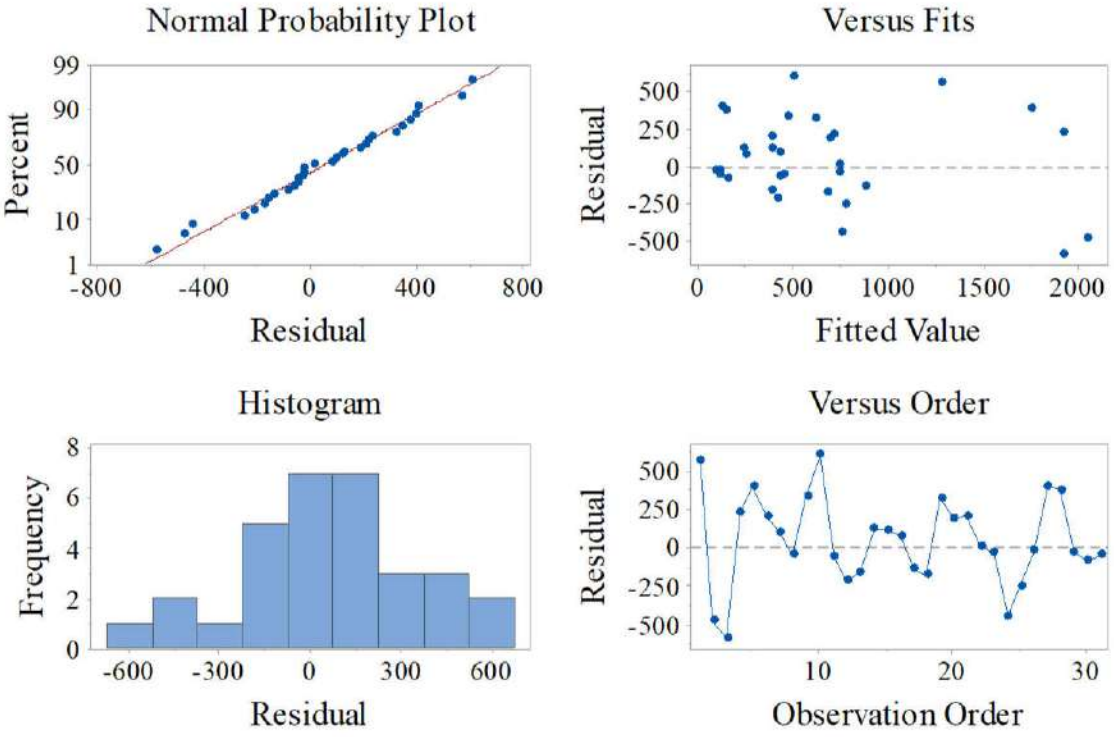

Figure 42. Residual plots for Equation 2 for walls without axial loads

3.2.3 Comparison of prediction of effective stiffness

Using Equations (40-43) for the calculation of theoretical stiffness and the reduction factors recommended by Luna (2015), ASCE (2005-2013), FEMA 356 (2000), ACI-318 (2014) and ASCE 41-17 (2017) the effective stiffness was calculated for each wall in the database described in Table 2. The factors are summarized in Table 7. Standards are not clear if these factors can be used for squat walls, only the factors proposed by Luna were determined specifically for squat walls.

Table 7: Reduction factors for effective stiffness

Component Flexure/Shear	Luna cracked	ASCE 43-05 uncracked	ASCE 43-05 cracked	ASCE 41-13 cracked	ACI 318-14 uncracked	ACI318-14 ASCE41-17 cracked	FEMA 356 uncracked	FEMA 356 cracked
(Flexure)EcIg=	0.5	1	0.5	0.5	0.7	0.35	0.8	0.5
(Shear)GcAg=	0.35	1	0.5	1	1	1	1	1

Figure 43 shows a graphic representation of the correlation of the calculated effective stiffness using the available factors vs the experimental effective stiffness. The diagonal line represents a ratio of predicted-to-experimental stiffness of 1.0. Any point falling on the line means an exact prediction of the effective stiffness. Any point above the diagonal line represents an over-prediction of stiffness and vice-versa. The farther the point from the diagonal represents a larger error on the estimate. It can be noted from Figure 43 that all the equation or factors produced significant scatter in the results.

Figures 44-45 present a graphic representation of the correlation of the calculated effective stiffness obtained with the two equations developed vs. the experimental effective stiffness. In these figures there is also a plot of the experimental and calculated values in function of the data number. Both plots give an idea of the level of accuracy of each of the equations in predicting the effective stiffness. The scatter is reduced when compared with the code/researcher predictions, at least with equations 47 and 48.

To numerically compare the observed behavior of the predictions with each equation or factor, Table 8 presents a summary of common central tendency and dispersion measures of the

experimental to predicted stiffness ratios. Mean and median values larger than 1.0 suggest that the equation or codes factors tends to underestimate the stiffness. On the other hand, the standard deviation and coefficient of variation (CoefVar) provide information on the dispersion (scatter) of the predictions. In other words, the mean and median values give useful information on the accuracy of the predictive equation while the standard deviation and coefficient of variation provide information regarding the precision of the equation. This descriptive statistical analysis shows that the Equations 1 and 2 developed in this study give the better results according to the statistical values based on the mean and median values that are close to one. However, from the two developed equations, Equation 47 has the lower coefficient of variation (CoefVar), variance and standard deviation (StDev). indicating that the scatter is reduced in comparison with the rest of the evaluated equations. Taking into account the Pearson's correlation coefficient, mean, median, coefficient of variation and standard deviation, Equation 1 gives the best predictions of the effective stiffness.

A correlation analysis was conducted relating effective stiffness calculated by codes, standards and Equations 47 and 48 vs experimental effective stiffness, using the Pearson correlation (Equation 45). The results are shown in Figure 46. Values closer to 1.0 means a good correlation with the experimental data. According to Figure 46, Equation 1 predicts with more accuracy the experimental effective stiffness because the correlation is closer to one than the rest of equations/factors.

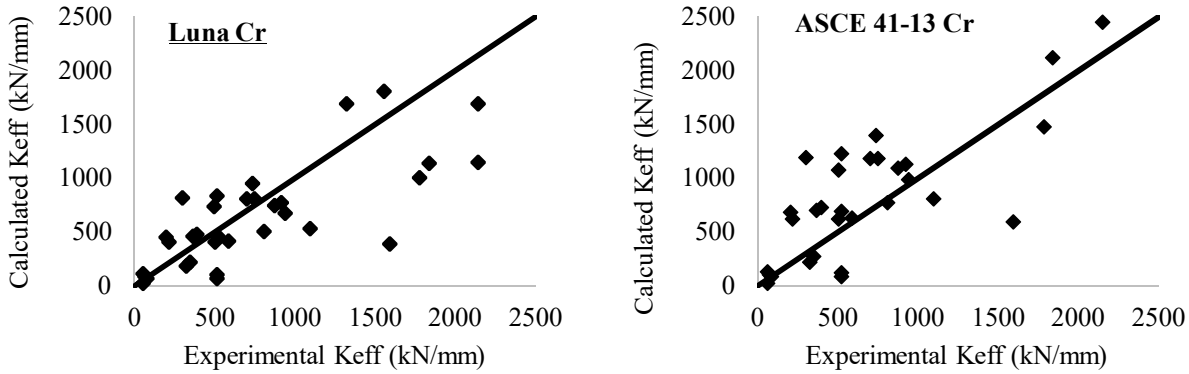

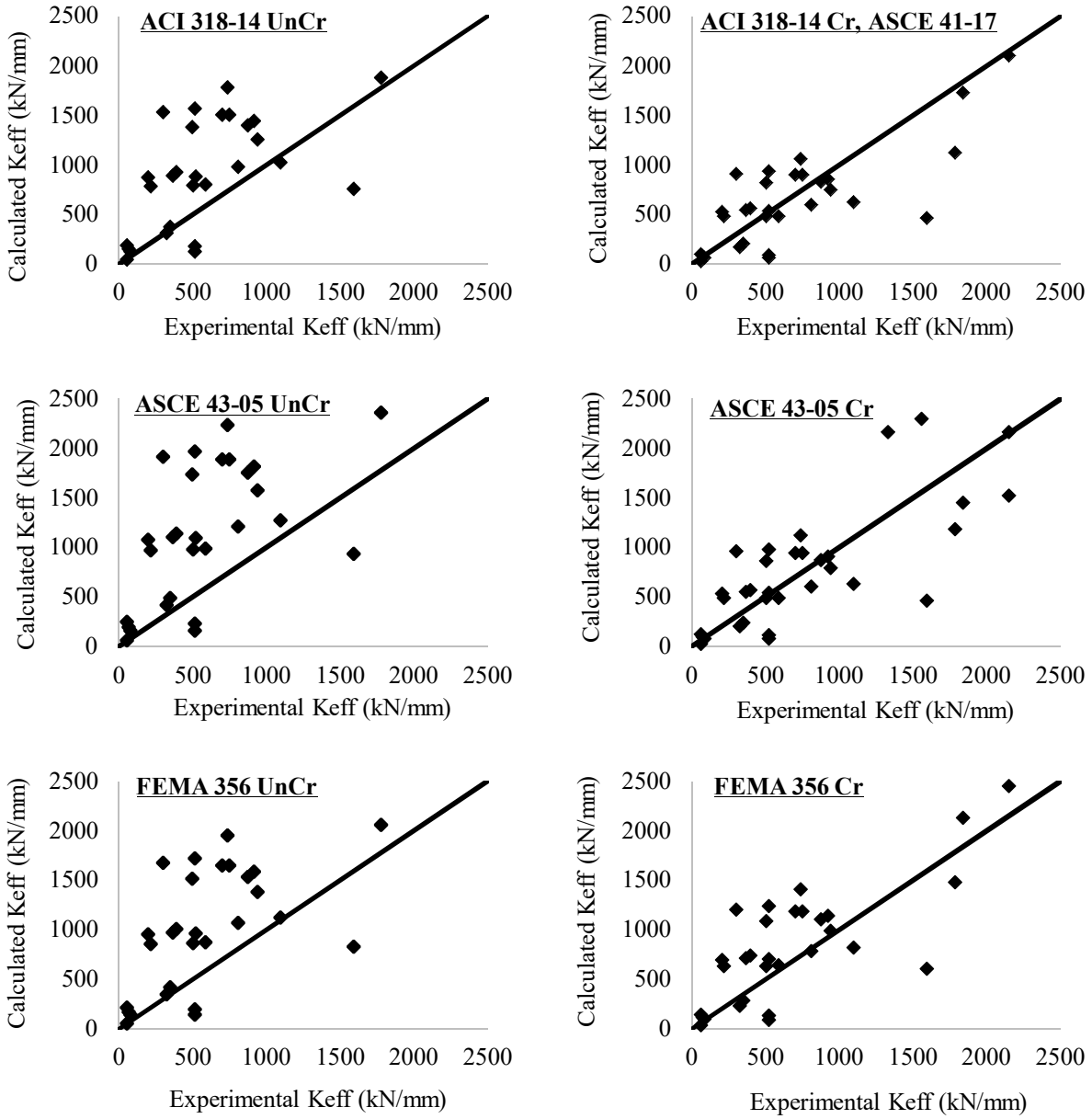

Figure 43. Correlation between calculated and experimental effective stiffness for walls without axial loads

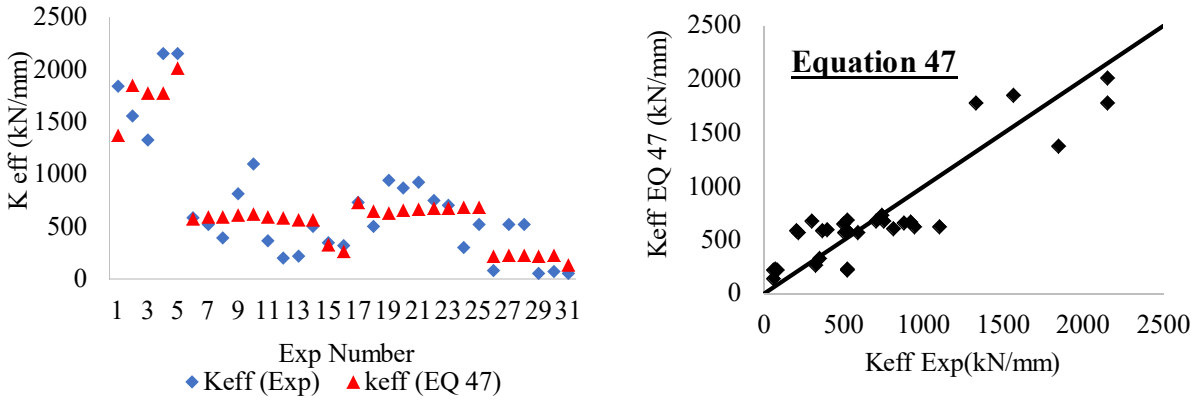

Figure 44. Correlation between prediction with Equation 47 and experimental data for walls without axial loads

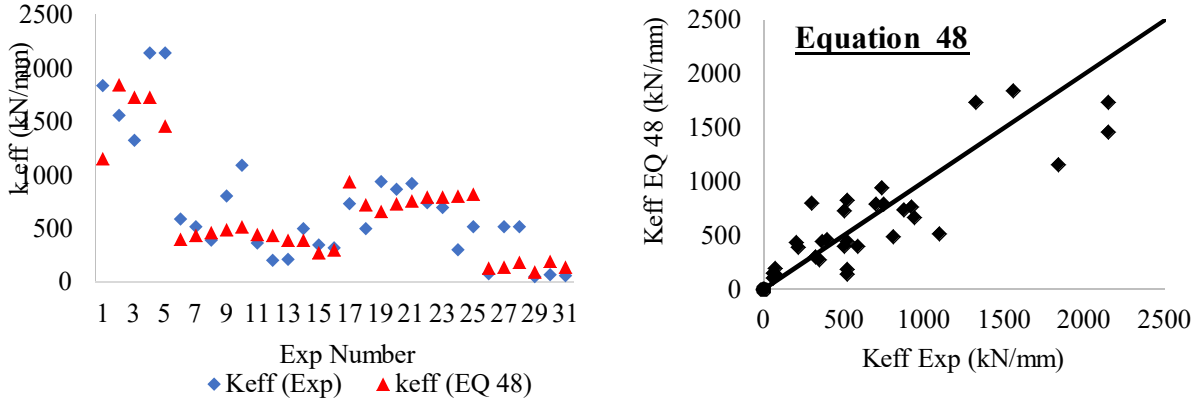

Figure 45. Correlation between prediction with Equation 48 and experimental data for walls without axial loads

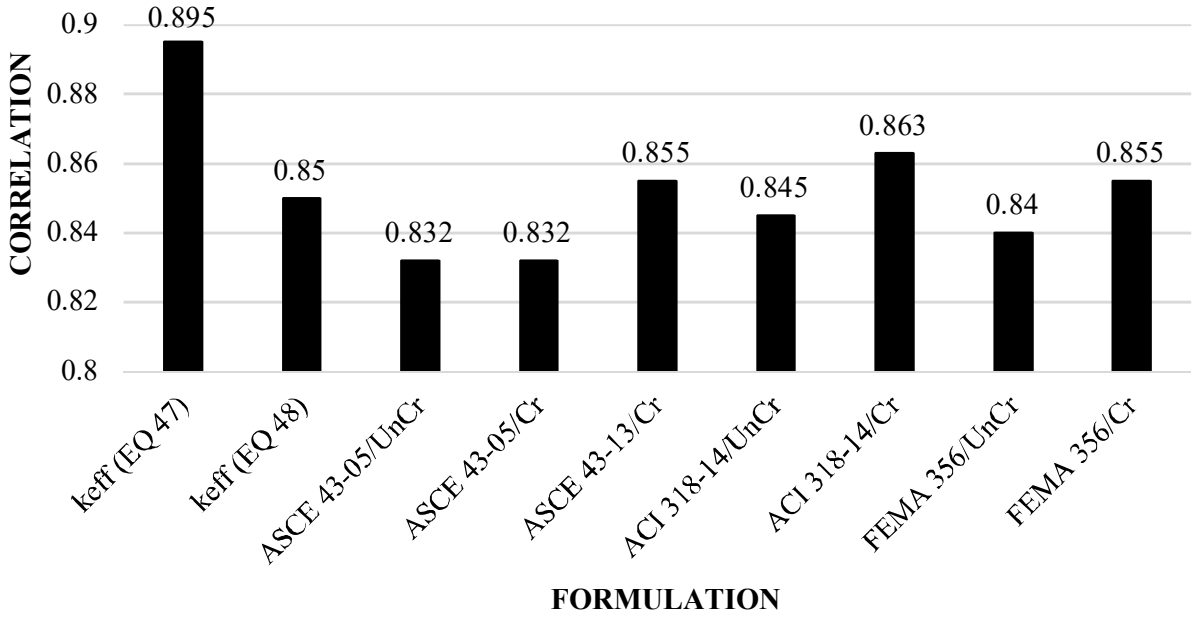

Figure 46. Correlation vs Equations for walls without axial load

Table 8: Statistics of the ratio of experimental to predicted stiffness for walls without axial load

Variable	Mean	SE Mean	StDev	Variance	CoefVar	Minimum	Median	Maximum
(EQ 47)	0.987	0.094	0.523	0.273	0.530	0.257	1.004	2.318
(EQ 48)	1.136	0.131	0.727	0.529	0.640	0.347	0.942	3.764
Luna Cr	1.396	0.231	1.285	1.652	0.920	0.366	1.126	6.829
ASCE 43-05 UnCr	0.611	0.109	0.606	0.367	0.992	0.156	0.484	3.192
ASCE 43-05 Cr	1.222	0.218	1.212	1.470	0.992	0.312	0.968	6.384
ASCE 41-13 Cr	1.019	0.204	1.135	1.288	1.114	0.250	0.742	5.866
ACI 318-14 UnCr	0.786	0.149	0.832	0.692	1.059	0.196	0.589	4.338
ACI 318-14 Cr	1.369	0.286	1.591	2.531	1.162	0.330	0.971	8.158
FEMA 356 UnCr	0.713	0.132	0.738	0.544	1.035	0.180	0.541	3.861
FEMA 356 Cr	1.019	0.204	1.135	1.288	1.114	0.250	0.742	5.866

Figure 47 shows a typical box and whisker plot comparing the distribution of the experimental-to-predicted/calculated effective stiffness for each presented equation. The graph shows the lower quartile (25th percentile), median marked with "•", upper quartile (75th percentile), the extreme values and the mean value marked with " ". The box in the box and whisker plot is constituted by the second and third quartile and represents the spread of the central 50% of the observations.

The range of this box is commonly known as the inter-quartile range (IQR), midspread or middle fifty. The narrower this range (or box in the graph) is, indicates the lesser the variability since the central 50% of the observations are nearer to the median value. The lower and upper whiskers of the plot represent the extreme values (outliers), the upper extreme is defined as third quartile (Q_3) plus 1.5 IQR and the lower extreme is defined as first quartile (Q_1) minus 1.5 IQR, where the interquartile range is $IQR=Q_3-Q_1$. Values higher and lower than those limits are known as outliers. According to Figure 47, the boxplot with better results correspond to Equation 1, because mean and median are almost coincident, but the IQR has a similar range compared to Luna, ASCE 43-05Cr, ACI 318-14 and ASCE 41-17 that indicates that these equations have a similar precision which is not as good as was expected.

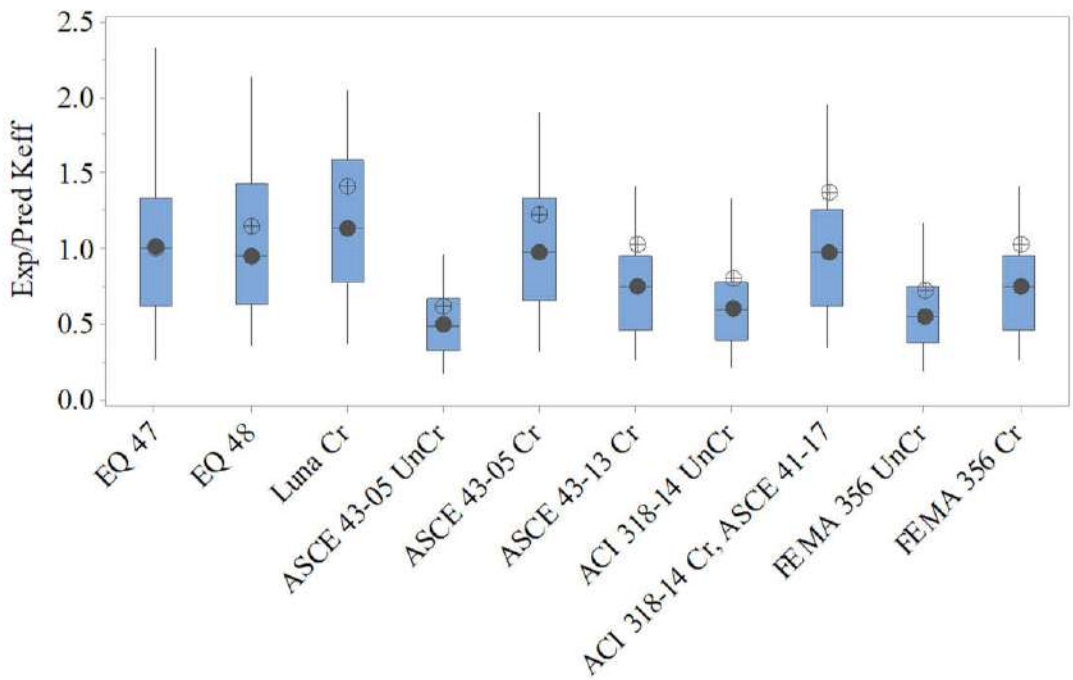

Figure 47. Box and whisker plot comparing different equations/factors for walls without axial loads

3.3 Effective stiffness equation for squat walls with axial loads

3.3.1 Data and variables for stiffness equation

To determine the effective stiffness equation for squat walls with axial loads, a total of 27 different squat walls from the database assembled by Adorno-Bonilla (2013) were used. Effective stiffness for each of these walls was calculated at forces less than 15% of peak strength and a drift ratio less than 0.025% from the test envelope curve (Table 9).

Table 9: Properties of squat walls with axial load from different authors

Researcher	ID	hw (mm)	lw (mm)	tw (mm)	hw /lw	lbe (mm)	ρ_{be} (%)	ρ_v (%)	ρ_h (%)	f'c MPa	fy_v MPa	Axial Load P (kN)	Keff kN/mm
Carrillo /Alcocer	MRN100 C	2400	5400	100	0.44	200	8.55	0.29	0.29	16.2	447	135	170
Carrillo /Alcocer	MRN50C	2400	5400	100	0.44	200	5.94	0.14	0.14	16.2	447	135	182
Carrillo /Alcocer	MCN50C	2400	2400	100	1.00	200	7.92	0.14	0.14	17.5	447	60	94
Carrillo /Alcocer	MCN100 C	2400	2400	100	1.00	200	11.40	0.29	0.29	17.5	447	60	117
Carrillo /Alcocer	MCS50C	2400	2400	100	1.00	200	7.92	0.14	0.14	22	447	60	26
Carrillo /Alcocer	MCS100 C	2400	2400	100	1.00	200	11.40	0.29	0.29	22	447	60	48
Carrillo /Alcocer	MCN50C -2	2400	2400	100	1.00	200	8.55	0.14	0.14	20	447	60	94
Carrillo /Alcocer	MCS50C -2	2400	2400	100	1.00	200	8.55	0.14	0.14	27.1	447	60	123
Carrillo /Alcocer	MCN100 D	1920	1920	80	1.00	160	12.38	0.28	0.28	24.7	435	38.4	83
Greifenhagen	M4	610	900	80	0.68	N/A	0.00	0.32	0.26	24.4	504	76	288
Terzioglu	SWT1N5 S1-10	750	1500	120	0.50	130	5.16	0.34	0.34	26.3	572	240	609
Terzioglu	SWT1N1 0S1-11	750	1500	120	0.50	130	5.16	0.34	0.34	27	572	480	925
Hwang/Sheu	SWN-1D	500	1000	100	0.5	N/A	0	0.40	0.54	26.7	468	320	248
Hwang/Sheu	SWN-5D	750	1000	100	0.75	N/A	0	0.40	0.55	28.0	468	337	241
Hirosawa	72	1600	1700	160	0.94	170	5.68	0.52	0.26	17.3	407	534	453
Hirosawa	73	1600	1700	160	0.94	170	5.68	0.52	0.26	20.8	407	534	401
Hirosawa	74	1600	1700	160	0.94	170	5.68	0.52	0.52	20.8	407	534	514
Hirosawa	75	1600	1700	160	0.94	170	5.68	0.52	0.52	13.7	407	534	423

Table 10: Properties of squat walls with axial load from different authors. (Cont)

Hirosawa	76	1600	1700	160	0.94	170	5.68	0.52	1.04	14.7	407	534	433
Hirosawa	77	1600	1700	160	0.94	170	5.68	0.52	1.04	18.3	407	534	479
Salonikios	LSW3	1200	1200	100	1.00	240	1.29	0.28	0.28	23.9	610	201	76
Park	S1	1500	1500	200	1.00	300	9.70	0.66	0.51	46.5	653	970	656
Park	S2	1500	1500	200	1.00	300	9.70	0.66	0.70	46.5	653	970	698
Park	S3	1500	1500	200	1.00	300	9.70	0.66	0.51	70.3	653	1470	633
Park	S5	1500	1500	200	1.00	200	9.70	0.36	0.25	46.1	653	970	449
Park	S6	1500	1500	200	1.00	200	9.70	0.36	0.25	70.3	653	1470	570
Park	S7	1500	1500	200	1.00	200	9.70	0.36	0.25	46.5	653	970	582

Like in previous section, several parameters and their combinations were evaluated to identify their impact on the effective stiffness of the walls with axial loads. Figures 48 (a) to (c) show a matrix with variables located in the diagonal and plots relating each variable with others. Row one of the matrix shows how each variable is related with effective stiffness. The variables that follow a defined behavior pattern are those of greatest interest for the development of an equation that to predict effective stiffness. Variables that follow a behavior pattern are highlighted with a red square.

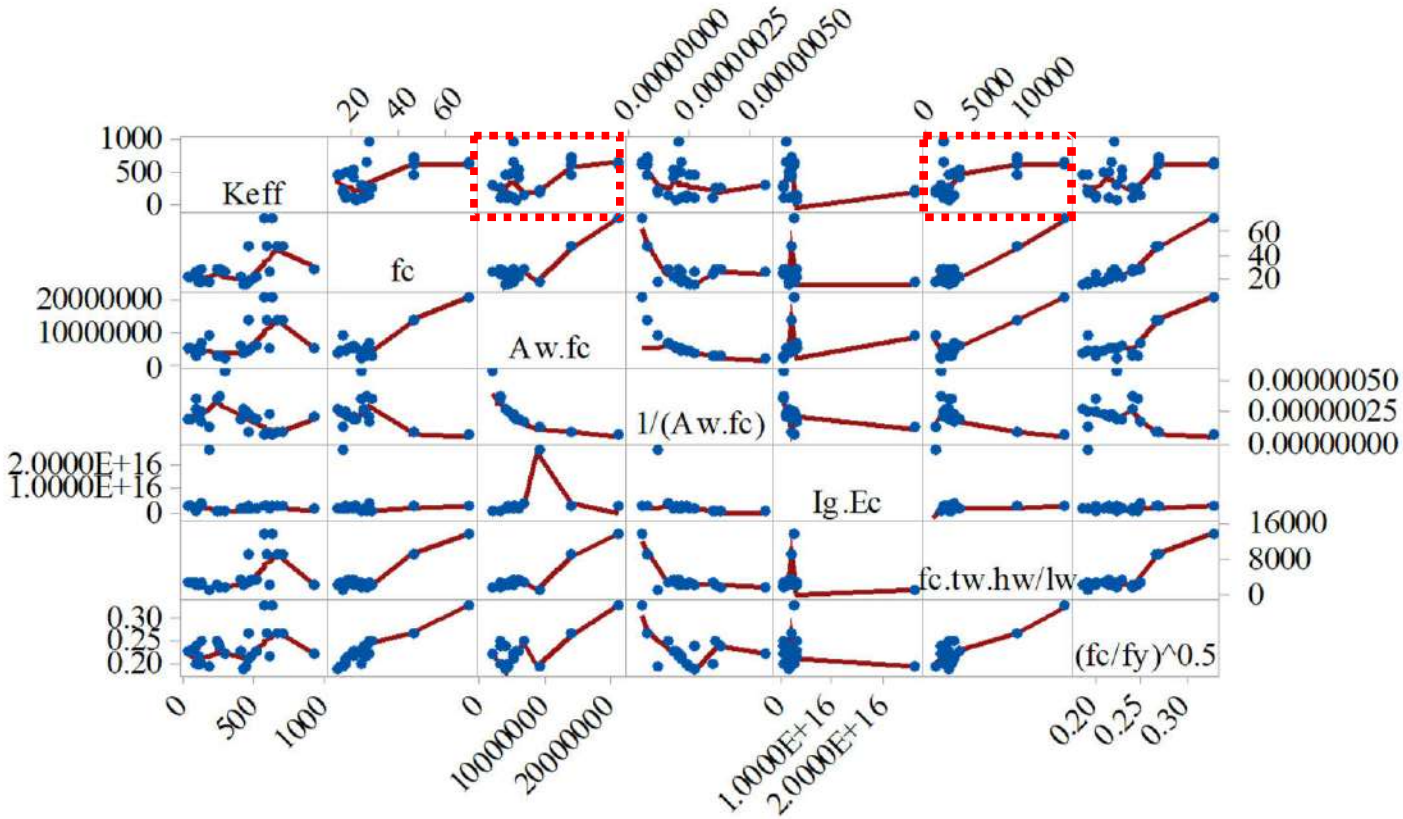

Figure 48. a) Variables and their impact on the effective stiffness of walls with axial load.

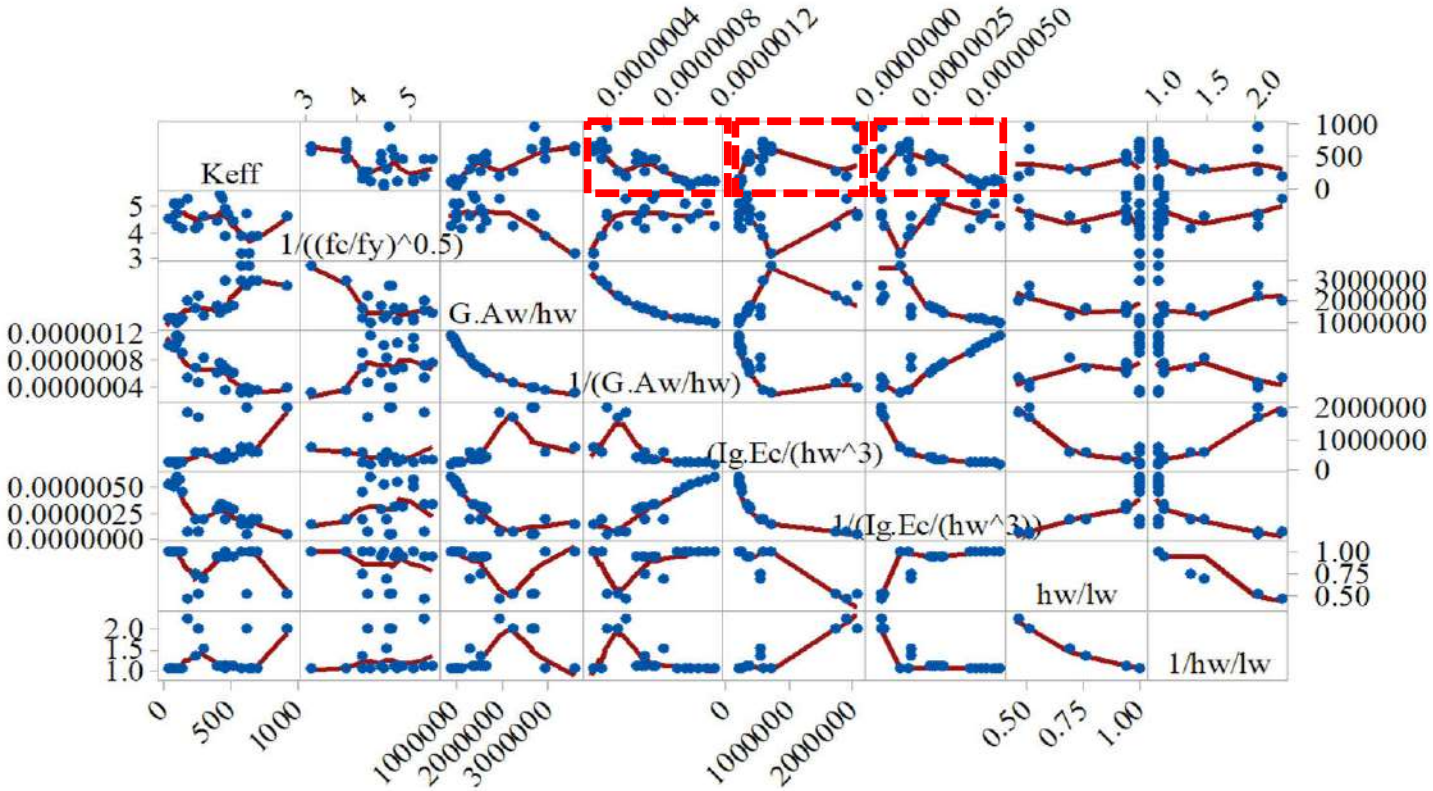

Figure 48. b) Variables and their impact on the effective stiffness of walls with axial load (Cont)

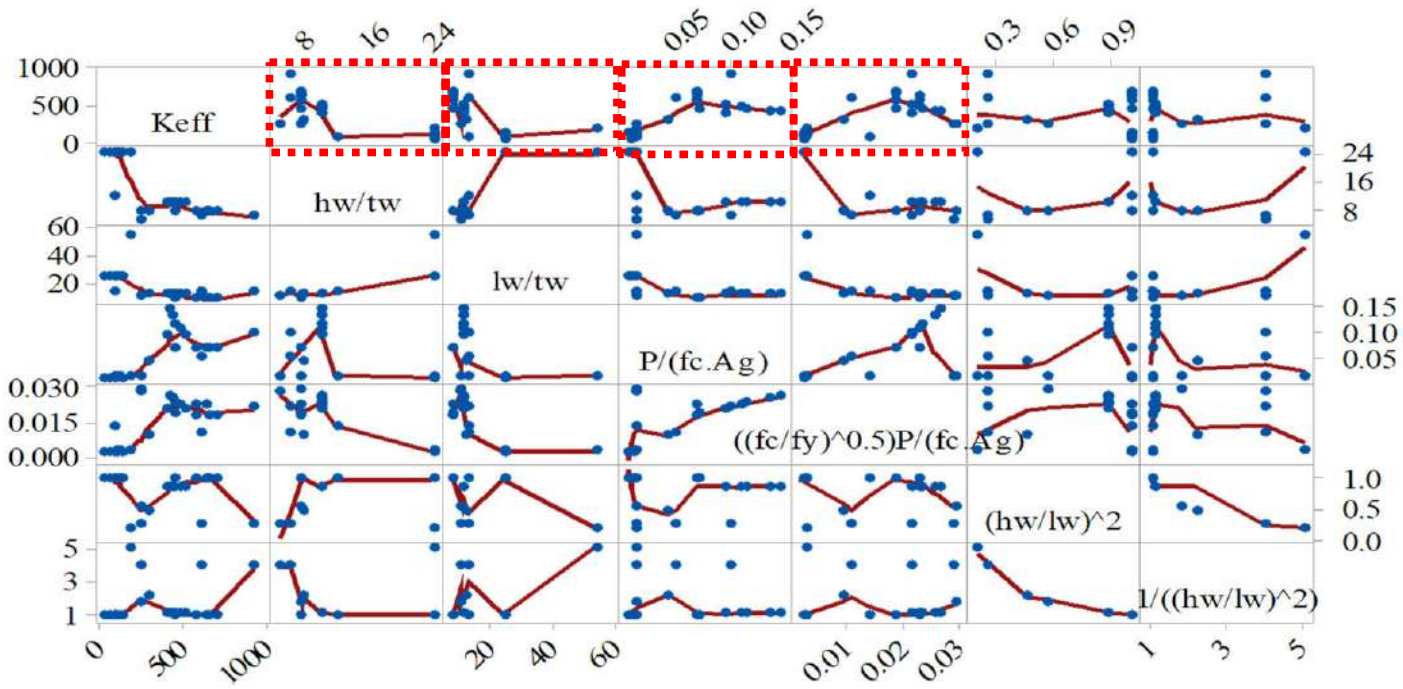

Figure 48. c) Variables and their impact on the effective stiffness of walls with axial load. (Cont)

Like in the previous section, the Pearson's correlation coefficient ("R" using Equation 45) and a P-value were calculated for each variable. As was explained before, when the value of R is close to -1 or +1 means a good correlation between effective stiffness and the variable. On the other hand, a P-value less than α=0.05 confirm the relationship between the variable and effective stiffness. These values are presented in Table 10.

Table 11: Correlations and P-values for variables

Variable	Correlation Coefficient	P-Value
f'c	0.507	0.007
Aw.fc	0.485	0.010
1/(Aw.fc)	-0.378	0.052
Ig*Ec	-0.232	0.244
fc.tw.hw/lw	0.532	0.004
(fc/fy)^0.5	0.427	0.026
1/((fc/fy)^0.5)	-0.411	0.033
G.Aw/hw	0.785	0.001
1/(G.Aw/hw)	-0.813	0.001
(Ig.Ec/(hw^3)	0.344	0.079
1/(Ig.Ec/(hw^3)	-0.664	0.001
hw/lw	-0.108	0.593
1/(hw/lw)	0.084	0.678
hw/tw	-0.783	0.001
lw/tw	-0.562	0.002
ρv/ρh	0.208	0.298
P/(fc.Ag)	0.565	0.002
((fc/fy)^0.5)P/(fc.Aw)	0.65	0.001
(hw/lw)^2	-0.116	0.564
1/((hw/lw)^2)	0.068	0.736

3.3.2 Determination of equations for walls with axial load

Using the software Minitab V18 (2017), two equations were determined by applying multiple regression analysis techniques to determine the factors and parameters that better match the effective stiffness. The program selects a combination of variables and its coefficients that better

correlate with the experimental values. Each variable must have a P-value less than α=0.05. Several equations can be determined combining the variables in several ways making this method an iterative process. Equations 49 and 50 were determined using the variables in Table 10 and its combinations. Table 11 presents the Pearson's correlation and P-values obtained for Equations 1 and 2. They show a good Pearson's correlation coefficient over 96%. Figures 49 and 50 show the residual equation plots that comply with almost a straight line in the Normal Probability Plot. A random distribution is noticed in the Residual vs Fitted Value and with Observation Order plots. An approximated bell form in the Histogram plots is observed.

Regression Equation C

$$keff = \frac{149}{10^6}\frac{G\ Aw}{w} + 2233\frac{P}{f'c\ Ag} \quad 3.1\frac{lw}{tw} \tag{49}$$

Regression Equation D

$$keff = \frac{G\ Aw}{10^6\ \ w}\left(\frac{1487\ P}{f'c\ Aw} + \frac{34}{10^6}\sqrt{\frac{fy}{f'c}} \quad \frac{4.2}{10^6}\right) \tag{50}$$

Table 12: Summary of goodness-of-fit statistics for Keff equations of walls with axial load

No.	S	R-sq	R-sq(adj)	R-sq(pred)
49	69.38	97.30%	96.95%	96.56%
50	61.67	97.87%	97.59%	97.18%

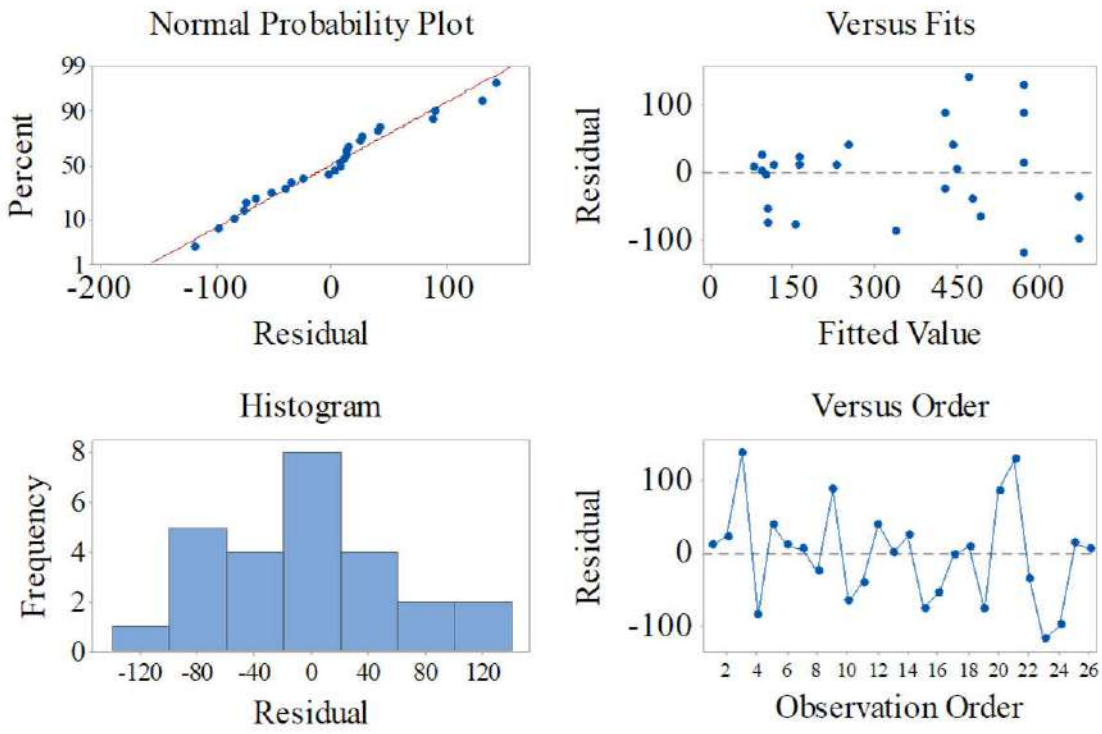

Figure 49. Residual plots for keff EQ 49 for walls with axial loads

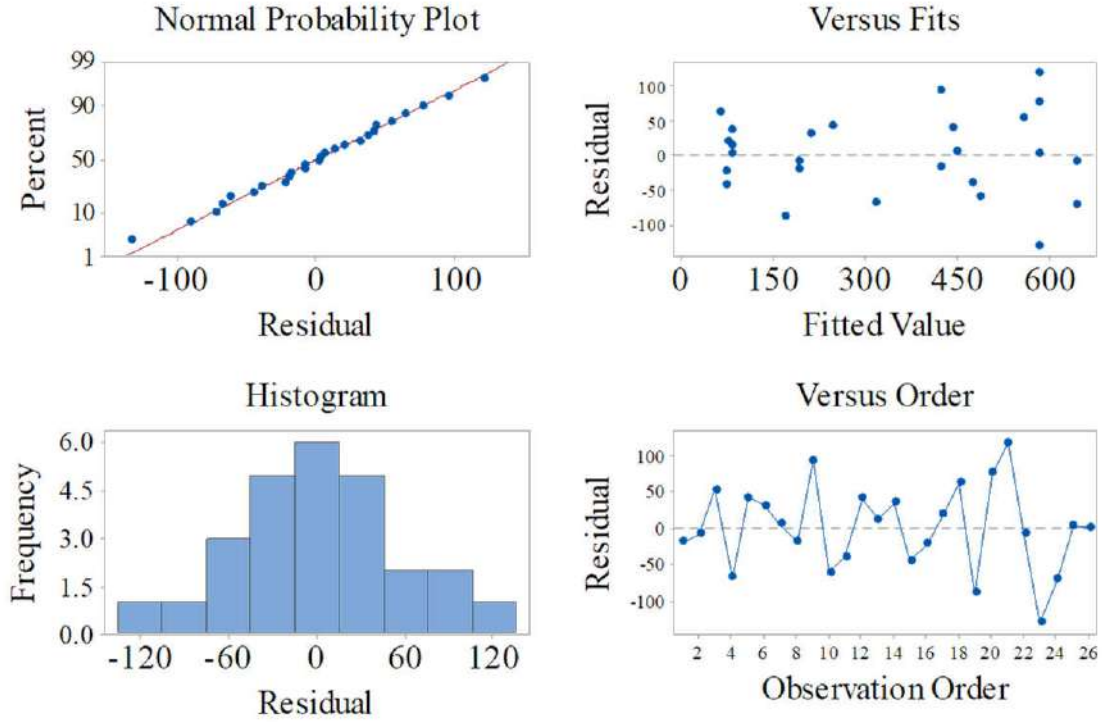

Figure 50. Residual plots for keff EQ 50 for walls with axial loads

3.3.3 Comparison of prediction of the effective stiffness

Similar to the equation for the walls without axial loads, the new equations for walls with axial loads were compared with the theoretical effective stiffness using equations (40-43) and the reduction factors recommended by Luna (2015), ASCE (2005-2013), FEMA 356 (2000), ACI-318 (2014) and ASCE 41-17(2017) summarized in Table 7. Effective stiffness was calculated for each wall in the database described in Table 9. Figure 51 shows the prediction from the mentioned standards and researchers compared with the experimental results. Similar to previous results, the diagonal line represents a ratio of predicted-to-experimental stiffness of 1.0. Any point falling on the line means an exact prediction of the shear strength. Any point above the diagonal line represents an over-prediction of stiffness and vice-versa. The farther the point is from the diagonal the larger the error on the estimate. It can be noted from Figure 51 that all the equations or factors produced significant scatter in the results. Figures 52 to 53 show the prediction from the developed Equations 49 and 50 compared with the experimental results, showing that the scatter in the results is significantly reduced.

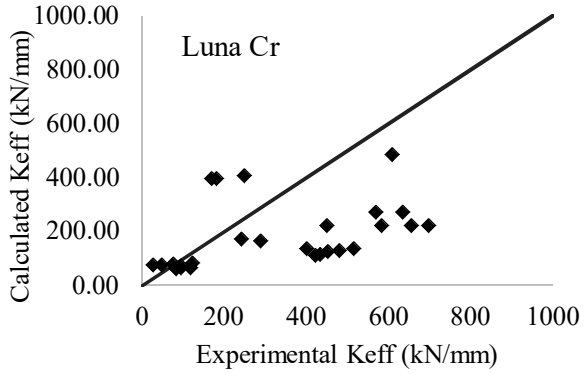

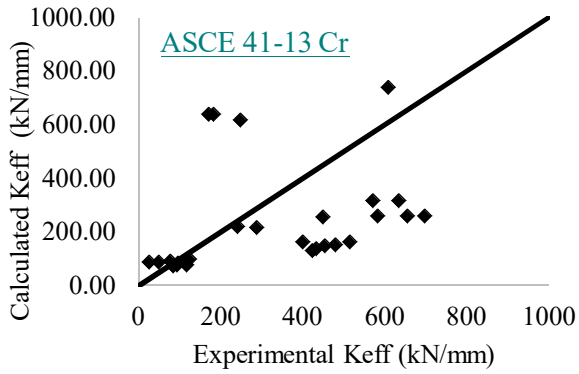

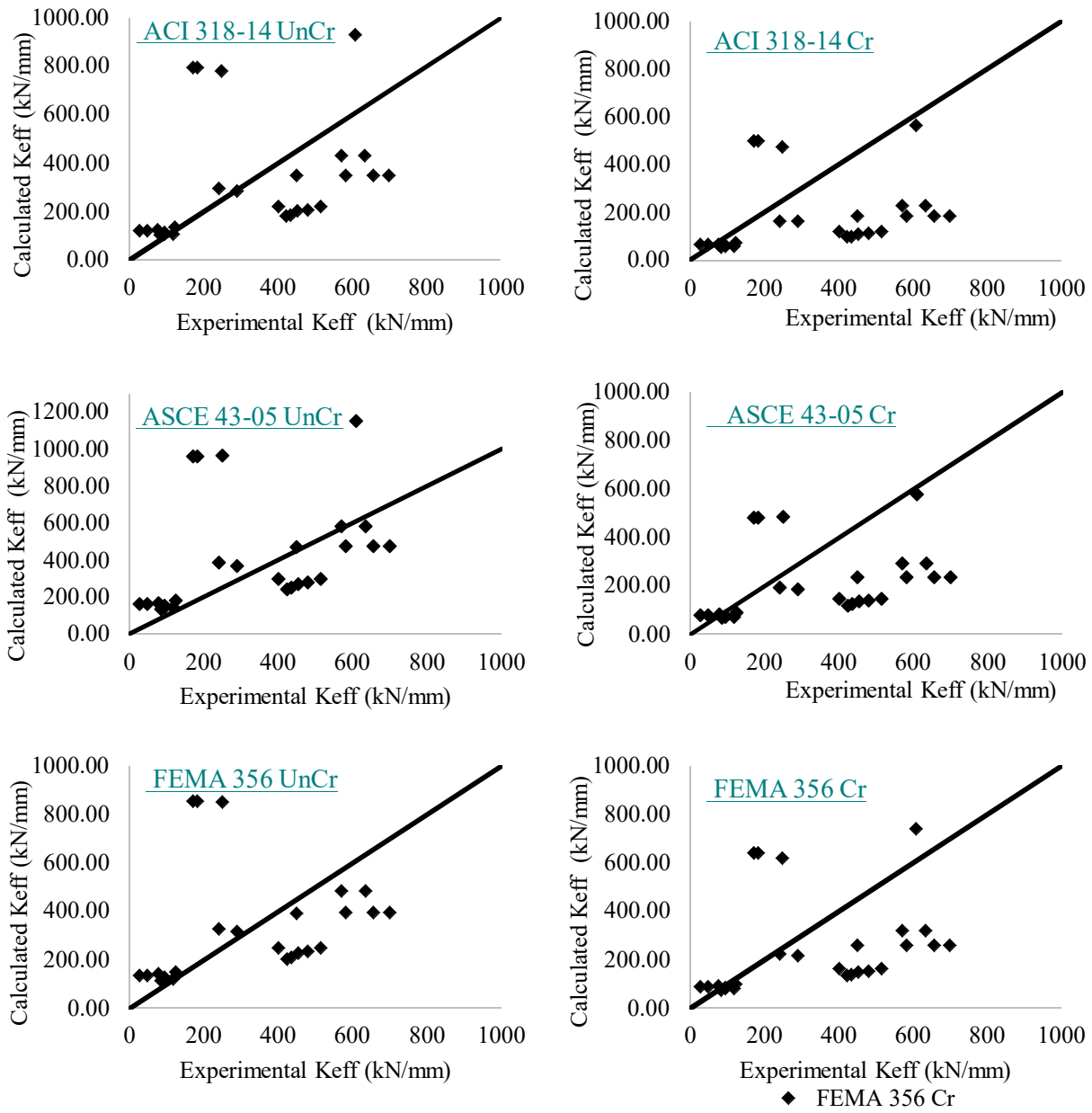

Figure 51. Keff Prediction other researchers and standards for walls with axial loads

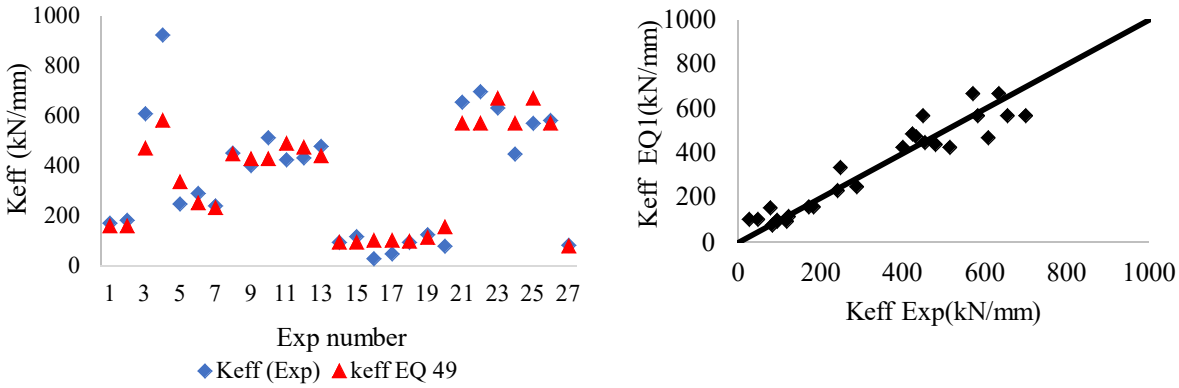

Figure 52. Keff prediction for Equation 49 for walls with axial loads

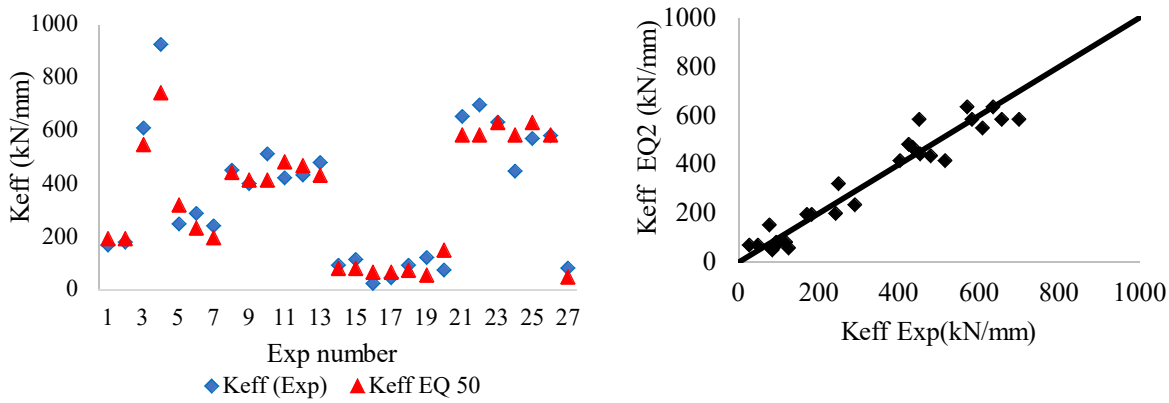

Figure 53. Keff prediction for Equation 50 for walls with axial loads

A correlation analysis was conducted relating effective stiffness determined by codes, standards and Equations 49 and 50 determined by multivariable analysis and experimental effective stiffness. The results of this analysis are shown in Figure 54. Equation 49 and 50 have similar correlations, very close to 1.0. The correlation with the experimental data obtained with the different codes/researchers is very low for wall with axial loads.

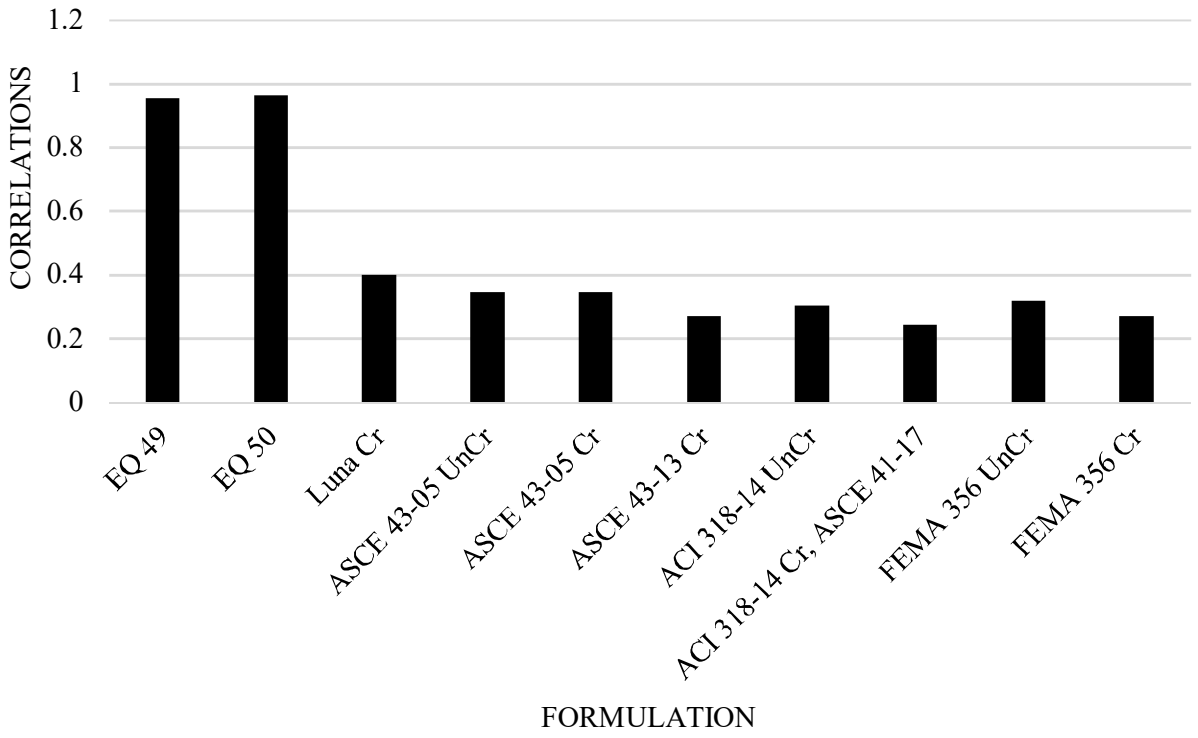

Figure 54. Correlation vs Equations for walls with axial load

A descriptive statistical analysis was conducted to determine the goodness of the predictions from the proposed equations and those standards/researchers. Table 12 shows the results from this analysis. The statistics are in terms of the experimental to predicted stiffness ratios. As shown in Table 12, the mean value of Equations 49 and 50 are close to 1.0 as well as the median value. Morover, the coefficient of variation (CoefVar) and standard deviation (StDev) that show that the smallest dispersions correspond to Equations 49 and 50. Despite that the two proposed equations give a good estimation of the effective stiffness for squat wall with axial loads, Equation 49 statistically gives better results than Equation 50. A box and whisker diagram is shown in Figure 55, this diagram indicates the statistical behavior of each equation compared with experimental results. As it is shown the median value marked with "•" and the mean value marked with " " of Equations 1 and 2 are very close to 1. The inter-quartile range (IQR box in the graph) is very small, indicating few variabilities of central 50% of the observations compared to the median value. According to Table 12, the standards that have statistically good predictions are the ASCE 43-05 UnCr with a mean value of 0.912 and a median of 0.787 with the lower standard deviation of the

codes. FEMA 356 UnCr also have a good mean value and median close to 1.0 with a standard deviation of 0.654. The worst results are obtained with ACI 318-14 Cr with mean and median closer to 2.0 and with the highest standard deviation value of 1.393.

Table 13: Statistics of the experimental to predicted stiffness ratios for walls with axial load

Exp/Prediction	Mean	SE Mean	StDev	Variance	CoefVar	Minimum	Median	Maximum
EQ 49	0.965	0.049	0.251	0.063	0.260	0.254	1.018	1.297
EQ 50	1.055	0.069	0.354	0.1251	0.335	0.371	1.010	2.153
Luna Cr	1.974	0.225	1.148	1.318	0.582	0.339	1.729	3.748
ASCE 43-05 UnCr	0.912	0.106	0.539	0.291	0.591	0.159	0.787	1.740
ASCE 43-05 Cr	1.825	0.212	1.079	1.163	0.591	0.317	1.574	3.481
ASCE 41-13 Cr	1.651	0.196	0.999	0.998	0.605	0.266	1.395	3.168
ACI 318-14 UnCr	1.229	0.144	0.736	0.542	0.599	0.215	1.047	2.352
ACI 318-14 Cr	2.284	0.273	1.393	1.94	0.610	0.342	1.915	4.392
FEMA 356 UnCr	1.097	0.128	0.654	0.428	0.596	0.192	0.939	2.097
FEMA 356 Cr	1.651	0.196	0.999	0.998	0.605	0.266	1.395	3.168

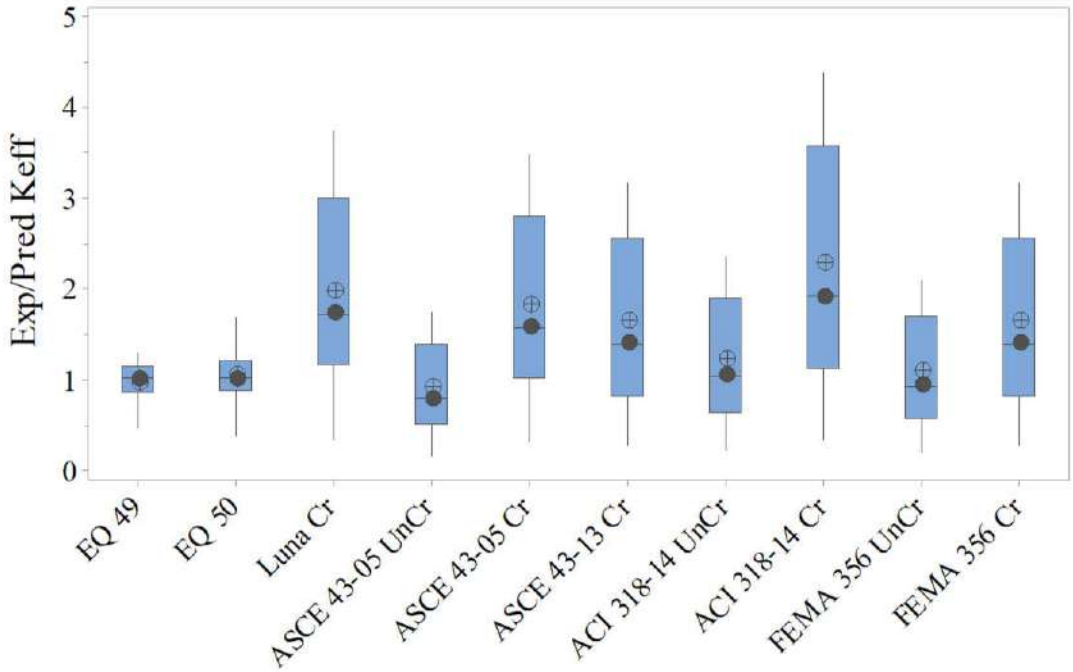

Figure 55. Box and whisker Diagram for walls with axial load.

3.4 Secant stiffness equation for squat walls at peak strength

Secant stiffness is an important parameter for designing structures using the displacement-based design method (Sullivan et al. 2004). In this method, the structure is characterized by the secant stiffness and the equivalent damping ratio of an equivalent single degree of freedom structure. Taking this into account, two equations for the estimation of the secant stiffness for squat walls are proposed: one equation for the estimation of secant stiffness for walls without axial load and walls with axial load.

3.4.1 Walls without axial load with and without boundary elements.

To determine the secant stiffness equation for squat walls without axial loads, a data for 32 different squat walls from different authors were used from the database assembled by Adorno-Bonilla (2013). The secant stiffness for each of these walls were calculated at peak strength and its respectively displacement from test envelope curve (Table 13).

Figures 56(a) to 56(c) show the variables and their combinations that have a considerable impact on the secant stiffness of the walls. The ones that follow a pattern are those who also have a good correlation (close to -1 or 1) and a P-value much lower than 0.05 according to Table 14. These variables are highlighted in Figures 56 (a) to (c) and in Table 14. The variables that have more impact on the secant stiffness are related to the geometry of the wall; hw/tw, hw/lw, Ig.Ec/(hw)^3 (related to the flexural stiffness), and GAw/hw (related to the shear stiffness).

Table 14: Properties for walls without axial loads by author for secant stiffness at peak.

Researcher	ID	hw (mm)	lw (mm)	tw (mm)	hw/lw	lb (mm)	ρ_{be} (%)	ρ_v (%)	ρ_h (%)	f'c (MPa)	fy_v (MPa)	Ksec (kN/mm)
Terzioglu	SWT2S1-1	750	1500	120	0.50	130	5.16	0.67	0.67	19.3	473	108.75
Terzioglu	SWT1S1-2	750	1500	120	0.50	130	5.16	0.34	0.34	23.7	473	111.67
Terzioglu	SWT2S2-3	750	1500	120	0.50	130	5.16	0.67	0.67	25.8	473	88.41
Terzioglu	SWT2S3-4	750	1500	120	0.50	130	5.16	0.67	0.67	29	572	134.06

Terzioglu	SWT3S1-5	750	1500	120	0.50	80	1.05	0.67	0.67	32.1	572	142.98
Terzioglu	SWT4S1-6	500	1500	120	0.33	130	3.95	0.67	0.67	34.8	572	352.93
Terzioglu	SWT5S1-7	1500	1500	120	1.00	130	9.75	0.34	0.67	35	572	66.99
Terzioglu	SWT6S1-8	1500	1500	120	1.00	130	9.75	0.67	0.67	22.6	572	54.06
Terzioglu	SWT1S2-9	750	1500	120	0.50	130	5.16	0.34	0.34	24	572	123.53
Wiradinata	Wall 2	500	2000	100	0.25	320	1.25	0.71	0.21	22.0	435	381.83
Wiradinata	Wall 1	1000	2000	100	0.50	320	1.25	0.71	0.21	25.0	435	67.15
Pilette	Wall4	1000	2000	100	0.50	320	1.25	0.71	0.80	33	480	56.63
Pilette	Wall 5	1000	2000	100	0.50	250	1.60	1.15	1.15	27	480	39.03
Synge	Wall 1	1500	3000	100	0.50	200	2.26	0.81	1.68	27.2	300	116.00
NEES-UB	SW1	2865	3048	203	0.94	0	0	0.71	0.71	24.8	462	30.21
NEES-UB	SW2	1646	3048	203	0.54	0	0	0.96	0.96	48.3	434	129.93
NEES-UB	SW3	1646	3048	203	0.54	0	0	0.71	0.71	53.8	434	80.50
NEES-UB	SW4	1646	3048	203	0.54	0	0	0.34	0.34	29	462	84.71
NEES-UB	SW5	1006	3048	203	0.33	0	0	0.96	0.96	29.7	462	255.84
NEES-UB	SW6	1006	3048	203	0.33	0	0	0.71	0.71	26.2	462	268.02
NEES-UB	SW7	1006	3048	203	0.33	0	0	0.34	0.34	26.2	462	305.90
NEES-UB	SW8	1646	3048	203	0.54	0	0	1.50	1.50	24.1	462	234.00
NEES-UB	SW9	1646	3048	203	0.54	0	0	1.50	0.71	29.7	462	245.75
NEES-UB	SW10	1646	3048	203	0.54	0	0	1.50	0.34	31.7	462	251.31
NEES-UB	SW11	1646	3048	203	0.54	380	1.54	0.71	0.71	34.5	462	167.79
NEES-UB	SW12	1646	3048	203	0.54	380	2.06	0.34	0.34	34.5	462	99.08
Whyte	Wall 1	1646	3048	203	0.54	0	0	0.71	0.71	35.5	464	123.58
Whyte	Wall 2	1646	3048	203	0.54	0	0	0.71	0.71	37.3	464	138.27
Doostdar	Wall 7	1500	2000	100	0.75	320	1.25	0.71	0.80	45.0	450	49.97
Doostdar	Wall 8	1500	1500	100	1.00	360	1.11	0.70	0.80	45.0	450	16.80
Salonikios	LSW1	1200	1200	100	1.00	240	1.73	0.57	0.42	22.2	610	43.37
Salonikios	LSW2	1200	1200	100	1.00	240	1.29	0.28	0.28	21.6	610	34.83

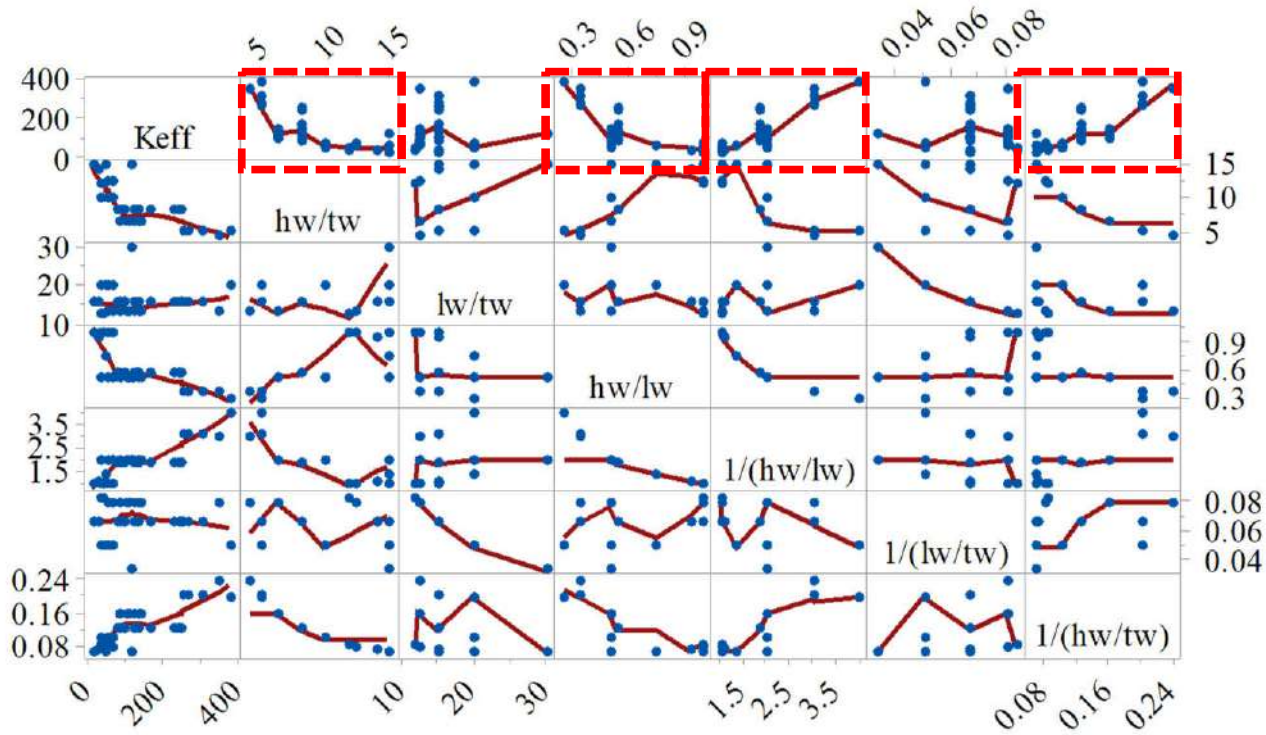

Figure 56 (a). Variables and their impact on the secant stiffness of squat walls without axial load.

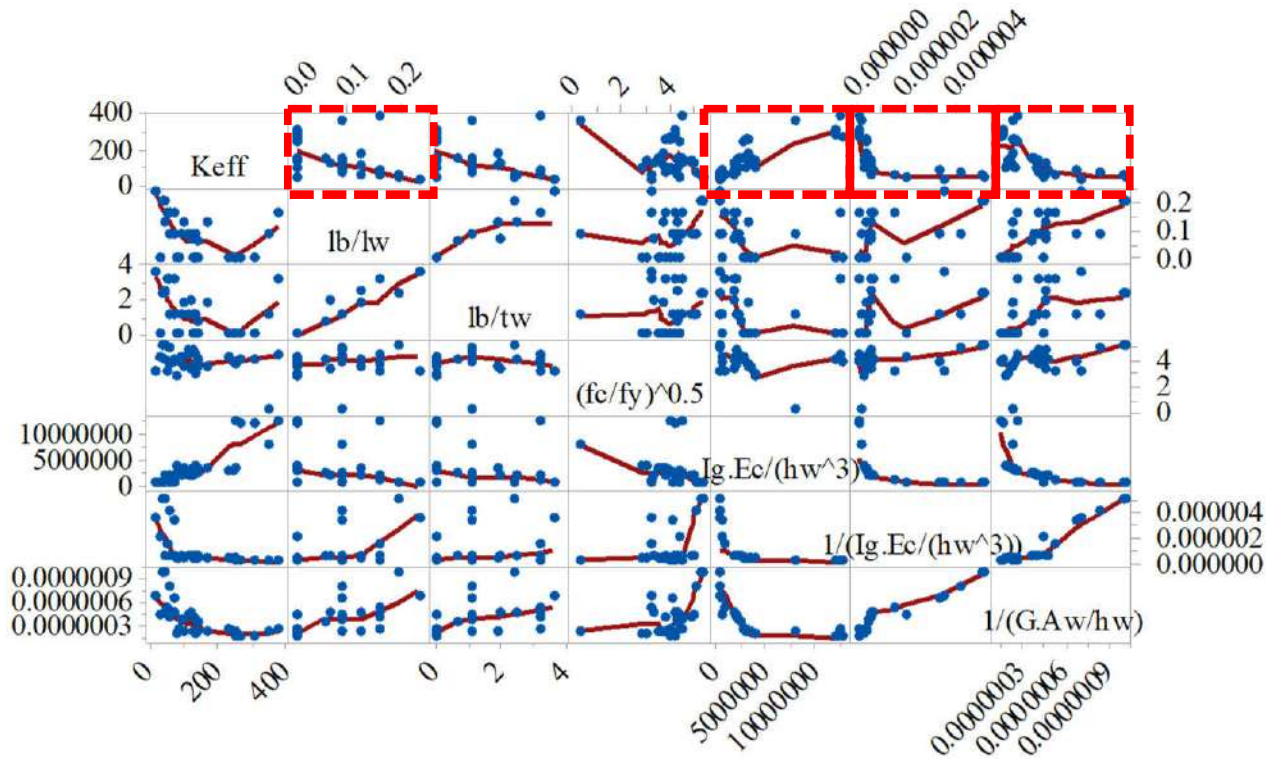

Figure 56 (b). Variables and their impact on the secant stiffness of squat walls without axial load (Cont)

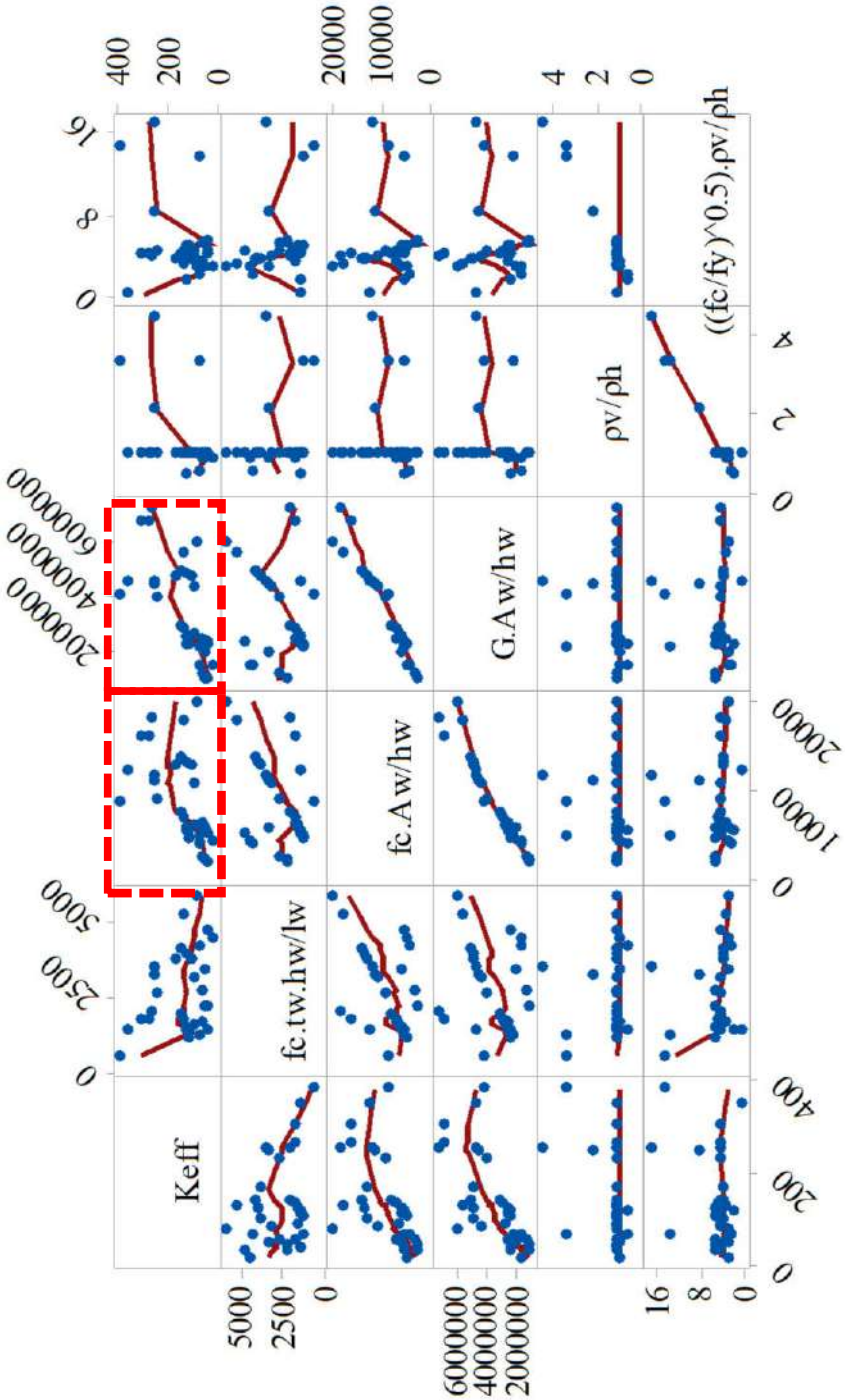

Figure 56(c). Variables and their impact on the secant stiffness of squat walls without axial load (Cont).

Table 15: Correlations and P-values for variables for Ksec of walls without axial loads

Variable	Correlations	P-Value
hw/tw	-0.701	0.001
lw/tw	-0.005	0.979
hw/lw	-0.701	0.001
1/(hw/lw)	0.832	0.001
1/(lw/tw)	-0.048	0.795
1/(hw/tw)	0.793	0.001
lb/lw	-0.395	0.025
lb/tw	-0.341	0.056
(fc/fy)^0.5	-0.295	0.101
Ig.Ec/(hw^3)	0.826	0.001
1/(Ig.Ec/(hw^3))	-0.538	0.001
1/(G.Aw/hw)	-0.621	0.001
fc.tw.hw/lw	-0.307	0.087
fc.Aw/hw	0.537	0.002
G.Aw/hw	0.665	0.001
ρv/ρh	0.384	0.030
((fc/fy)^0.5).ρv	0.297	0.099

Regression Equation E

$$Ksec = 410.2\left(\frac{lw\ tw}{w^2}\right) + 31.4\frac{\rho v}{\rho} \quad 14.29\frac{lb}{tw} \tag{51}$$

Regression Equation F

$$Ksec = 373.7\left(\frac{lw\ tw}{w^2}\right) + 0.002587\ \frac{f'c\ Aw\ \rho v}{w\ \rho} \tag{52}$$

Table 16: Summary of goodness-of-fit statistics for Ksec equations of walls without axial load

No.	S	R-sq	R-sq(adj)	R-sq(pred)
51	43.30	93.99%	93.37%	92.64%
52	20.07	96.55%	96.31%	94.89%

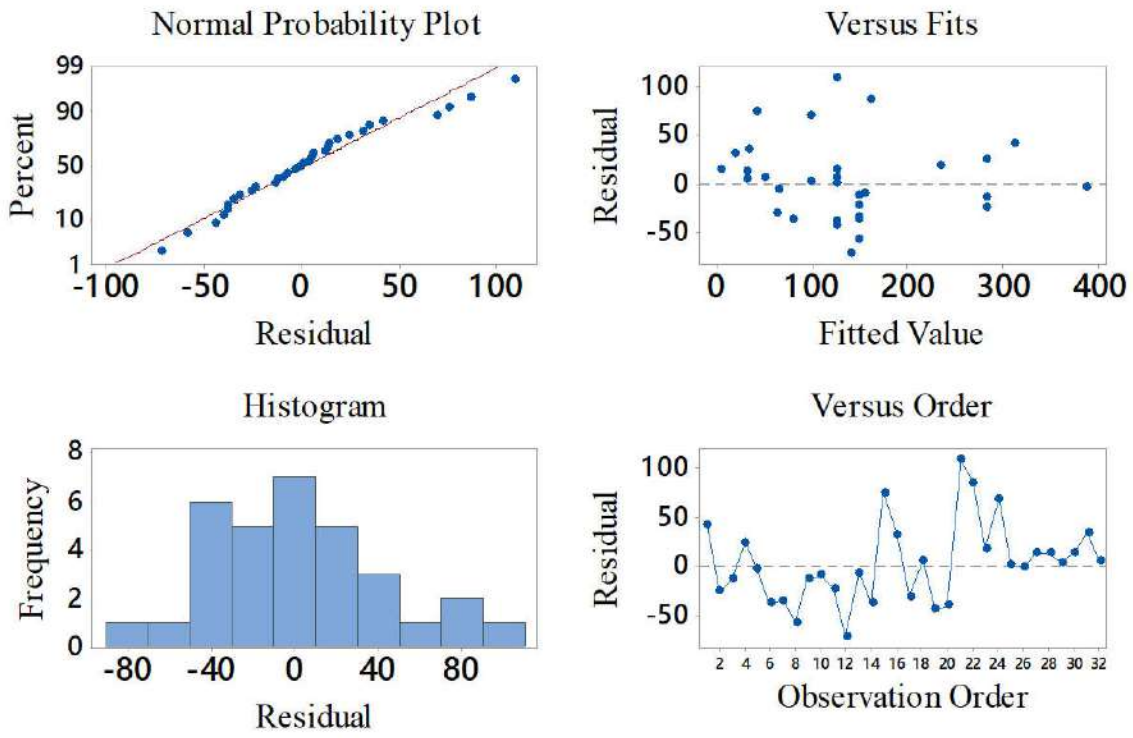

Figure 57. Residual plots of Ksec obtained with EQ1

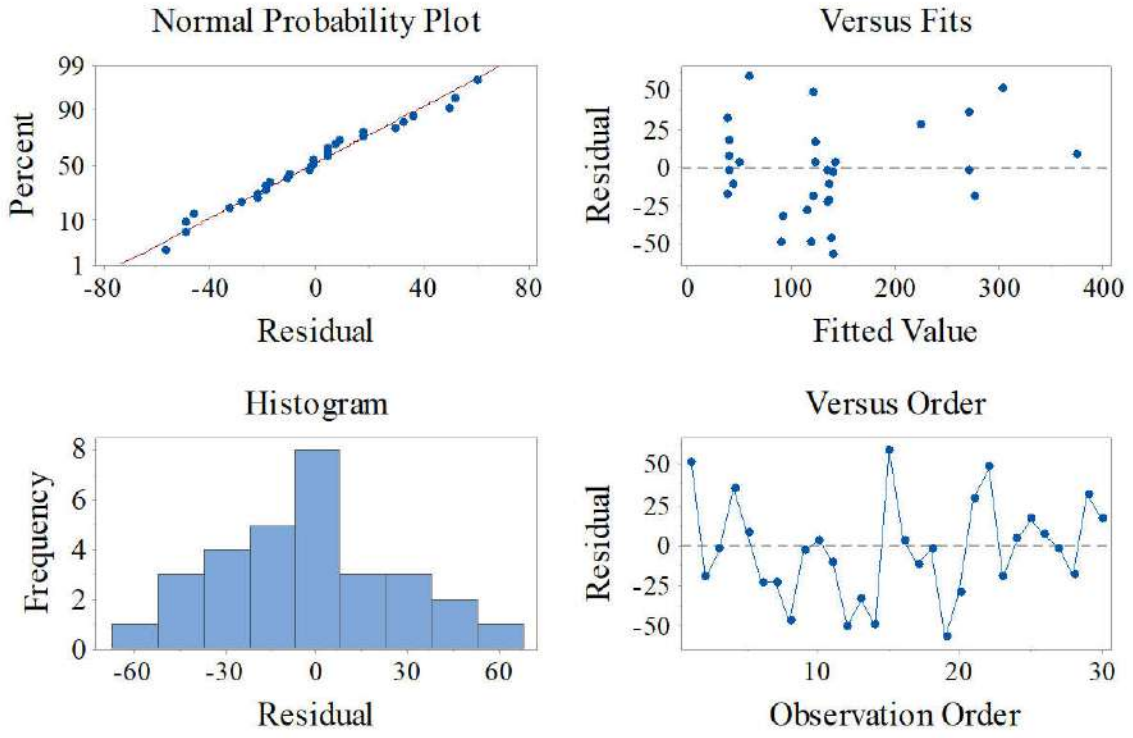

Figure 58. Residual plots of Ksec obtained with EQ2

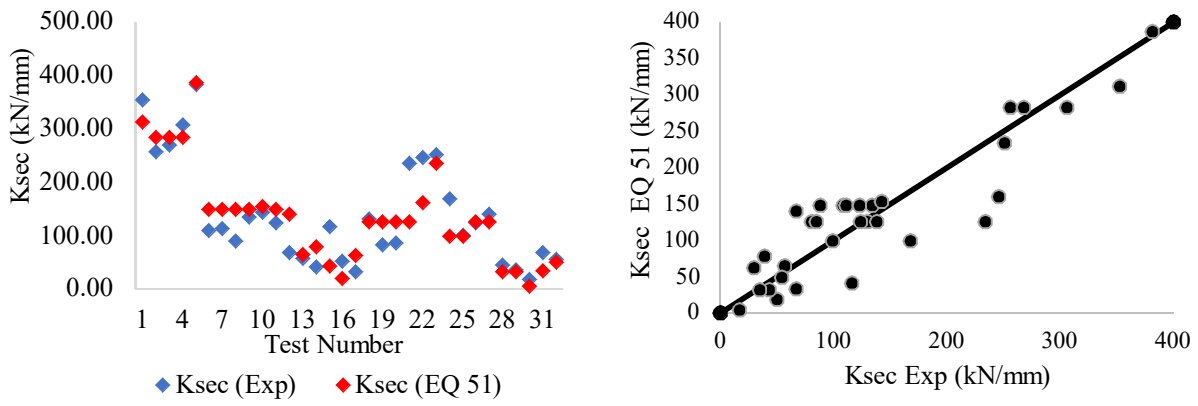

Figure 59. Ksec prediction of Equation 51 for walls without axial loads

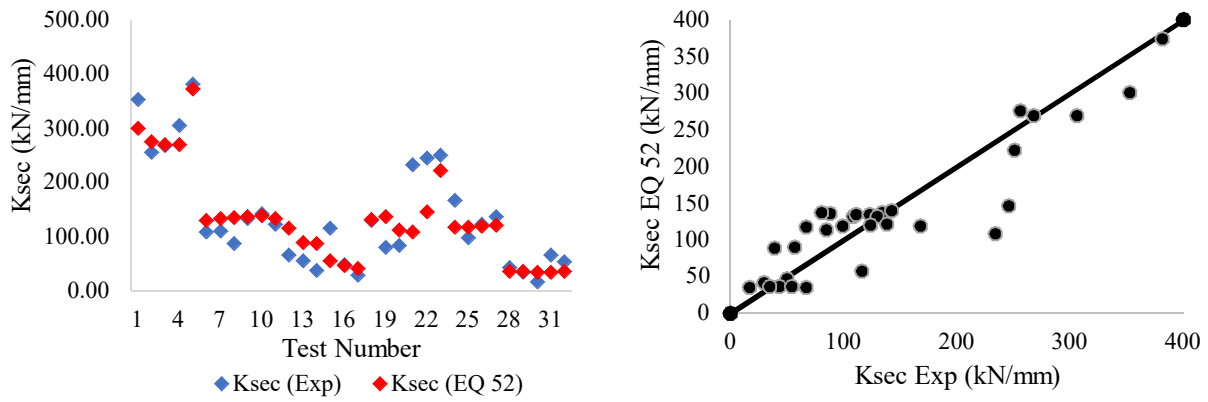

Figure 60. Ksec prediction of Equation 52 for walls without axial loads

3.4.2 Walls with axial load and with boundary element.

To determine the secant stiffness equation for squat walls with axial load with boundary elements (lb) a data of 25 different squat walls from different authors were used. The data is shown in Table 16 which was obtained from the assembled database of Adorno-Bonilla (2013).

Table 17. Properties for walls with axial loads by author for Ksec at peak.

Researcher	ID	hw (mm)	lw (mm)	tw (mm)	hw/lw	lbe (mm)	ρ_{be} (%)	ρ_v (%)	ρ_h (%)	f'c (MPa)	fy_v (MPa)	P (kN)	Ksec peak (kN/mm)
Carrillo/Alcocer	MRN100C	2400	5400	100	0.44	200	8.55	0.29	0.29	16.2	447	135	52.75
Carrillo/Alcocer	MRN50C	2400	5400	100	0.44	200	5.94	0.14	0.14	16.2	447	135	40.43
Carrillo/Alcocer	MCN50C	2400	2400	100	1.00	200	7.92	0.14	0.14	17.5	447	60	22.32
Carrillo/Alcocer	MCN100C	2400	2400	100	1.00	200	11.40	0.29	0.29	17.5	447	60	23.35
Carrillo/Alcocer	MCS50C	2400	2400	100	1.00	200	7.92	0.14	0.14	22	447	60	15.43
Carrillo/Alcocer	MCS100C	2400	2400	100	1.00	200	11.40	0.29	0.29	22	447	60	18.92
Carrillo/Alcocer	MCN50C-2	2400	2400	100	1.00	200	8.55	0.14	0.14	20	447	60	31.51
Carrillo/Alcocer	MCS50C-2	2400	2400	100	1.00	200	8.55	0.14	0.14	27.1	447	60	33.81
Terzioglu	SW-T1-N5-S1-10	750	1500	120	0.50	130	5.16	0.34	0.34	26.3	572	240	131.58
Terzioglu	SW-T1-N10-S1-11	750	1500	120	0.50	130	5.16	0.34	0.34	27	572	480	132.80
Hirosawa	72	1600	1700	160	0.94	170	5.68	0.52	0.26	17.3	407	534	94.14
Hirosawa	73	1600	1700	160	0.94	170	5.68	0.52	0.26	20.8	407	534	68.74
Hirosawa	74	1600	1700	160	0.94	170	5.68	0.52	0.52	20.8	407	534	98.60
Hirosawa	75	1600	1700	160	0.94	170	5.68	0.52	0.52	13.7	407	534	36.97
Hirosawa	76	1600	1700	160	0.94	170	5.68	0.52	1.04	14.7	407	534	95.08
Hirosawa	77	1600	1700	160	0.94	170	5.68	0.52	1.04	18.3	407	534	55.34
Park	S1	1500	1500	200	1.00	300	9.70	0.66	0.51	46.5	653	970	142.42
Park	S2	1500	1500	200	1.00	300	9.70	0.66	0.70	46.5	653	970	153.20
Park	S3	1500	1500	200	1.00	300	9.70	0.66	0.51	70.3	653	1470	169.98
Park	S5	1500	1500	200	1.00	200	9.70	0.36	0.25	46.1	653	970	124.50
Park	S6	1500	1500	200	1.00	200	9.70	0.36	0.25	70.3	653	1470	130.98
Park	S7	1500	1500	200	1.00	200	9.70	0.36	0.25	46.5	653	970	139.42
Salonikios	MSW3	1800	1200	100	1.50	240	1.29	0.28	0.28	24.1	610	202	16.66
Salonikios	LSW3	1200	1200	100	1.00	240	1.29	0.28	0.28	23.9	610	201	50.20
Carrillo/Alcocer	MCN100D	1920	1920	80	1.00	160	12.38	0.28	0.28	24.7	435	38.4	27.14

Figure 61 shows the variables and their combinations that have a considerable impact on the secant stiffness of the walls. The variables that follow a pattern are those who also have a good correlation (close to -1 or 1) and a P-value much lower than 0.05 (Table 17). These variables are highlighted in Figure 61 and in Table 17.

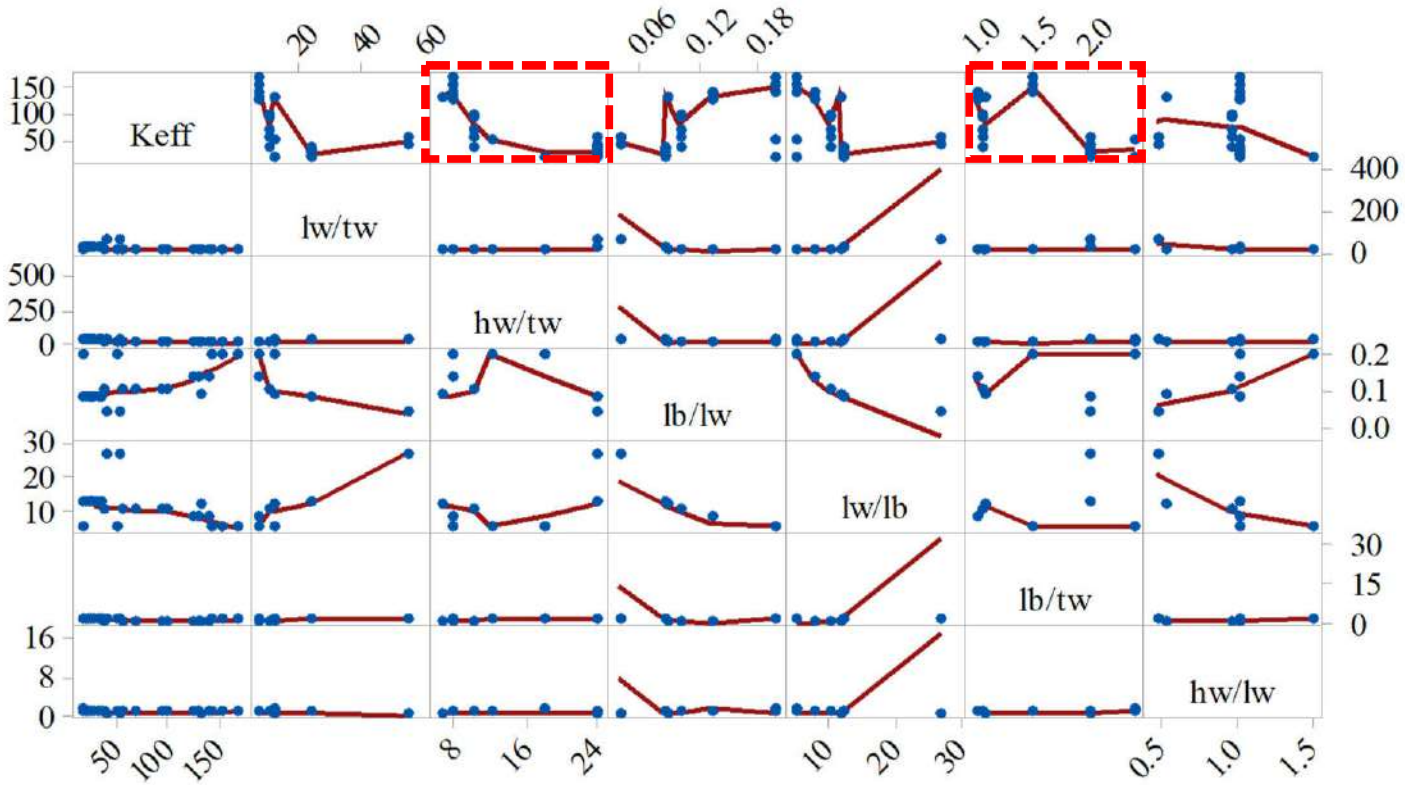

Figure 61 (a). Variables and their impact on the secant stiffness of squat walls with axial load and lb

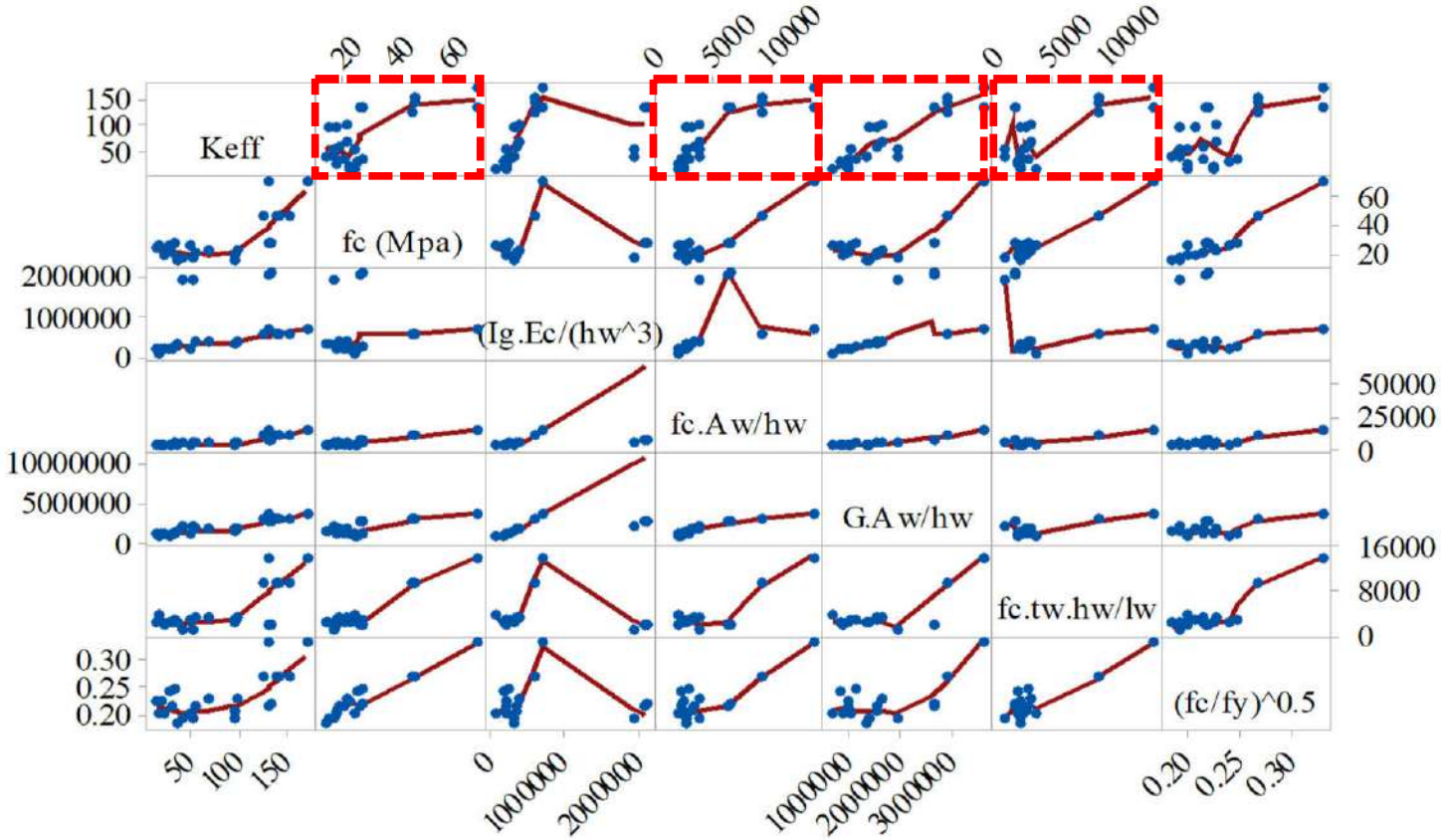

Figure 61(b). Variables and their impact on the secant stiffness of squat walls with axial load and lb (Cont)

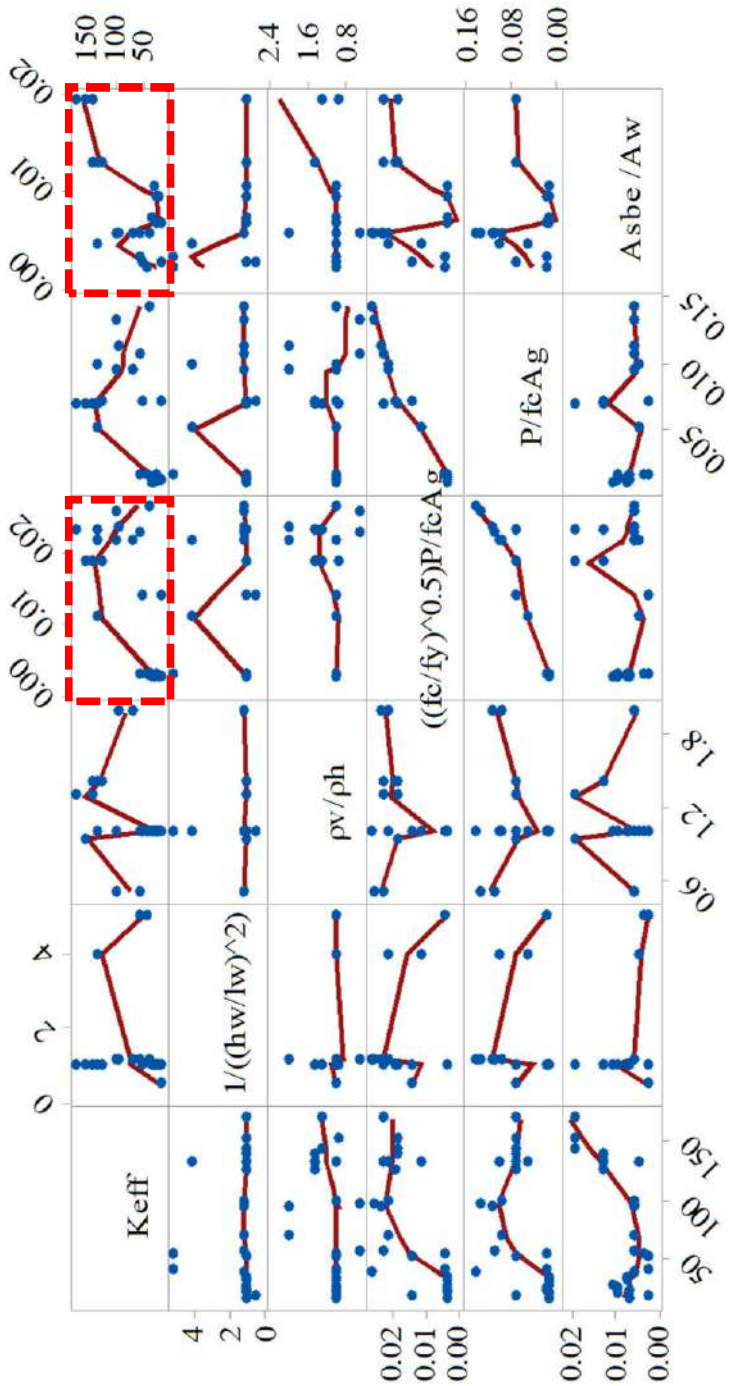

Figure 61(c). Variables and their impact on the secant stiffness of squat walls with axial load and lb (Cont).

Table 18: Correlations and P-values for variables of walls with axial loads and lb

Variable	Correlations	P-Value
lw/tw	-0.544	0.005
hw/tw	-0.842	0.001
lb/lw	0.474	0.017
lw/lb	-0.4	0.047
lb/tw	-0.671	0.001
hw/lw	-0.188	0.369
fc	0.727	0.001
(Ig.Ec/(hw^3)	0.367	0.071
fc.Aw/hw	0.863	0.001
G.Aw/hw	0.919	0.001
fc.tw.hw/lw	0.722	0.001
(fc/fy)^0.5	0.667	0.001
1/((hw/lw)^2)	0.077	0.715
ρv/ρh	0.293	0.155
((fc/fy)^0.5)P/fcA	0.652	0.001
P/fc.Ag	0.452	0.023
As.be /Aw	0.609	0.001

Regression Equation G

$$Ksec = \frac{0.000072\ G.Aw}{w} \quad 1.284\frac{lw}{tw} \quad \frac{0.007\ f'c.Aw}{w} \tag{53}$$

Regression Equation H

$$Ksec = 365.2\frac{lb}{lw} \quad \frac{0.000049\ G.Aw}{w} \quad 25.24\frac{lb}{tw} \quad \frac{0.00382\ f'c.tw.\ \ w}{lw} \tag{54}$$

Table 19: Summary of goodness-of-fit statistics for Ksec equations of walls with axial load

No.	S	R-sq	R-sq(adj)	R-sq(pred)
53	14.44	97.80%	97.50%	96.86%
54	14.69	97.82%	97.41%	96.99%

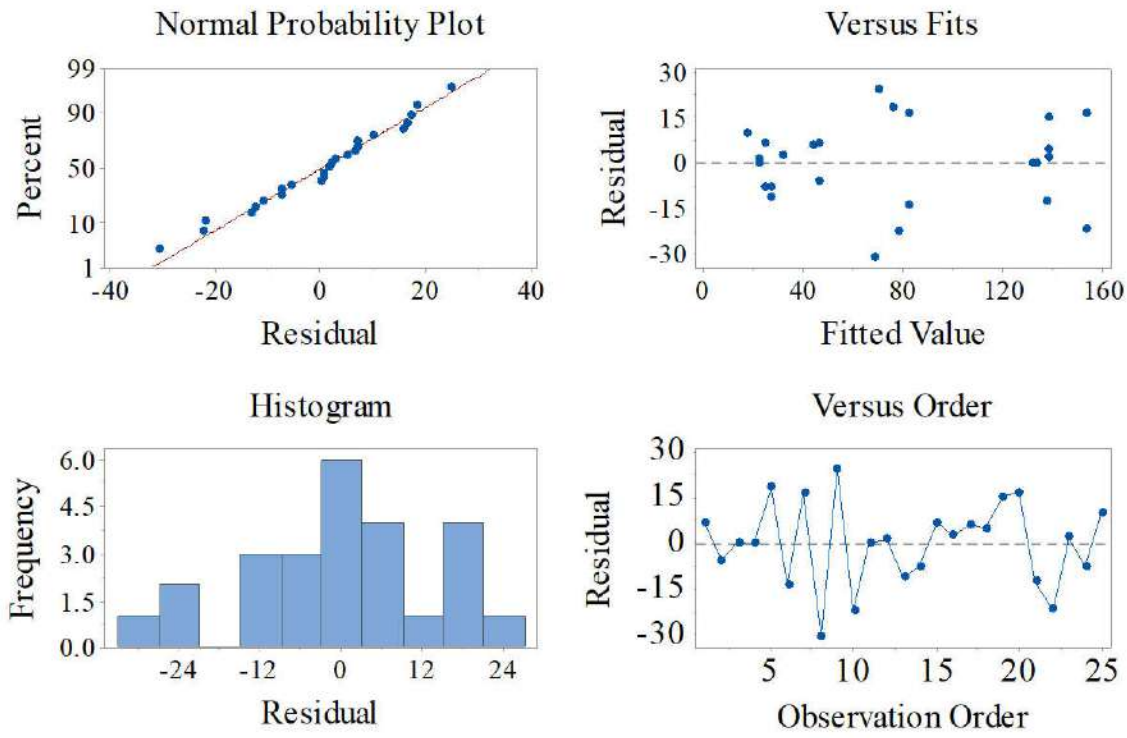

Figure 62. Residual plots of Ksec obtained with EQ1

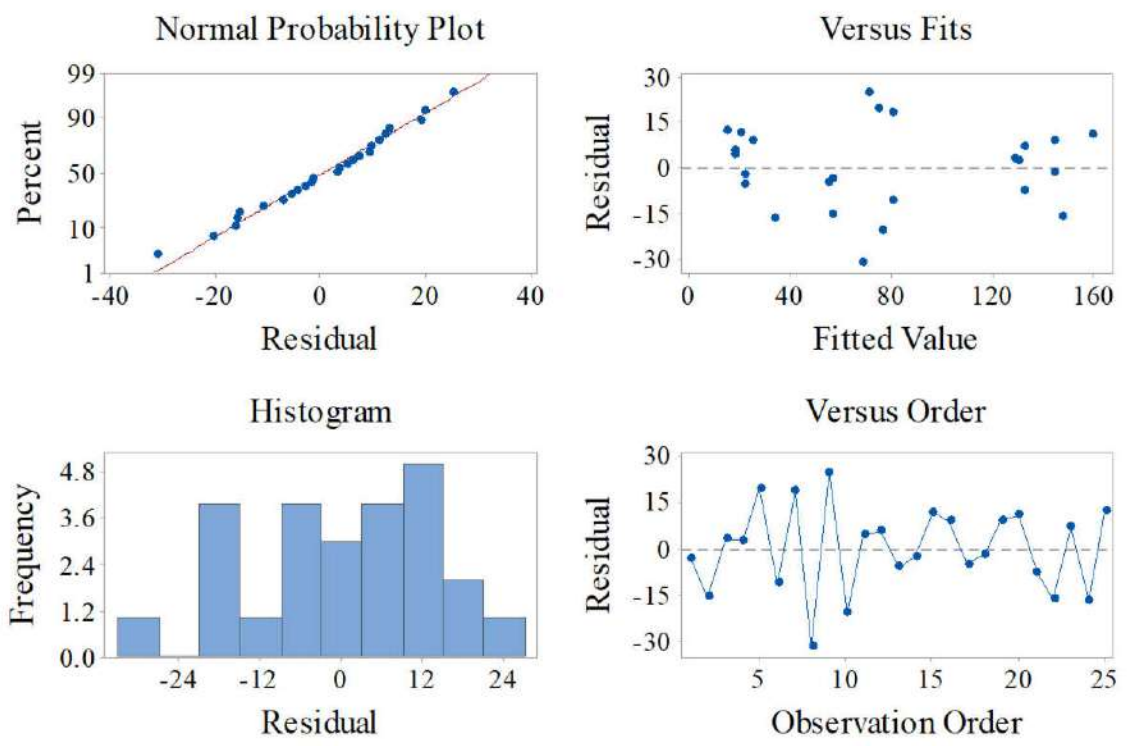

Figure 63. Residual plots of Ksec obtained with EQ2

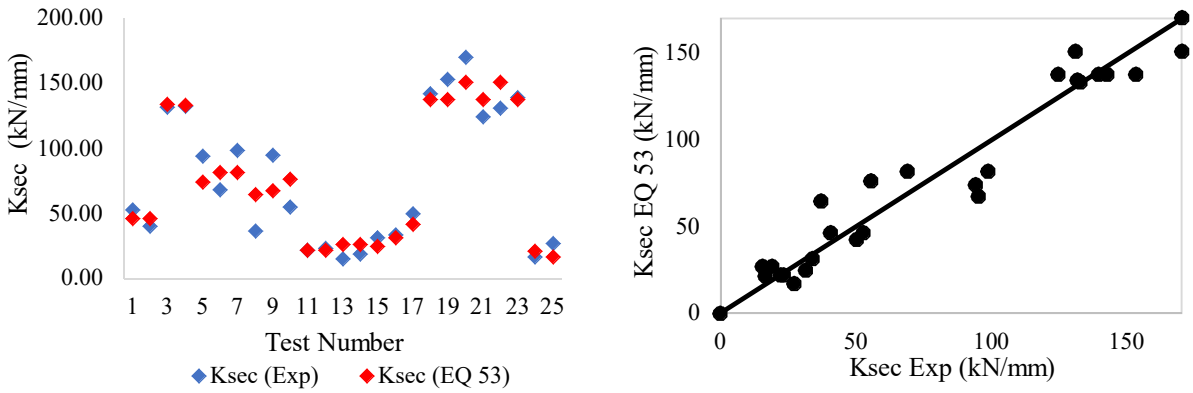

Figure 64. Prediction of Equation 1 for Ksec

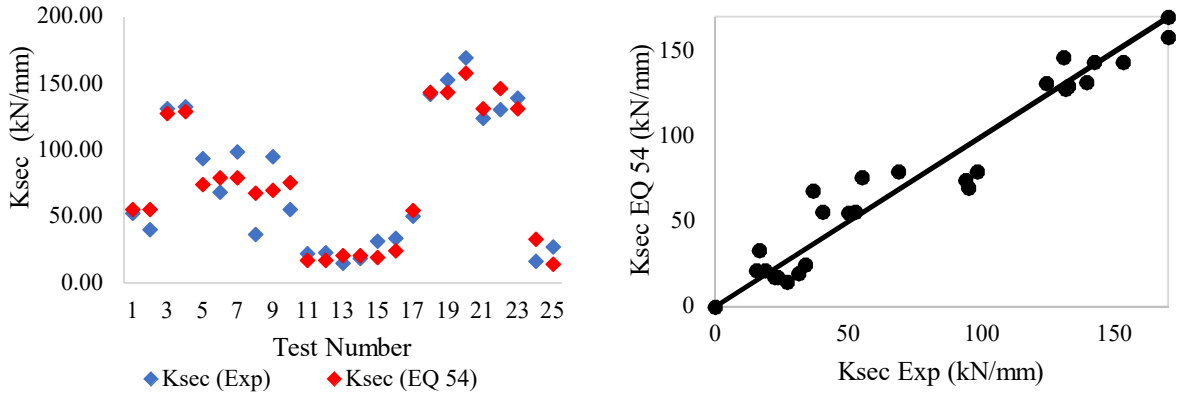

Figure 65. Prediction of Equation 2 for Ksec

3.4.3 Statistical analysis for secant stiffness at peak strength equations

Four equations were determined for calculations of secant stiffness at peak strength, two for squat walls without axial loads with and without boundary element and two for squat walls with axial load with boundary elements. These equations were compared with the secant stiffness calculated from equation of Adorno-Bonilla (2016) to estimate the peak shear and peak displacement as part of his Ph.D. dissertation. These equations are described below.

Peak Shear:

$$Vn = \left(0.35 + 0.068f'c \quad 0.08f'c\,\frac{w}{l_w} + 0.41\frac{P}{A_g} + 0.47\rho_{se}\,f_{yse} + 0.39\rho_{be}\,f_{ybe}\right)A_{cv} \tag{55}$$

$$f_{yse} = Af_{yv} + Bf_{yh} \tag{56}$$

$$\rho_{se} = A\rho_v + B\rho_h \tag{57}$$

$$\rho_{be} = \frac{A_{sbe}}{A_{cv}} \tag{58}$$

Where ρ_{be} is the longitudinal boundary element reinforcement ratio; A_{sbe} is the longitudinal boundary reinforcement area (mm^2); and constants A and B are calculated as follow depending on the aspect ratio h_w/l_w:

If, $h_w/l_w \leq 0.5$	A = 1	B = 0
If $0.5 < h_w/l_w \leq 1.5$	A = $-h_w/l_w + 1.5$	B = $h_w/l_w - 0.5$
If $h_w/l_w \geq 1.5$	A = 0	B = 1

Drift at peak strength

$$R_{peak} = 0.0094 \quad 0.000006\,f_{yh} + 0.000063\,f'_c \quad 0.00044\,\frac{S_h}{t_w} \tag{59}$$

The displacement can be calculated as $D_{peak} = R_{peak}.h_w$ and the secant stiffness can be calculated as Ksec = Vn/D_{peak}. Figure 66 shows the prediction for walls without axial load and with axial load.

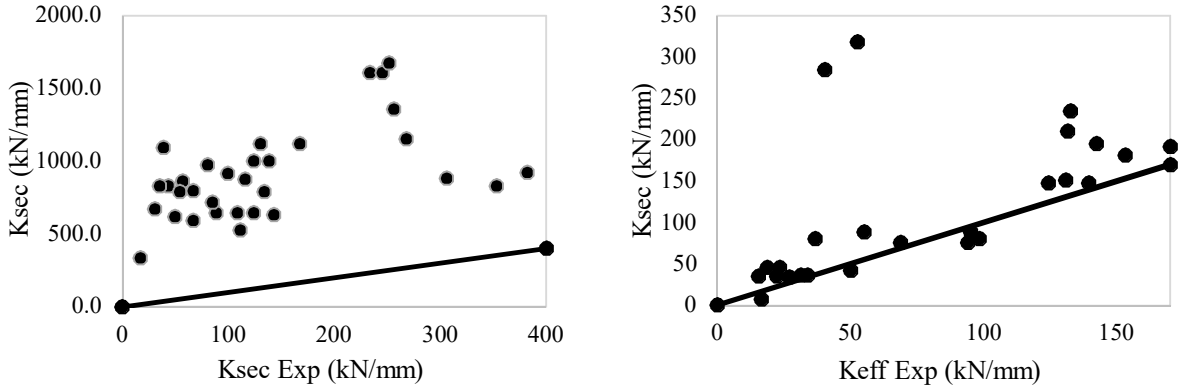

a) **b)**

Figure 66. Prediction for Ksec of Adorno-Bonilla equation for walls (a) without axial loads and (b) with axial loads

Table 19 shows a statistical comparison of Equation 51, 52 for squat walls without axial and the prediction using the equations of Adorno-Bonilla. As it is shown, the Equations 51 and 52 have median and mean values closer to one. The coefficient of variation and standard deviation show that the smallest dispersions are obtained with Equation 52. It means that Equation 52 gives better results for the calculation of secant stiffness for squat walls without axial load with and without boundary element. This result is corroborated in the box and whisker diagram that shows that the mean and median of Equation 52 are almost coincident and close to one.

Table 20: Descriptive statistics of the experimental to predicted secant stiffness ratios walls without axial load

Exp/Prediction	Mean	SE Mean	StDev	Variance	CoefVar	Minimum	Median	Maximum
EQ 51	1.247	0.154	0.870	0.757	0.698	0.481	0.999	4.874
EQ 52	1.050	0.075	0.424	0.179	0.403	0.440	0.987	2.151
Adorno-Bonilla	0.149	0.017	0.097	0.009	0.653	0.036	0.135	0.425

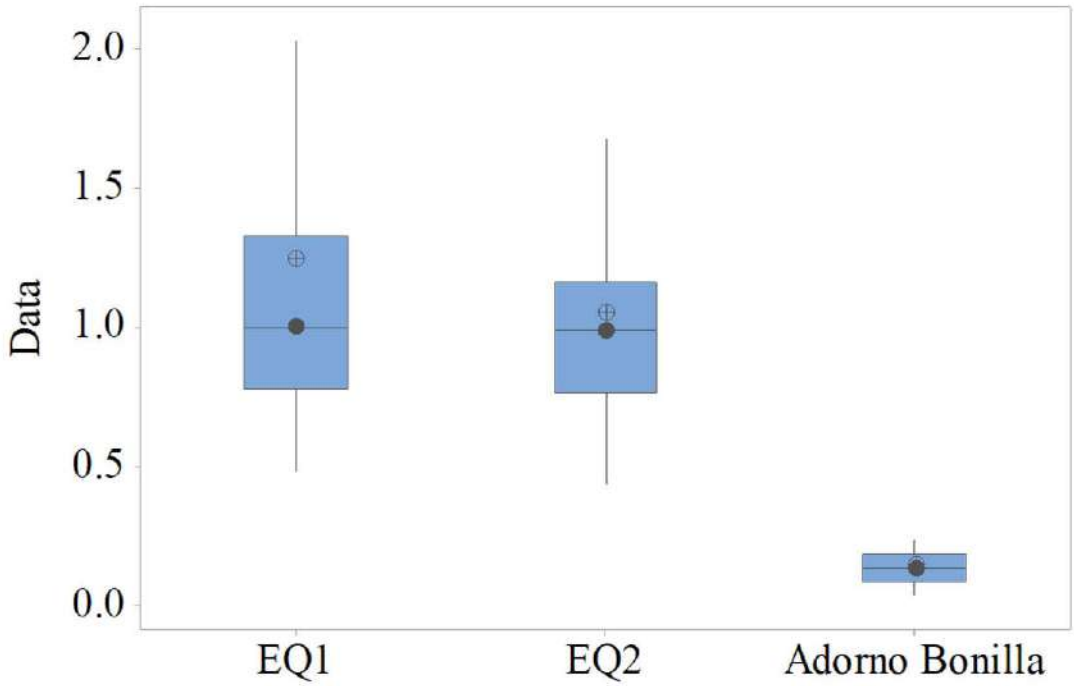

Figure 67. Box and whisker diagram for secant stiffness equations for squat walls without axial load.

Table 20 shows a statistical comparison of Equation 53 and 54 for squat walls with axial and the prediction using the equations of Adorno-Bonilla. As it is shown, Equations 53 and 54 have a good approximation to one in the values of median and the mean. The coefficient of variation and the standard deviation show that the smallest dispersions are obtained with Equation 53. It means that Equation 53 gives better results for the calculation of secant stiffness for squat walls with axial load with and without boundary element.

Table 21: Descriptive statistics of the experimental to predicted secant stiffness ratios for walls with axial load

Exp/Prediction	Mean	SE Mean	StDev	Variance	CoefVar	Minimum	Median	Maximum
EQ 53	1.013	0.050	0.248	0.062	0.245	0.548	1.028	1.604
EQ 54	1.055	0.064	0.321	0.103	0.304	0.503	1.026	1.899
Adorno-Bonilla	0.811	0.086	0.429	0.184	0.529	0.142	0.843	2.309

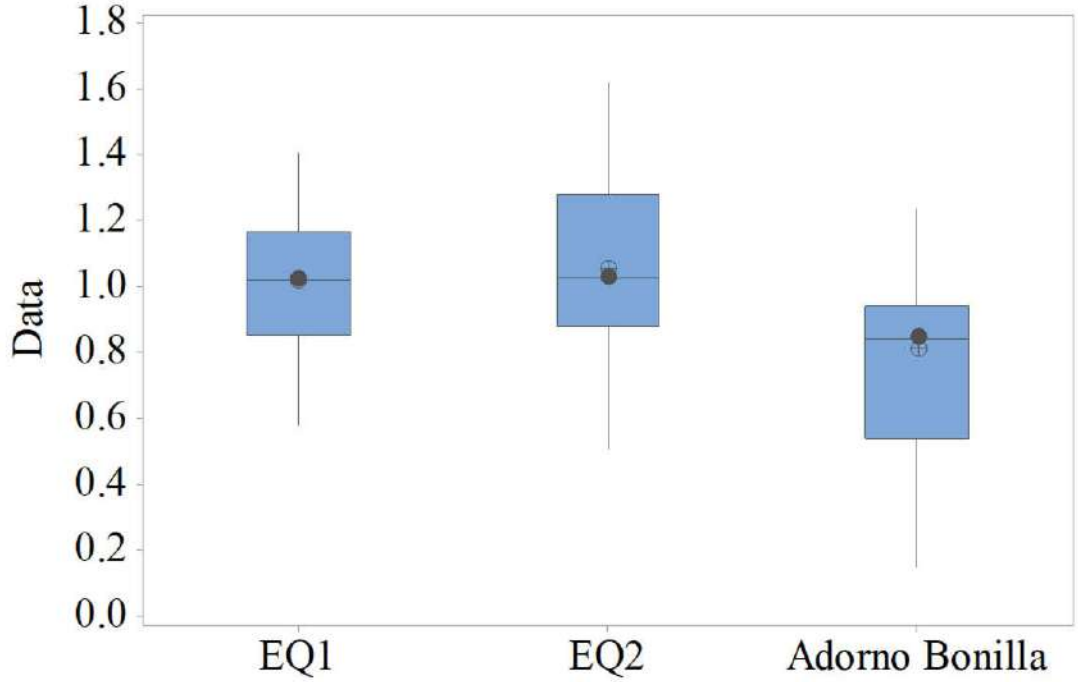

Figure 68. Box and whisker diagram for secant stiffness equations for walls with axial loads.

3.4.2 Summary

Eight equations were developed, and four equations were selected in this chapter for squat walls with $h_w/l_w \leq 1.0$, two equations to estimate the effective stiffness and the other two equations to estimate the secant stiffness at peak strength. Table 21 gives a summary and a description of each equation.

Table 22: Equations for calculations of effective stiffness and secant stiffness on squat walls

EQ #	Equations	Description
48	$Keff = \frac{0.000097\ Ec\ Ig}{w^3} + 200.3\ \frac{lw}{w}$	Effective stiffness for squat walls **without** axial load.
50	$keff = \frac{0.000149G\ Aw}{w} + 2233\frac{P}{f'c\ Ag} \quad 3.1\frac{lw}{tw}$	Effective stiffness for squat walls **with** axial load.
53	$Ksec = 373.7\left(\frac{lw\ tw}{w^2}\right) + 0.002587\ \frac{f'c\ Aw\ \rho v}{w\ \rho}$	Secant stiffness for squat walls **without** axial load.

54	$Ksec = \frac{0.000072\, G.Aw}{w} \quad 1.284\frac{lw}{tw} \quad \frac{0.007\, f'c.Aw}{w}$	Secant stiffness for squat walls **with** axial load.

According to the statistical analysis and boxplot figures for each equation, it was observed that:

- Equation 48 for effective stiffness without axial load gives a minimal improvement in the results when compared to existing equations. Although the statistical results are better when compared with the more simplified equations of Luna or ASCE 43-05, perhaps its use is not that practical for design environment applications. If more accurate results are needed, the Equation (48) is a good option.
- Equation 51 for effective stiffness with axial load gives much better results when compared with those from other researchers and standards. For this reason, this equation is highly recommended, and it represents a more realistic behavior because most walls are subjected to axial loads.
- Both equations for secant stiffness give a statistically good result. Nevertheless, no other equation was not found in the literature to compare with these equations. Several researchers have developed equations to compute stiffness, but from the slope of a line that pass by the yield point and then extrapolated to the level of the nominal strength. For this reason, no direct comparison was possible.
- Adorno-Bonilla (2016) derived two equations to estimate the peak shear for squat walls and the displacement at maximum shear force. These equations were combined to determine the secant stiffness at peak shear. The agreement of these equations with the experimental data is more effective for walls with axial loads than for walls without axial load.
- It was noticed that the secant stiffness for walls without axial loads is influenced more by the compressive concrete strength ant the reinforcement strength and its amount. At peak shear stresses, the cracking patterns changes making the contribution of the compressive strength more significant for the stiffness and strength.

CHAPTER IV. VERIFICATION OF PROPOSED EQUATIONS

4.1 Introduction

The equations proposed in Chapter III were determined using multivariable regressions analysis. Two of these equations were determined to estimate the effective initial stiffness for walls without axial loads and the other for walls with axial loads. In addition, two other equations were determined to estimate the secant stiffness of squat walls, one for walls without axial loads and the others with axial loads. In this chapter, additional validation of the developed equations is performed. Considering the good estimation of effective and secant stiffness calculated using the finite element models with the Concrete Damage Plasticity constitutive material implemented in the software Abaqus, additional RC squat walls were modeled to validate the results obtained with the equations. These tests were part of a project that sought to optimize the construction of concrete walls for typical housing in Mexico, sponsored by the Engineering Institute of UNAM and the CEMEX company. In the first stage they tested a total of sixteen walls subjected to monotonic and cyclic loads. Figure 69 shows the wall dimensions and reinforcing steel configuration. The properties of the selected wall are shown in Table 22 (shaded row). In this table, ρ_b corresponds to the reinforcement ratio of the boundary element, ρ_h and ρ_v correspond to the reinforcement ratio of the web for horizontal and vertical reinforcement, t_w is the thickness of the wall, h_w is the height of the wall and l_w is the length of the wall, P is the axial load in the walls, f'c and fy correspond to the concrete compressive strength and rebar yield strength, respectively. Based on the calibrated MCN100C wall model, seven new models were created and analyzed preserving the same material properties of initial tested walls and changing its thickness in incremental values of 50mm, 75mm and 100mm and the level of axial load.

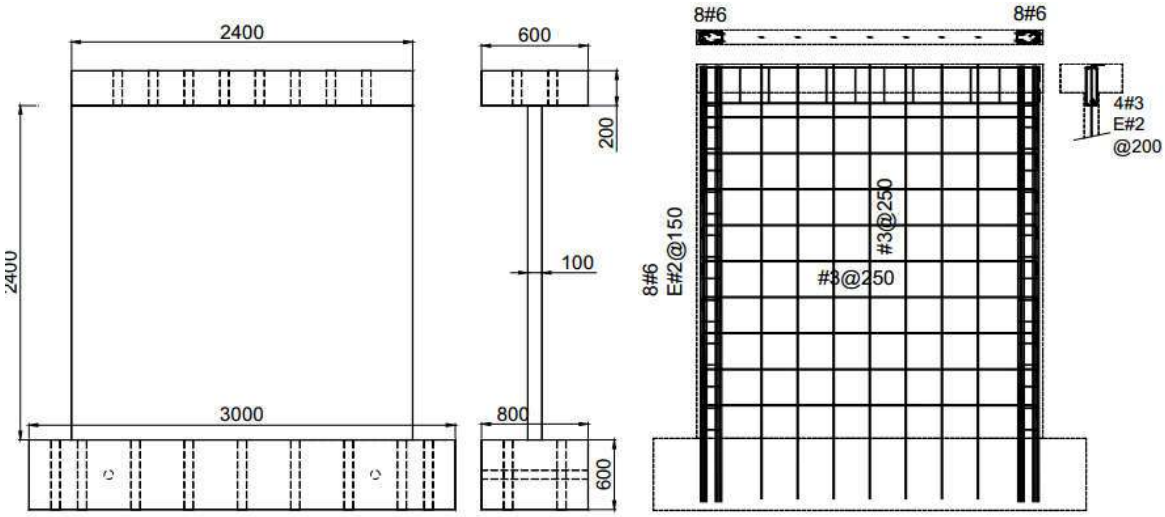

Figure 69.Geometric dimensions and reinforcement of wall MCN100C
(Figure from Flores el at 2007)

Also, five additional walls without boundary elements were modeled based on the walls designated as SW1, SW2 and SW6 tested at the NEES facility at University at Buffalo (Rocks 2012). For calibrated models SW1, SW2 and SW6, an axial load was added corresponding to 5% of f_c'Ag and its thickness was incremented for each wall in 100mm, creating six new wall models to analyze and to compare the results of effective and secant stiffness with the proposed equations. Table 23 shows the properties for the SW wall models. The variables are the same as in Table 22.

Table 23: Properties for walls MCN100C and its variations

Wall	hw (mm)	lw (mm)	tw (mm)	hw /lw	lb (mm)	ρ_{be} (%)	ρ_v (%)	ρ_h (%)	f'c (MPa)	fy (MPa)	P/f'cAg (%)
MCN100C	2400	2400	100	1.00	200	11.40	0.29	0.29	17.5	447	1.43
MCN100Cv1	2400	2400	150	1.00	200	7.60	0.19	0.19	17.5	447	0.95
MCN100Cv2	2400	2400	150	1.00	200	7.60	0.19	0.19	17.5	447	5.00
MCN100Cv3	2400	2400	175	1.00	200	6.51	0.16	0.16	17.5	447	0.82
MCN100Cv4	2400	2400	175	1.00	200	6.51	0.16	0.16	17.5	447	0.00
MCN100Cv5	2400	2400	200	1.00	200	5.70	0.14	0.14	17.5	447	0.71
MCN100Cv6	2400	2400	200	1.00	200	5.70	0.14	0.14	17.5	447	5.00
MCN100Cv7	2400	2400	100	1.00	200	11.40	0.29	0.29	17.5	447	5.71

Table 24: Properties for variations of walls WS1, WS2 and WS5

Wall	hw (mm)	lw (mm)	tw (mm)	hw/lw	lbe (mm)	ρ_{be} (%)	ρ_h (%)	f'c (Mpa)	fy (Mpa)	P/f'cAg (%)
SW1	2865	3048	203	0.94	N/A	0	0.71	24.8	462	0
SW1v1	2865	3048	303	0.94	N/A	0	0.48	24.8	462	0
SW3	1646	3048	203	0.54	N/A	0	0.71	53.8	434	0
SW3v1	1646	3048	203	0.54	N/A	0	0.71	53.8	434	5.01676
SW3v2	1646	3048	303	0.54	N/A	0	0.48	53.8	434	0
SW6	1006	3048	203	0.33	N/A	0	0.71	26.2	462	0
SW6v1	1006	3048	203	0.33	N/A	0	0.71	26.2	462	5.67513
SW6v2	1006	3048	303	0.33	N/A	0	0.48	26.2	462	0

4.2 Model in Abaqus for squat walls MCN100C and its variations

4.2.1 Material and plasticity criterion definition

All new squat wall models were analyzed as 3D models using brick elements with 8 nodes linear reduced integration hexagonal elements (C3D8R) and a large-strain formulation with hourglass control as defined in Chapter 2 (Figure. 24). The constitutive material for modeling the concrete was the CDP with the parameters obtained from the parametric study performed in Chapter 2. The dilation angle was set to 56° with the Kc and fb_0/fc_0 equal to 0.67 and 1.16, respectively. The reinforcement was included into the shell element as shown in Chapter 2 (Figure 26). The Concrete in boundary elements were modeled as confined because of the presence of stirrups and longitudinal bars forming a small column into the wall. To define the confined concrete, the Mander (1988) model was used (Equations 60-66). The web of the wall with a single face of reinforcement was considered as unconfined concrete defined by the relationship proposed by Popovics (1973). The reinforcement was modeled with the constitutive model proposed by Chang and Mander (1994).

$$f_c = \frac{n\left(\frac{\varepsilon_c}{\varepsilon_{cc}}\right) f'_{cc}}{(n \quad 1) + \left(\frac{\varepsilon_c}{\varepsilon_{cc}}\right)^n} \tag{60}$$

$$n = \frac{E_c}{E_c \quad E_{sec}} \tag{61}$$

$$E_c = 5000\sqrt{f'_c} \tag{62}$$

$$E_{sec} = \frac{f'_{cc}}{\varepsilon_{cc}} \tag{63}$$

$$\varepsilon_{cc} = \varepsilon_{co}\left[1 + 5\left(\frac{f'_{cc}}{f'_c} \quad 1\right)\right] \tag{64}$$

$$f'_{cc} = f'_c\left(\quad 1.254 + 2.254\sqrt{1 + \frac{7.94 f'_l}{f'_c}} \quad 2\frac{f'_l}{f'_c}\right) \tag{65}$$

Where f'_c is the unconfined concrete compressive strength (MPa), ε_{co} is the unconfined concrete strain, E_c is the modulus of elasticity unconfined concrete, E_{sec} is the secant modulus for confined concrete, $f'l = fl.k_e$ is the lateral pressure from the transverse reinforcement, assumed to be uniformly distributed over the surface of the concrete core, $k_e = A_e/A_{cc}$ is the confinement effectiveness coefficient; A_e is the area of the effectively confined concrete core (mm^2); A_{cc} is the $A_c(1-\rho_{cc})$, ρ_{cc} is the ratio of area of the longitudinal reinforcement to area of the core of section; A_c is the area of the core of section enclosed by center lines of the perimeter spiral or hoop (mm^2); fl is the $\rho_x.f_{yh}$, where f_{yh} is the yield strength of transverse reinforcement (MPa) and $\rho_x = A_{sx}/(s.d_c)$ is the ratio of transverse reinforcement in the x direction. Figure 70 shows some of the parameters for the confined core of a rectangular section.

For a rectangular section, the confinement coefficient k_e is calculated as:

$$k_e = \frac{\left(1 \quad \sum_{i=1}^{n}\frac{(w'_i)^2}{6\, b_c d_c}\right)\left(1 \quad \frac{s'}{2\, b_c}\right)\left(1 \quad \frac{s'}{2\, d_c}\right)}{(1 \quad \rho_{cc})} \tag{66}$$

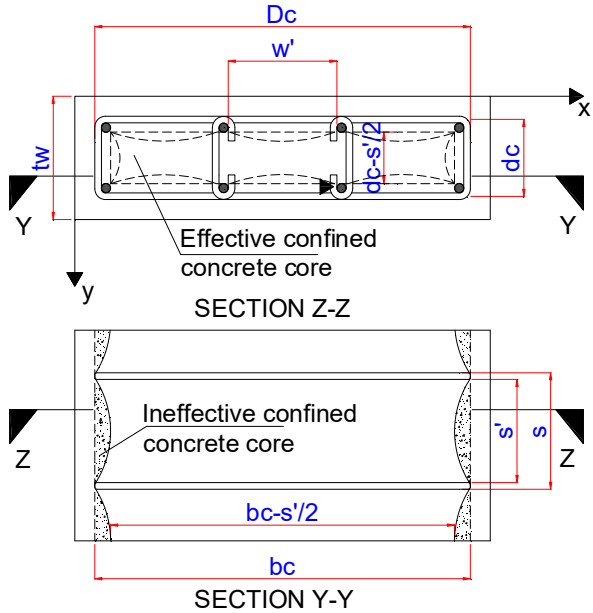

Figure 70. Effectively confined core for rectangular hoop reinforcement.

Figure 71 presents the compressive stress and strain concrete curves for the unconfined and confined concrete of the squat wall MCN100C and its variations.

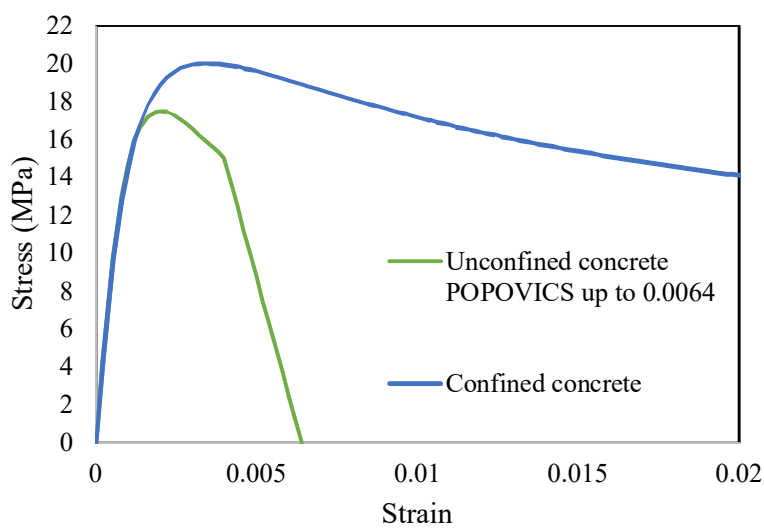

Figure 71. Compressive stress and strain concrete curves for squat walls.

4.2.2 Model analysis in Abaqus

The results of base shear and drifts of wall MCN100C obtained from Abaqus were compared with the experimental results of the mean value from positive and negative envelope base shear-drift experimental backbone curves (Figure 72). Variations of the calibrated model were also analyzed, and their effective stiffness and secant stiffness were compared with proposed equations. Based on the results of new models based on SW series, effective stiffness and secant stiffness were calculated for each wall and compare with the proposed equations. As explained in previous chapter the effective stiffness was calculated as the ratio of 15% of the shear peak and its respectively displacement and the secant stiffness were calculated as the ratio of shear peak and its respectively displacement. Some shear walls models do not show a clear peak shear, and for that reason it was necessary to calculate an average from peak shear values to get the secant stiffness. Figure 74 shows the base shear vs drift of new walls based on the original calibrated wall MCN100C, showing how these changes affect the original behavior of the wall.

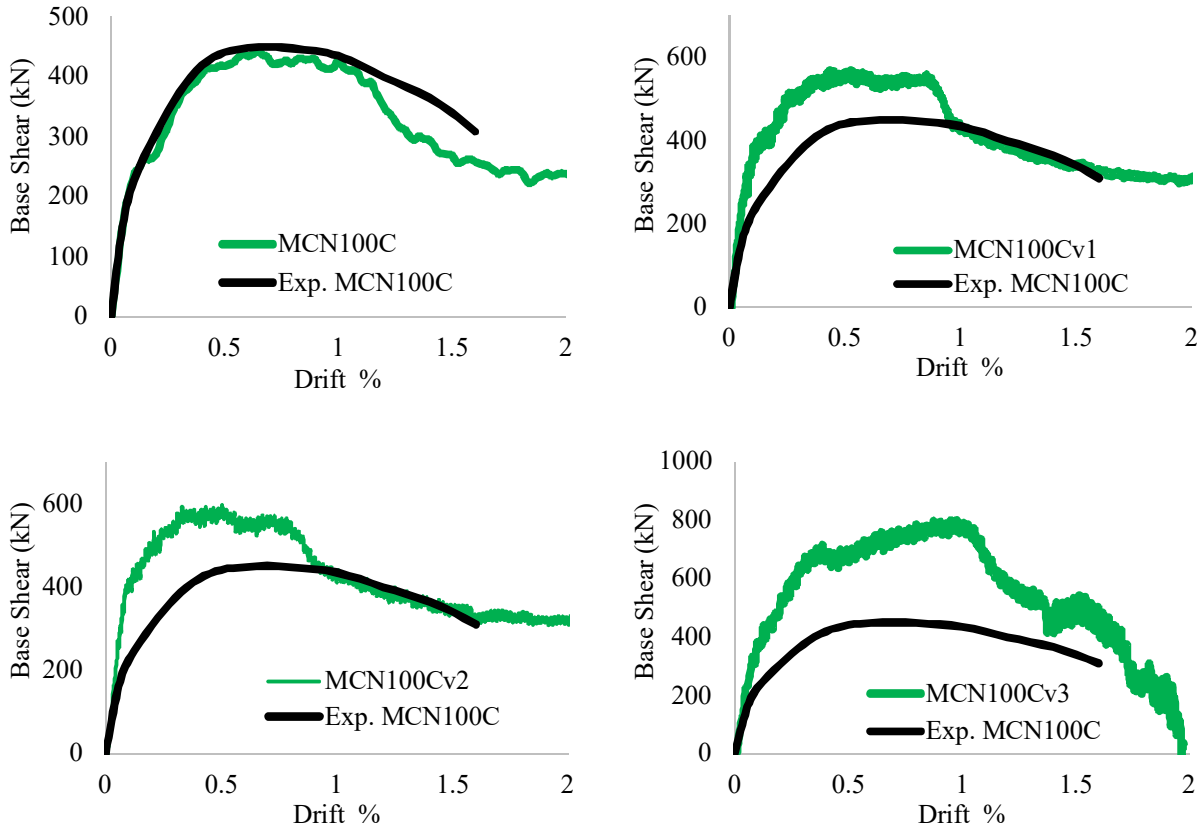

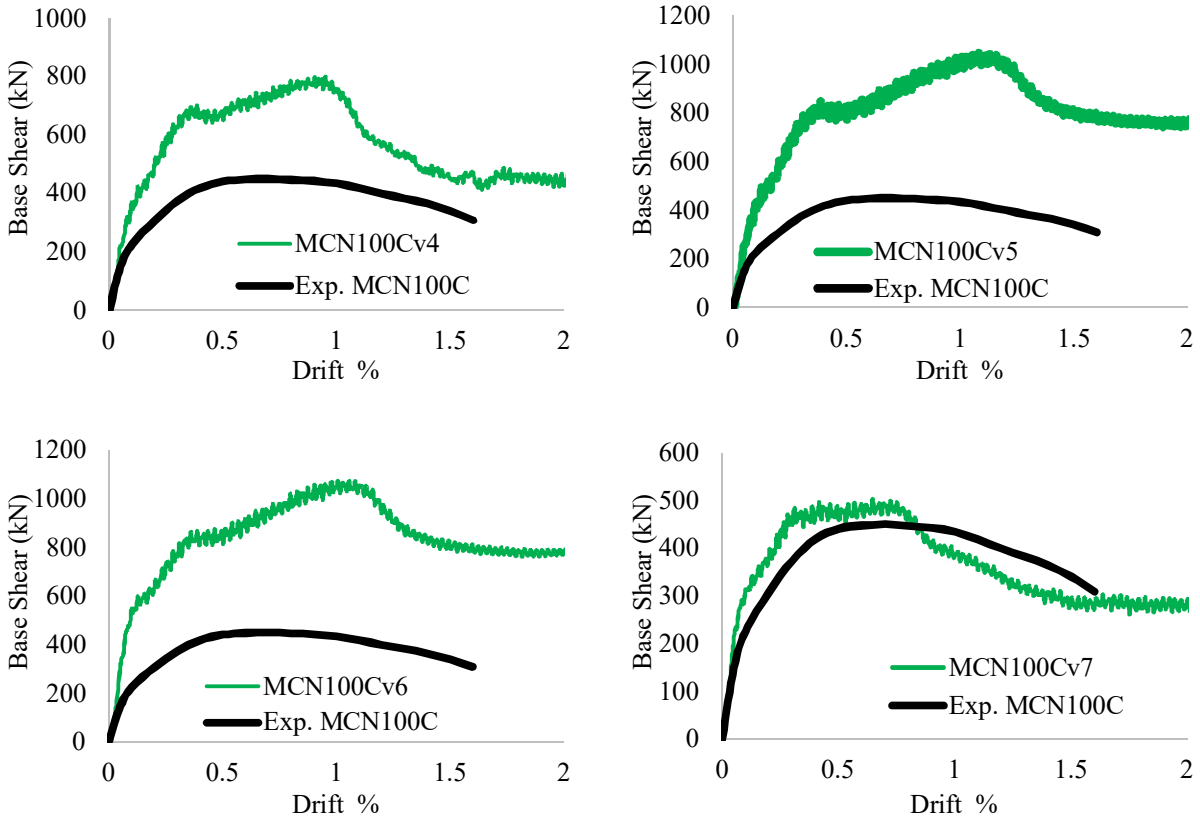

Figure 72. Experimental vs analytical base shear-drift envelopes for variations of the model MCN100C in Abaqus

Figure 73 shows the base shear vs drift of new walls based on the SW series and the original experimental walls, showing how these changes affect the original behavior of the wall.

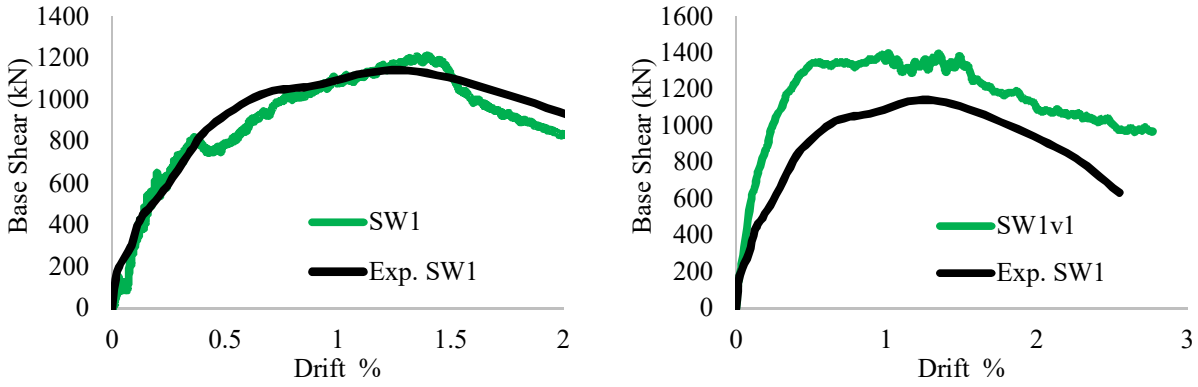

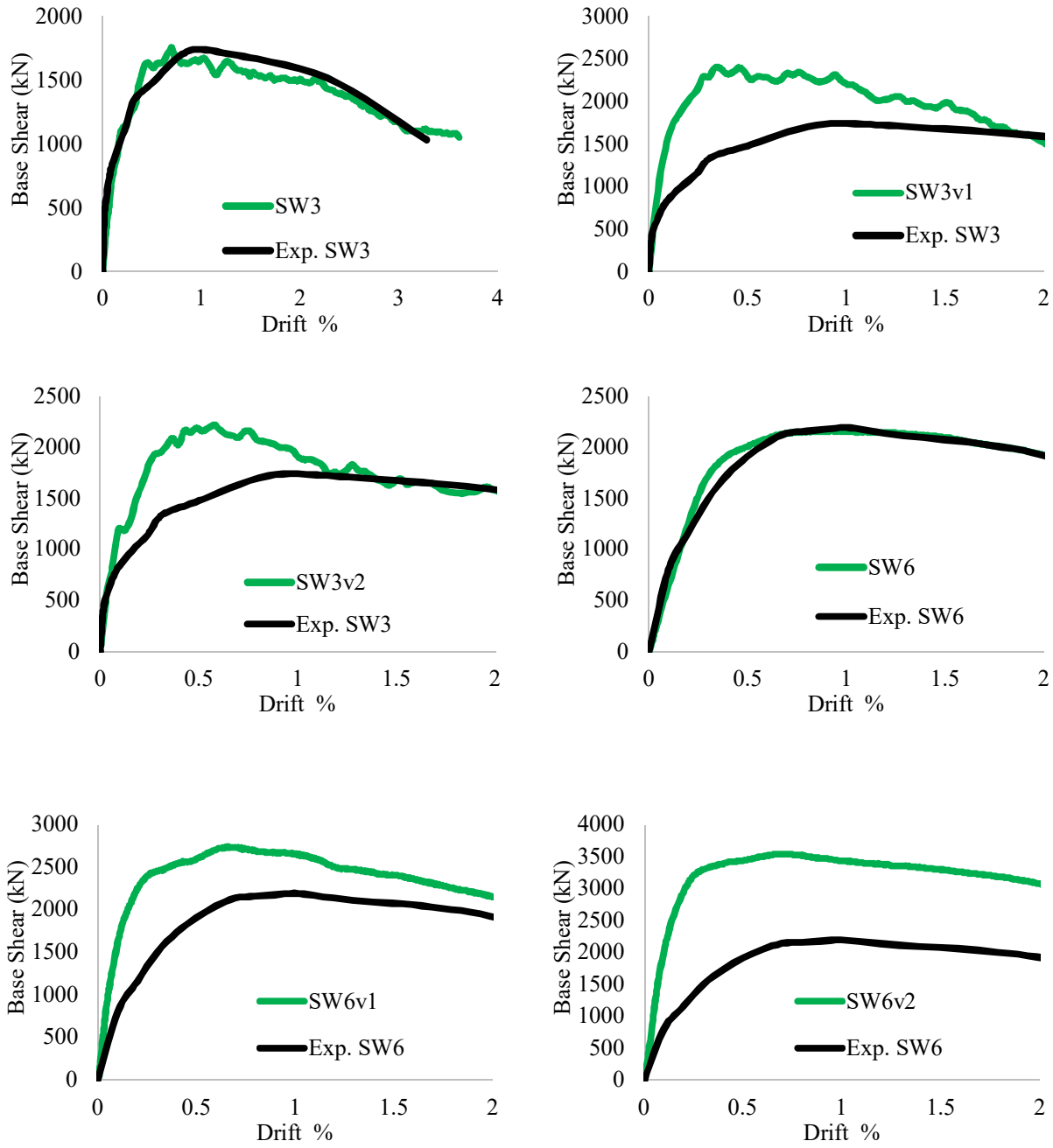

Figure 73. Experimental vs analytical base shear-drift envelopes for variations of models SW1-SW6 in Abaqus

Tables 24-27 show the results of effective stiffness and secant stiffness for the modified walls based on the MCN100C and SW series calculated using Abaqus, the proposed equations and standards. The standards used are shown in Table 24 for effective stiffness. The standards do not specify any equation to estimate the secant stiffness of walls.

Table 25: Effective stiffness of wall MCN100C and variations using Abaqus, equations and standards.

Wall ID	Keff, Abaqus	Keff EQ48, 51	Luna cracked	ASCE 43-05 Uncracked	ASCE 43-05 Cracked	ASCE 43-13 Cracked	ACI 318-14 Uncracked	ACI 318-14 Cracked	FEMA 356 Uncracked	FEMA 356 Cracked
MCN100C	123.59	91.51	68.26	146.01	73.00	79.45	107.44	57.13	120.73	79.45
MCN100Cv1	141.97	147.88	102.38	219.01	109.51	119.18	161.16	85.70	181.09	119.18
MCN100Cv2	152.00	238.27	102.38	219.01	109.51	119.18	161.16	85.70	181.09	119.18
MCN100Cv3	165.00	178.35	119.45	255.51	127.76	139.04	188.02	99.98	211.27	139.04
MCN100Cv4	155.00	229.89	119.45	255.51	127.76	139.04	188.02	99.98	211.27	139.04
MCN100Cv5	178.00	209.57	136.51	292.02	146.01	158.91	214.88	114.26	241.45	158.91
MCN100Cv6	205.00	305.27	136.51	292.02	146.01	158.91	214.88	114.26	241.45	158.91
MCN100Cv7	136.00	187.21	68.26	146.01	73.00	79.45	107.44	57.13	120.73	79.45
SW1	322.23	262.29	193.09	415.96	207.98	228.54	307.78	164.86	345.19	228.54
SW1v1	531.42	286.53	288.22	620.87	310.44	341.12	459.40	246.08	515.23	341.12
SW3	882.80	753.03	1010.45	2366.67	1183.33	1478.46	1882.08	1118.62	2057.63	1478.46
SW3v1	1092.19	948.76	1010.45	2366.67	1183.33	1478.46	1882.08	1118.62	2057.63	1478.46
SW3v2	1487.95	941.27	1508.20	3532.51	1766.26	2206.76	2809.22	1669.66	3071.24	2206.76
SW6	1325.69	1774.91	1700.09	4333.04	2166.52	3186.44	3754.10	2597.33	3975.41	3186.44
SW6v1	1325.69	1088.71	1700.09	4333.04	2166.52	3186.44	3754.10	2597.33	3975.41	3186.44
SW6v2	1325.69	2350.30	2537.57	6467.54	3233.77	4756.11	5603.41	3876.80	5933.74	4756.11

Table 25 show the secant stiffness estimated using the proposed equations (53,54) and the approximation using the equations of Adorno-Bonilla (2016) EQs (55-59)

Table 26: Secant stiffness of wall MCN100C and variations

Wall ID	Ksec Exp, Abaqus	Ksec EQ 53,55	|% Error| Abaqus vs EQ 53,55	Ksec Bonilla	|% Error| Abaqus vs Bonilla
MCN100C	28.85	21.69	24.82	11.20	61.17
MCN100Cv1	34.18	47.95	40.27	11.62	66.00
MCN100Cv2	41.17	47.95	16.45	11.63	71.76
MCN100Cv3	34.19	61.07	78.64	11.95	65.05
MCN100Cv4	35.13	61.07	73.84	11.95	65.99
MCN100Cv5	40.31	74.20	84.08	12.31	69.46
MCN100Cv6	44.49	74.20	66.77	12.32	72.31
MCN100Cv7	36.40	21.69	40.41	11.26	69.07
SW1	29.00	42.03	44.92	48.13	65.96
SW1v1	51.16	62.73	22.60	49.77	2.72
SW3	122.86	137.66	12.05	125.51	2.16

SW3v1	297.75	265.97	10.67	125.67	57.79
SW3v2	233.37	205.48	11.95	155.57	33.34
SW6	219.10	270.16	23.31	237.12	8.22
SW6v1	415.00	355.26	14.39	237.43	42.79
SW6v2	505.43	403.25	20.22	288.30	42.96

To compare the prediction of proposed equations (51, 52) and standards in the estimation of effective stiffness a statistical analysis was conducted in the program Minitab V18 (Tables 28 and 29). The analysis was based on the ratio of stiffness calculated with Abaqus and effective stiffness calculated using the proposed equations and standards (Table 26).

Table 27: Ratio of effective stiffness obtained with Abaqus to predicted with equations and standards

	Ratio $K_{effeAbaqus\ or\ Exp}$/ $K_{effepredictions}$								
Wall	Keff	Luna	ASCE 43-05	ASCE 43-05	ASCE 41-13	ACI 318-14	ACI 318-14	FEMA 356	FEMA 356
ID	EQ 48, 51	cracked	Uncracked	Cracked	Cracked	Uncracked	Cracked	Uncracked	Cracked
MCN100C	1.35	1.81	0.85	1.69	1.56	1.15	2.16	1.02	1.56
MCN100Cv1	0.96	1.39	0.65	1.30	1.19	0.88	1.66	0.78	1.19
MCN100Cv2	0.64	1.48	0.69	1.39	1.28	0.94	1.77	0.84	1.28
MCN100Cv3	0.93	1.38	0.65	1.29	1.19	0.88	1.65	0.78	1.19
MCN100Cv4	0.67	1.30	0.61	1.21	1.11	0.82	1.55	0.73	1.11
MCN100Cv5	0.85	1.30	0.61	1.22	1.12	0.83	1.56	0.74	1.12
MCN100Cv6	0.67	1.50	0.70	1.40	1.29	0.95	1.79	0.85	1.29
MCN100Cv7	0.73	1.99	0.93	1.86	1.71	1.27	2.38	1.13	1.71
SW1	1.23	1.67	0.77	1.55	1.41	1.05	1.95	0.93	1.41
SW1v1	1.85	1.84	0.86	1.71	1.56	1.16	2.16	1.03	1.56
SW3	1.17	0.87	0.37	0.75	0.60	0.47	0.79	0.43	0.60
SW3v1	1.15	1.08	0.46	0.92	0.74	0.58	0.98	0.53	0.74
SW3v2	1.58	0.99	0.42	0.84	0.67	0.53	0.89	0.48	0.67
SW6	0.75	0.78	0.31	0.61	0.42	0.35	0.51	0.33	0.42
SW6v1	1.22	0.78	0.31	0.61	0.42	0.35	0.51	0.33	0.42
SW6v2	0.56	0.52	0.20	0.41	0.28	0.24	0.34	0.22	0.28

The same ratio was calculated for the secant stiffness, in which the secant stiffness from Abaqus was divided by results from equation 53 and 54 and the secant stiffness using the equation of Adorno-Bonilla (Table 27).

Table 28: Ratio of secant stiffness obtained with Abaqus to predicted with equations

Wall	Ratio $K_{secAbaqus}/K_{secpredictions}$	
ID	K_{sec}	K_{sec}
	EQ (53,54)	_Bonilla
MCN100C	1.33	2.58
MCN100Cv1	0.71	2.94
MCN100Cv2	0.86	3.54
MCN100Cv3	0.56	2.86
MCN100Cv4	0.58	2.94
MCN100Cv5	0.54	3.27
MCN100Cv6	0.60	3.61
MCN100Cv7	1.68	3.23
SW1	0.69	0.60
SW1v1	0.82	1.03
SW3	0.89	0.98
SW3v1	1.12	2.37
SW3v2	1.14	1.50
SW6	0.81	0.92
SW6v1	1.17	1.75
SW6v2	1.25	1.75

Tables 28 and 29 show the descriptive statistical analysis results for the effective and secant stiffness. These tables show the mean, standard deviation, variance, coefficient of variation, median, maximum and minimum of the ratio between Abaqus results and predictions using the equations or standards. As shown in Table 28, the standards “ACI 318-14 Cr” and “FEMA 356 Cr” have a mean value close to 1.0 but the standard deviation and coefficient of variation are high indicating a wide range of dispersion. Equations 48 and 51 have a mean and median value very similar and relatively close to 1.0, however their standard deviation and standard error of the mean value are the lowest compared with the standards. The Luna standard deviation values for effective stiffness are comparable with the proposed equation, but their mean values are much higher. This result can be corroborated with the diagram of box and whiskers shown in Figure 74.

Table 29: Statistical analysis for effective stiffness prediction equations and standards of calibrated models

Variable	Mean	SE mean	StDev	Variance	CoefVar	Minimum	Median	Maximum
EQ 48 51	1.020	0.092	0.369	0.136	0.362	0.564	0.943	1.855
Luna	1.293	0.107	0.427	0.182	0.330	0.522	1.343	1.993
ASCE 43-05 UnCr	0.587	0.055	0.219	0.048	0.373	0.205	0.628	0.932
ASCE 43-05 Cr	1.173	0.109	0.438	0.192	0.373	0.410	1.255	1.863
ASCE 41-13 Cr	1.033	0.113	0.453	0.205	0.439	0.279	1.153	1.712
ACI 318-14 UnCr	0.778	0.080	0.319	0.102	0.410	0.237	0.853	1.266
ACI 318-14 Cr	1.416	0.163	0.654	0.427	0.462	0.342	1.604	2.380
FEMA 356 UnCr	0.698	0.069	0.277	0.077	0.397	0.223	0.759	1.127
FEMA 356 Cr	1.033	0.113	0.453	0.205	0.439	0.279	1.153	1.712

As shown in Figure 74, the interquartile range of Equations 48 and 51 are better distributed than standards values, as shown at least 50% of the data is located between 0.75 and 1.25. Also, the mean and median value are very coincident as shown by the symbols "• " (mean) and " " (median value). It is shown that the data from the proposed equations (48,51) are equally distributed around the median and mean value. It is demonstrated that the proposed equations can predict the effective stiffness of squat walls with a lower range of uncertainty.

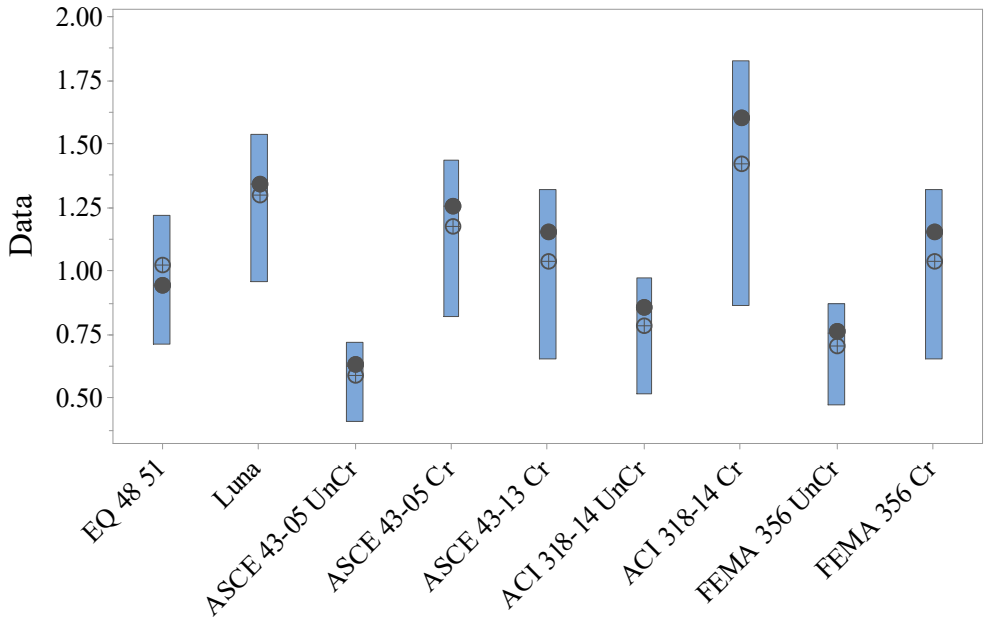

Figure 74. Box and whisker diagram for effective stiffness predictions of equations and standards compared with calibrated models in Abaqus.

The predictions for secant stiffness using Equations 53 and 54 compare well with those from the Adorno-Bonilla equations considering that the mean and median value are very close to 1.0 (Table 29). Figure 75 shows that the equations have a good prediction in the estimation of secant stiffness as shown, 50% of the data lies between 0.75 and 1.25.

Table 30: Statistical analysis for secant stiffness prediction equations and Adorno-Bonilla (2016)

Variable	Mean	SE mean	StDev	Variance	CoefVar	Minimum	Median	Maximum
K sec EQ (53,55)	0.922	0.082	0.329	0.108	0.356	0.543	0.837	1.678
K Sec Adorno-Bonilla	2.243	0.255	1.021	1.042	0.455	0.603	2.472	3.612

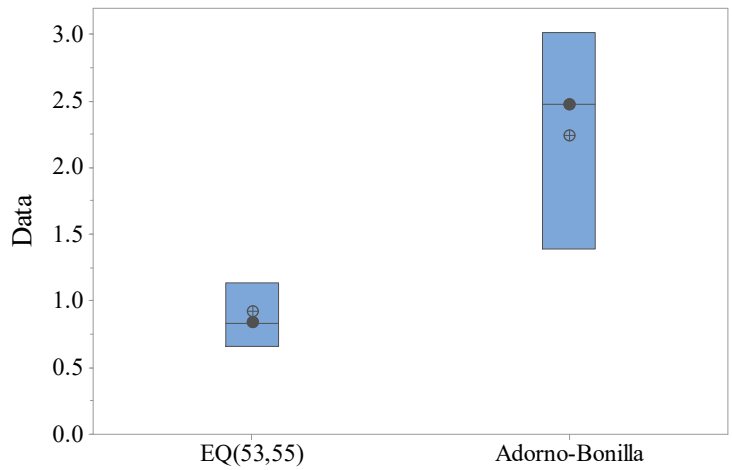

Figure 75. Box and whisker diagram for secant stiffness predictions of equations.

4.3 Summary

Due to the difficulties to find new data of squat walls with aspect ratios (hw/lw) less than 1.0, thirteen new models were created based on calibrated models MCN100C and SW1, SW3 and SW6, the main variations were the thickness and the axial load according to Tables 22 and 23. The effective stiffness and secant stiffness obtained from these models were compared with the proposed equations to determine the effective stiffness (EQ 48,51) and secant stiffness (EQ 53, 54). A statistical analysis was performed to determine the effectiveness of the equations in the estimation of the effective and secant stiffness results. These analyses determined that the

equations can be used to determine the effective and secant stiffness because of the good estimations compared with other equations and standard coefficients. However, the use of these equations is restricted to the range of variables used to develop it. The equations proposed were determined using data from experimental squat walls with different characteristics. Figures 76 to 79 show different histograms with the frequency of occurrence of each parameter used to develop each of the equations. This information can be used to assess the range of applicability of the proposed equations. The use for walls with height to thickness ratios higher than 16 and higher than 25 for walls without and with axial loads, respectively are not recommended. Accuracy of the developed equations is better for walls with axial loads. For effective stiffness calculations with walls with axial loads, it is recommended that hw/tw be less than 20.

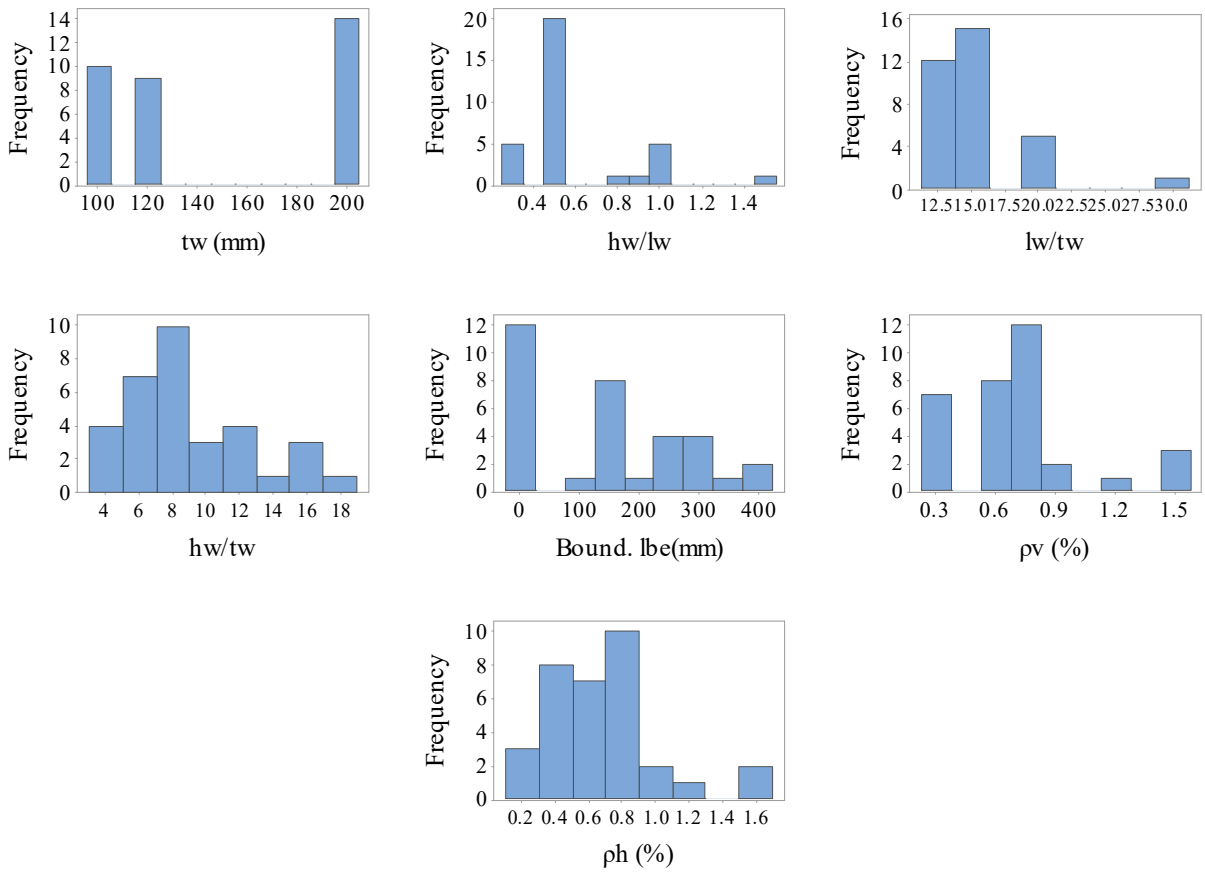

Figure 76. Histograms for variables used to develop the effective stiffness equations of squat walls without axial loads

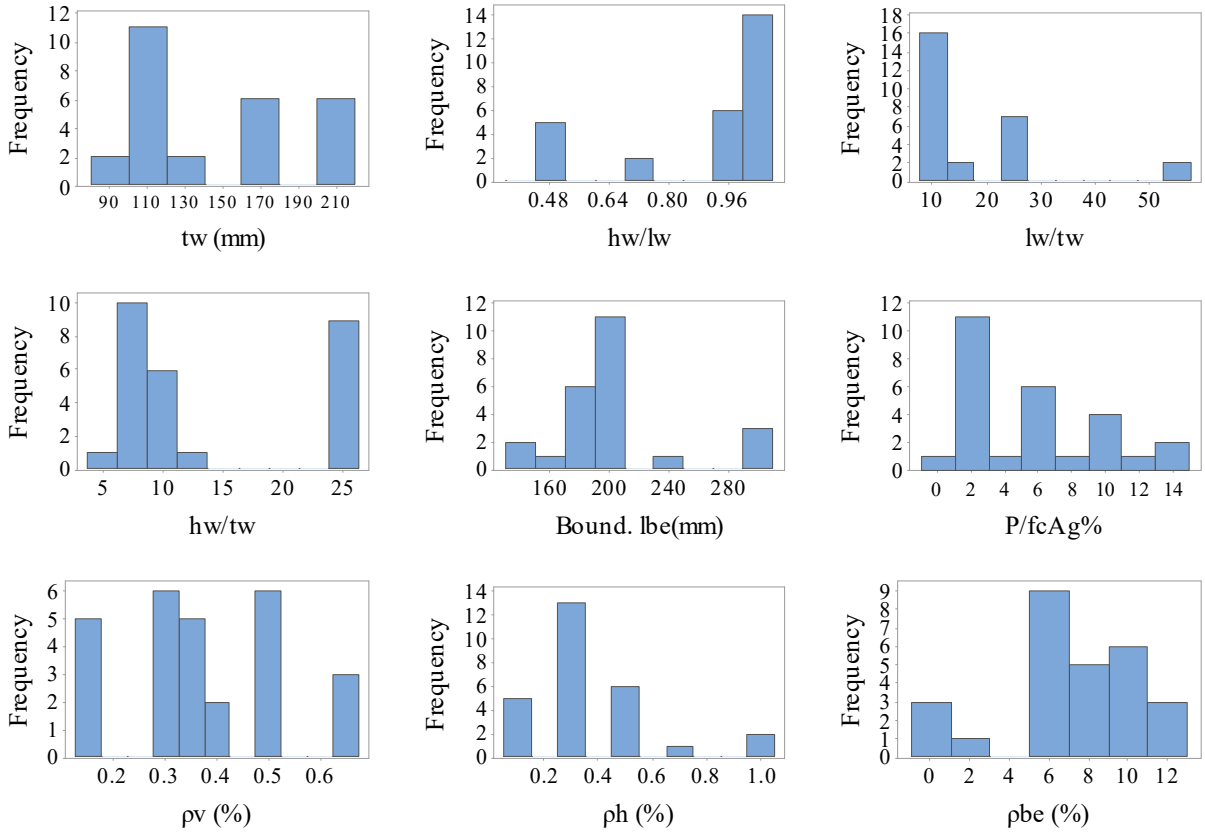

Figure 77. Histograms for variables used to develop the effective stiffness equations of squat walls with axial loads

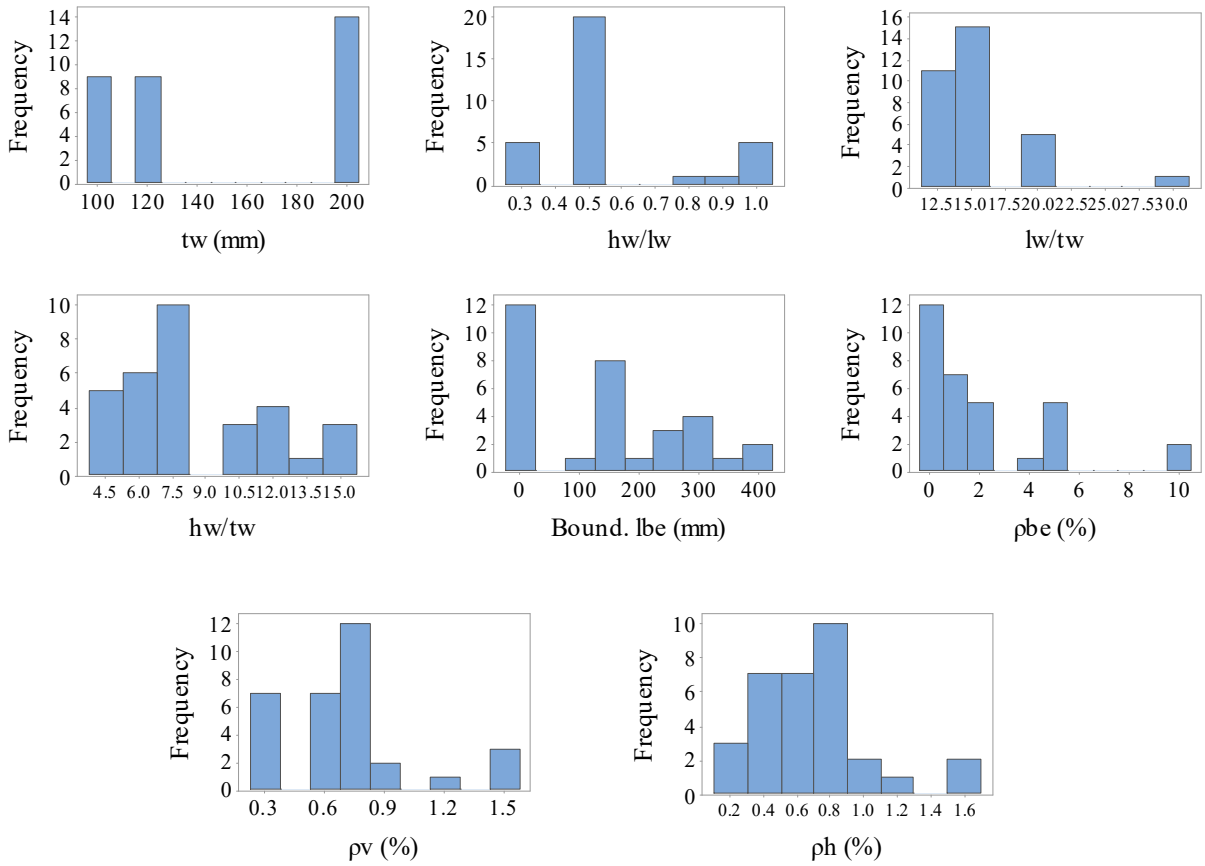

Figure 78. Histograms for variables used to develop the secant stiffness equations of walls without axial load with and without boundary elements (lb).

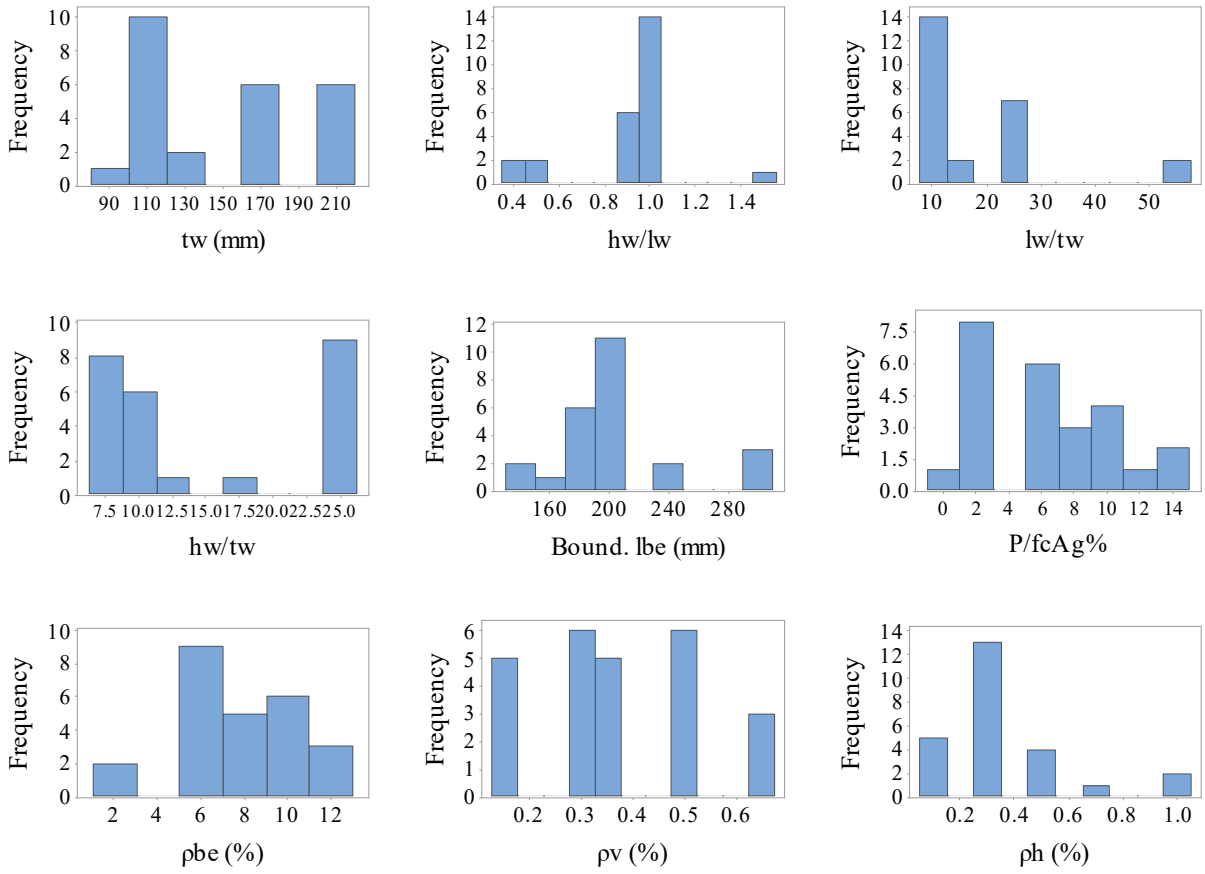

Figure 79. Histograms for variables used to develop the secant stiffness equation for walls with axial load and with boundary element (lb).

CHAPTER V. CONCLUSIONS AND FUTURE WORK

5.1 Conclusions

Finite element models were developed in Abaqus to determine the parameters that have the most important influence in the prediction of lateral stiffness of squat reinforced concrete walls. Equations were also developed to predict the effective and secant stiffness of these walls.

- According to the finite element analyses in Abaqus and using the Concrete Damage Plasticity Model as constitutive material for the concrete, it was found that:
  - ✓ The parameter that has more influence in the response of the walls analyzed in this study was the dilation angle of the concrete. An angle of 56° better captures the response of these walls and provides accurate results of lateral stiffness and peak shear values.
  - ✓ Different mesh sizes mostly affect the peak shear strength and post peak responses.
  - ✓ The prediction of the lateral response (shear vs drift) of the walls analyzed in this research was better obtained with the constitutive relationship of the concrete based on the Popovics curve.
- From the evaluation of existing lateral stiffness factors and equations, it was assessed that the reduction factors that provide a better approximation of the effective stiffness are the factors proposed by Luna, FEMA 356 and ASCE 43-05 for cracked walls. The finite element models developed in Abaqus provide results that are in good agreement with the experimental data.
- The Shear-Flexure Interaction Multiple-Vertical-Line-Element Model developed in OpenSees was also evaluated to determine its modeling capabilities for squat RC walls. From these analyses, it was determined the following:

- The height factor where the relative rotation between top and bottom of rigid beams (ch) is concentrated and the shape parameter have great influence in the response and convergence of the analyses.
- The convergence of the results is greatly affected by the mesh size; number of horizontal and vertical fibers.
- A very small dowel action parameter is needed to run the analyses.
- The friction coefficient has less impact in the wall response.
- The convergence of this model was not possible for drifts higher than 0.5%.
- Further improvements of this model are needed to be used for squat RC walls.

❖ Four equations were developed for squat walls with $h_w/l_w \leq 1.0$, two equations to estimate the effective stiffness and the other two equations to estimate the secant stiffness at peak strength. According to the statistical analysis for each equation and boxplot figures, it was observed that:

- The equation for effective stiffness without axial load gives a minimal improvement in the results when compared to existing equations. Although the statistical results are better when compared with the more simplified equations of Luna or ASCE 43-05, perhaps its use is not that practical for design environment applications. If more accurate results are needed, Equation (48) is a good option.
- Equation (51) for effective stiffness with axial load gives much better results when compared with these from other research and standards. For this reason, this equation is highly recommended, and represents a more realistic condition because most walls are subjected to axial loads.
- The equations for secant stiffness both give a statistical good result. Nevertheless, another equation was not found in the literature to compare with the proposed equations. Several researchers have developed equations to compute stiffness, but from the slope of a line that pass by the yield point and then extrapolated to the level of the nominal strength. For this reason, no direct comparison was possible.
- However, Adorno-Bonilla (2016), derived two equations to estimate the peak shear for squat walls and the displacement at maximum shear force. These equations were combined

to determine the secant stiffness at peak shear. The agreement of these equations with the experimental data is more effective for walls with axial loads than for walls without axial load.

- It was also noticed that the secant stiffness for walls with axial loads is influenced more by the compressive concrete strength. At peak shear stresses, the cracking patterns change making the contribution of the compressive strength more significant for the stiffness and strength.

❖ From the verification of the proposed equations to estimate the effective and secant stiffness, with calibrated models in Abaqus of walls MCN100C, SW1 to SW6, and assessing their results (effective and secant stiffness), it was concluded that the equations can predict the effective stiffness and secant stiffness with variable accuracy. Secant stiffness equations can be improved as new data from experimental testing becomes available.

5.2 Future work

❖ In order to improve the capability of the finite element model presented in chapter 2 for modeling squat RC walls, additional calibration of the concrete parameters based on experimental data is needed. Further work can be done in the calibration of another concrete hysteretic model using more experimental data and incorporate this model in Abaqus to improve the post peak response of these walls.

❖ Substantial work must be performed to incorporate models in Abaqus and OpenSees to predict with more accuracy the cyclic response of reinforced concrete squat walls. However, this task seems to be limited by the availability of digital data enough tests in order to obtain a robust model calibration.

REFERENCES

American Concrete Institute. (2014). "Building code requirements for structural concrete (ACI 318-14) and commentary." ACI, Farmington Hills, MI.

American Society of Civil Engineers (ASCE). (2005). "Seismic design criteria for structures, systems, and components in nuclear facilities (ASCE/SEI 43-05)." Reston, VA.

American Society of Civil Engineers (ASCE). (2013). "Seismic rehabilitation of buildings (ASCE/SEI 41-13)." ASCE, Reston, VA.

Abaqus-2016, (2016), "Abaqus 2016 User Documentation – User Mannual", Dassult Systems Simulia Corp., Providence, RI, USA.

Adorno Bonilla C. (2016), "Shear strength and displacement capacity of squat reinforced concrete shear walls." PhD dissertation, University of Puerto Rico, Mayaguez Puerto Rico.

Belarbi H. and Hsu T.C. (1994), "Constitutive Laws of Concrete in Tension and Reinforcing Bars Stiffened by Concrete," ACI Structural Journal, 91(4), 465-474.

Bismarck N. Luna. (2015). Seismic Response of Low Aspect Ratio Reinforced Concrete Walls for Buildings and Safety-Related Nuclear Applications. PhD Dissertation, University of New York at Buffalo. Retrieved from http://gradworks.umi.com/10/01/10013563.html

Chang, G. A. and Mander, J. B. (1994). "Seismic Energy Based Fatigue Damage Analysis of Bridge Columns: Part I - Evaluation of Seismic Capacity," Technical Report No. NCEER–94–0006, State University of New York, Buffalo, New York

Epackachi, S., Luna, B., & Whittaker, A. S. (2015). Numerical Investigation of the in-Plane Behavior of Low Aspect Ratio Reinforced Concrete Shear Walls. *Transactions, SMiRT-23*.

Fenwick, R., and Bull, D. (2000). What is the stiffness of reinforced concrete walls. SESOC Journal, 13(2), 23–32.

FEMA 356 (2000) "Prestandard and Commentary for the Seismic Rehabilitation of Buildings", federal Emergency Management Agency, Washington D.C., USA.

Filippou, F. C.; Popov, E. G.; and Bertero, V. V. (1983). "Effects of bond deterioration on hysteretic behavior of reinforced concrete joints," EERC Report No. UCB/EERC–83/19, Earthquake Engineering Research Center, University of California, Berkeley, California.

Gulec, Cevdet Kerem, and Andrew Whittaker. (2009). "Performance-Based Assessment and Design of Squat Reinforced Concrete Shear Walls." *Report No. MCEER-09-0010, Multidisciplinary Center for Earthquake Engineering Research, Buffalo, NY, 2009.*

Gulec, C. K., and Whittaker, A. (2009). Performance-based assessment and design of squat reinforced concrete shear walls. Report No. MCEER-09-0010, Multidisciplinary Center for Earthquake Engineering Research, Buffalo, NY, 2009.

Kolozvari, K., Tran, T. A., Orakcal, K., & Wallace, J. W. (2014). Modeling of Cyclic Shear-Flexure Interaction in Reinforced Concrete Structural Walls. II: Experimental Validation. Journal of Structural Engineering, 141(5), 04014136. https://doi.org/10.1061/(ASCE)ST.1943-541X.0001083

Massone L.M., O. K. and J. . W. (2006). Shear-flexure interaction for structural walls Shear-Flexure Interaction for Structural Walls. International Concrete Abstracts Portal, 236(November 2016), 127–150.

Menegotto, M. and Pinto, E. (1973). "Method of Analysis for Cyclically Loaded Reinforced Concrete Plane Frames Including Changes in Geometry and Non-Elastic Behavior of Elements under Combined Normal Force and Bending," Proceedings, IABSE Symposium. Lisbon, Portugal.

Massone L.M., O. K. and Wallace J. . W. (2006). Shear-flexure interaction for structural walls Shear-Flexure Interaction for Structural Walls. International Concrete Abstracts Portal, 236(November 2016), 127–150.

Li, B., & Xiang, W. (2011). Effective Stiffness of Squat Structural Walls. *Journal of Structural Engineering*, *137*(December), 1470–1479. https://doi.org/10.1061/(ASCE)ST.1943-541X.0000386

Lubliner, J., Oliver, J., Oller, S., & Oñate, E. (1989). A plastic-damage model for concrete. International Journal of Solids and Structures, 25(3), 299–326. https://doi.org/10.1016/0020-7683(89)90050-4.

"OpenSees – Open System for Earthquake Engineering Simulation", Pacific Earthquake Engineering Research Center, University of California, Berkeley.

Paulay, T., and Priestley, M. J.N. (1992). Seismic design of reinforced concrete and masonry buildings, Wiley, New York, 744.

Popovics, S. (1973). "A numerical approach to the complete stress-strain curve of concrete." *Cement and Concrete Research*, 3(5), 583-599.

Rocks, J. F. (2012). *Large Scale Testing of Low Aspect Ratio Reinforced Concrete Walls*. State University of New York, University at Buffalo.

Sozen, M. A., and Moehle, J. P. (1993). "Stiffness of reinforced concrete walls resisting in-plane shear." *Report No. EPRI TR-102731*, Electrical Power Research Institute, Palo Alto, CA.

Tang, T. O., & Su, R. K. L. (2014). Shear and Flexural Stiffnesses of Reinforced Concrete Shear Walls Subjected to Cyclic Loading. *The Open Construction and Building Technology Journal*, 104–121.

Tran, T. A. (2012). *Experimental and Analytical Studies of Moderate Aspect Ratio Reinforced Concrete Structural Walls*. PhD dissertation, University of California. Retrieved from http://escholarship.org/uc/item/1538q2p8

Tang, T. O., & Su, R. K. L. (2014). Shear and Flexural Stiffnesses of Reinforced Concrete Shear Walls Subjected to Cyclic Loading. *The Open Construction and Building Technology Journal*, 104–121.

Thomson, E., & Flórez-lópez, J. (2004). Simplified Damage Model for Shear Dominated Reinforced Concrete Walls Under Lateral Forces. *13th World Conference on Earthquake Engineering*, (844).

Tran, T. A. (2012). *Experimental and Analytical Studies of Moderate Aspect Ratio Reinforced Concrete Structural Walls*. PhD dissertation, University of California. Retrieved from http://escholarship.org/uc/item/1538q2p8

Ulugtekin, D. (2010). “Analytical modeling of reinforced concrete panel elements under reversed cyclic loadings.” M.S. thesis, Bogazici Univ., Istanbul, Turkey.